INTERPLAY OF CHARGE CURRENT AND SPIN IN NANOSTRUCTURES

INTERPLAY OF CHARGE CURRENT AND SPIN IN NANOSTRUCTURES

Proefschrift

ter verkrijging van de graad van doctor
aan de Technische Universiteit Delft,
op gezag van de Rector Magnificus prof. ir. K. C. A. M. Luyben,
voorzitter van het College voor Promoties,
in het openbaar te verdedigen op maandag 7 april 2014 om 15:00 uur

door

Fatemeh KAKO JOIBARI

Master of Science in Solid State Physics and Electronics
geboren te Sari, Iran.

Dit concept-proefschrift is goedgekeurd door de promotors:

Prof. dr. ir. G. E. W. Bauer
Prof. dr. Y. M. Blanter

Samenstelling promotiecommissie:

Rector Magnificus,	voorzitter
Prof. dr. ir. G. E. W. Bauer,	Technische Universiteit Delft, promotor
Prof. dr. Y. M. Blanter,	Technische Universiteit Delft, copromotor
Prof. dr. Y. V. Nazarov,	Technische Universiteit Delft
Prof. dr. L. D. A. Siebbeles,	Technische Universiteit Delft
Prof. dr. J. Aarts,	Universiteit Leiden
Dr. R. A. Duine,	Universiteit Utrecht
Dr. P. Yan,	Technische Universiteit Delft

Printed by: Gildeprint

Front & Back: Designed by Zahra Hamidi

Casimir PhD Series, Delft-Leiden 2014-6

ISBN 978-90-8593-181-2

An electronic version of this dissertation is available at
http://repository.tudelft.nl/

To my beloved family

PREFACE

It was almost July 2009 when I moved to the Netherlands. I started my PhD with two theses on ultrafast switching magnetization, an interesting and challenging topic which was very different from my background. Now, this journey comes to the end with this thesis.

Reaching the end of my PhD, I must admit that what I have learned during this time went way beyond the science aspect: Working around the world in different countries and meeting international people taught me far more than I expected. I met people with whom I enjoyed spending my time, friends without whom it would not have been nearly as fun nor pleasant. Here, I owe a debt of gratitude to all the people who had any contribution to my learning experiences, joyful moments and health by accompanying me in sports.

As for the academic aspect of my PhD, there are lots of people I would like to thank for discussing science with me. To Gerrit, who offered me the job and gave me the freedom to choose how to tackle the problems. Thanks to you I had the chance to collaborate and discuss science with people from all around the world. To Yaroslav, for not only discussing physics with me, but also being such a kind and caring person. To Peng, from whom I have learned so many things, especially while collaborating on DW project. To Yi, for having great discussions over many conferences and visits. To Jiang, for such a good hospitality, when I visited Fudan university in Shanghai, and great scientific discussions. To Akash and François, for all our fruitful white-board discussions. To Stefan, Mihajlo, Chris, Frans, Kim and Erin for discussing my work with me, and science in a more general aspect in our leisure time.

My work environment in Delft was also a place full of enthusiastic people who I have enjoyed talking to. Those of you I have had chances to get to know better and those who joined the group only recently. Mireia, Fatemeh and Alina, thank you for starting off my PhD with a warm welcome. Mireia, special thanks to you for helping me find myself quickly in the new environment when I first moved here. To Tony, Marnix, Marcin, Ciprian, Yanting, Yunshan, and Rodrigo, for so many pleasant discussions over coffee breaks, and occasional breaks. To Yuli, who always motivated scientific discussions and a better scientific presentation. Miriam and Jos, I have enjoyed our many discussions, including the ones about science. To Marjolein, and Erika who have made our lives in the group much easier, by helping us

with work related formalities. The people who joined our group more recently and made the group lively again: Anton, Michael, Wouter, Jose, Alwin, Mohammad, Adriaan, Albert, Xiaoli, Sebastian, Rafał. Special thank to Mohammad and Wouter, for their useful feedbacks of the final version of the thesis, and to Alwin who very much voluntarily lent me his chair. You guys are all very friendly, and pleasant to talk to. Have a great time in theory group!

During these years, I also enjoyed participating in sports, so I would like to thank all people who shared the same interests with me, and motivate me to work out. To Kim, for going to the gym with me: if it wasn't for you, I would be too lazy to go to the gym so often! To Gio and Chris for our so-called Saturday morning workout tradition! To Mickael for taking me to climbing with him. To Ruta, for being my tennis partner for over the last two years.

My experience in the Netherlands was completed with a great circle of friends who I spent time after work. People who I could truly connect with, for whom the difference in culture did not become a barrier for us to become good friends. I would like to thank you all, for being such good friends, teaching me so many things, and sharing your cultures with me.

To Stefan, who is warm-hearted, and has a broad knowledge on different subjects. You are a friend, who I could count on. To Hedyeh and Fatemeh, for our occasional Persian girls' evenings out. You are kind and enjoyable to hang out with. To Frans, I have always enjoyed discussing with you on so many divergent topics. I also especially thank you for translating my summary and propositions to Dutch. To you and Denise who showed me that Dutch food is great! To Akash, who I could always talk to, about anything from science to fun! You are a caring, warm and energetic person. To Nicole and Rakesh, for throwing cool parties. I hope you more success next time sledging. To Gabriele and Maria, who are fun, and experts in making fabulous brunches. To Olya and Dave, who are a very relaxed and cool couple! I have always enjoyed spending time with you.

To Chris, Vanessa, Gio, and Keti who their friendship made me to feel stronger. You have always offered me help when I needed it. With you guys, I could put the tiredness aside, and be relaxed and happy. Our circle was complete when Joost and Tungky joined us. To Joost, who is of the most optimistic and caring people I have met. To Tungky, who always smiles regardless of the situation! You people make me to feel very happy.

To Kim and Erin, you have been such great company, and so supportive to me all these years. I can truly say that meeting you was one of my greatest fortunes in the last couple of years. I believe we will always stay good friends, regardless of the distance.

To Zahra, who has been one of my best friends for over half our lives! (The number shall remain a secret.) You have always been supportive, kind, and gener-

ous. When you moved to the Netherlands, my happiness became amplified, as we say in Persian.

To Andy, for all the happy and pleasant moments and adventures we have shared. Dankeschön Liebling: for being so cheerful and supportive since I met you. To the Fognini family, who has always welcomed and treated me like one of the family. Having you around made it easier to be so far from my own.

And to my dearest family:

به پدر و مادر مهربان ، و خواهر نازنینم. سپاس بیش از همه به شما که هیچ زمان حمایت و محبتتان را از من دریغ نکردید. به هنگام شـادی با من خندیدید و در هنگام خستگی و دلتنگی آغوشـتان همیشه برایم باز بود. پس تقدیم به شما با عشـق.

Fateme Joibari
Delft, March 2014

CONTENTS

1

INTRODUCTION

MAGNETISM has led to revolutionary advances in data storage, and offers new possibilities for novel computing paradigms. Thus, its fundamental understanding is of paramount importance for future applications. Currently, magnetic recording in commercially available hard drives offers large storage capacity, random access to data, and non-volatility, all at a low cost per byte. However, as data processing power and speed is ever increasing, understanding and finding ways to control the technological matters spawned the field of *spintronics* [1]. Spintronics, or spin electronics, is the science and technology field that strives to study and control spin, the intrinsic angular momentum of the electron. An important phenomenon in spintronics is magnetism, i.e. spontaneous ordering of the spins even far above room temperature.

Magnetization can be controlled by various means. The most straightforward and traditional way of controlling the magnetization is using magnetic fields, that orient the magnetization direction by the Zeeman interaction. However, the desire to make data storage *faster* and *smaller* requires new approaches due to the practical limitations of generating magnetic fields in small structures.

For *faster* control of the magnetization, alternatives such as all optical control had been introduced [2, 3]. This is shown to have magnetization reversal at the sub-picosecond time scales: currently one of the fastest means of switching. To go *smaller*, Domain Wall (DW) seems to be a promising tool to extend the scaling of spintronic devices to much smaller dimensions [4–6]. This inspired fundamental studies during the last decade on the spin transfer effect, where an electrical current is used to displace DWs along magnetic tracks [7]. Thus, studying the effect of

an electric current on the spin state of the material is essential.

As a *reciprocal* phenomena, the spin of particles in a system could also affect the conductance properties of a material. The Aharonov-Casher effect is a good example of this. It shows the importance of spins, as controlled by Rashba spin orbit interaction (SOI), on conducting behaviors of materials. This will be explained in more details in Section 1.3.

1.1 BASICS OF MAGNETISM

Magnetism has been known already to the Greek and Chinese for almost two millennia. Historically, it attracted attention due to its mysterious nature: magnetic materials repel and attract each other or certain kinds of objects without having contact with them. This was, in ancient times, attributed to magic. According to the legends magnetism was discovered by a shepherd who noticed that the metal tips of his shoes were stuck to a black stone he was standing on. The stone was found in an area named Magnesia, thus, it is believed that the word 'Magnetism' originated from this name [8]. Later, it was found that magnetic slivers floating on the surface of water, or otherwise properly suspended from their center of mass, would spin around their centers until one end of the magnet always pointed north. The Chinese appear to be the first who could use this technique to orient themselves in the oceans by simple compasses [9].

To study the magnetic materials, one could look at magnetism from two different perspectives: One is the classical picture, and the other, which is the more recent realization, discusses magnetization quantum mechanically.

1.1.1 CLASSICAL DESCRIPTION

Magnetization is a material property for which the classical concept was known long before the discovery of quantum mechanics. The most direct manifestation of magnetism is the force of attraction or repulsion between two magnets. This phenomenon can be described by assuming that there are 'free' magnetic poles on the ends of each magnet that exert forces on one another.

Magnets are materials with a net magnetic moment, the quantity which determines the amplitude of torque that a magnetic field applies on it. These magnetic moments originate from the angular momentum of charged particles, with an elementary charge of q. An oversimplified but intuitive model treats elementary charges as spherical particles with charge uniformly distributed throughout its volume. A rotating particle with angular momentum $\mathbf{L}$ has a magnetic dipole moment of

$$\boldsymbol{\mu} = \frac{q}{2m}\mathbf{L}, \tag{1.1}$$

where m and q are the mass and charge of the particle, respectively. While the above expression is correct for orbital angular momentum, it is off by a factor from the spin magnetic moment, as will be shown in Section 1.1.2.

1.1.2 QUANTUM MECHANICAL DESCRIPTION

The discovery of quantum mechanics provided a more precise perspective to magnetization. Quantum mechanics introduced a second type of angular momentum, which differs from the ordinary orbital angular momentum. This new type known as spin, the analogue of which is absent in classical mechanics, is an intrinsic form of angular momentum carried by elementary particles. Similar to a rotating electrically charged bodies in classical mechanics, a magnetic dipole is allocated to particles with spin. The intrinsic magnetic moment for a particle with spin **S**, charge q, and mass m is

$$\boldsymbol{\mu} = \frac{g_s q}{2m}\mathbf{S}. \tag{1.2}$$

where g_s is the dimensionless factor absent in the classical picture of Eq. (1.1) and is called the g-factor. The above equation is usually written in terms of Bohr magneton, μ_B:

$$\boldsymbol{\mu} = g_s \mu_B \frac{\mathbf{L}}{\hbar}, \tag{1.3}$$

where $\hbar$ is the planck constant.

Based on their magnetic properties, materials are either ferromagnetic or non-ferromagnetic. In ferromagnetic materials, the electron spins are partially aligned, producing a macroscopic non-zero magnetic field, i.e. finite magnetization. However, this macroscopic magnetic field vanishes above the Curie temperature. This is the critical temperature beyond which the spins are randomized and the magnetization is lost. In non-ferromagnet materials, individual dipoles in the absence of external magnetic fields are always randomly oriented, producing a net zero magnetic field.

1.2 CONTROL OF MAGNETIZATION

The technological aspect of magnetic storage derives research aimed at finding fast and efficient ways to control the magnetization. Magnetization switching, or reversal, i.e. a 180° reorientation of the magnetization vector with respect to its original direction, is one of the most important processes in magnetic data storage. The reason is that with each magnetization direction a binary '0' or '1' can be saved. By increasing the demand for faster and faster computers, it is necessary to

find ways to store data on shorter time scales as well. An applied magnetic field is historically the first tool to control the magnetization. The magnetic field applies a torque on the magnetization, which tends to align it with the field. Thus, to switch the magnetization, an external field opposite to the initial magnetization orientation is usually applied. This can be experimentally challenging if a switching time shorter than a nanosecond is necessary.

Alternatively, one can inject a spin polarized current from a ferromagnet into the magnetic domain to switch its magnetization [10–12]. If the polarization of the conducting electrons is not aligned with the magnetization of the domain, conducting electrons exert a torque on magnetization because of exchange interaction. If the spin current density is high enough, a sufficiently large torque will be generated, and the magnetization switches. Such a switching has been performed on the hundreds of picoseconds time scale, for current densities above a few 10^6A cm^{-2} [13, 14].

Optical tools provide another alternative to control the magnetization. This method is currently the fastest tool for switching magnetization with reversal at sub-picosecond time scales [2, 3]. This will be discussed in more depth in Section 1.2.1. These are the commonly known ways of controlling the magnetization.

In addition to these methods, one can control the magnetization with unpolarized current in the presence of an electric field, and noncollinear magnetization texture. These two methods, and the non absorbing optical control of magnetization are the focus of this thesis, and will be discussed in the sequel.

1.2.1 MAGNETO OPTICS: INVERSE FARADAY EFFECT

It has been shown that the magnetization can be switched by all optical tools [2, 3]. All optical switching refers to a method where the magnetization in a ferromagnet is switched using a circular polarized light, where the orientation of the magnetization is determined by the helicity of the light. Optical pulses can be made very short, in femtosecond time scales, allowing ultrafast switching of the magnetization. One possible mechanism for all optical switching is the Inverse Faraday effect (IFE) [15, 16]. Originally, this effect is non-absorbing, i.e. the photons are not absorbed by the medium.

IFE is reciprocal to the original Faraday effect (FE), which was discovered by Faraday in 1845 [17]. FE was one of the first evidences demonstrating that light and magnetization interact. FE describes the rotation of the polarization plane of linearly polarized light when passing through a material subject to an external magnetic field, or a ferromagnet, with magnetic field or a magnetization component parallel to the light vector, respectively. Linearly polarized light is a superposition of right and left handed circularly polarized light with equal amplitudes and

different phases. These two polarizations propagate with a slightly different velocity in a magnetic material. This property, known as circular birefringence, is rooted in the difference of the refractive indices of lights with opposite helicities in optically active materials. The difference is a measure of the strength of optical activity, which is a material characteristic. Thus, upon exiting the magnetic material, the two polarizations acquire a relative phase shift, which is equivalent to a rotation of the orientation of the linear polarization upon transmission. This effect for light traversing a material subjected to an external magnetic field B, in the direction of propagation, can be formulated as follows:

$$\beta = \mathcal{V} B d \tag{1.4}$$

where β is the angle of rotation, d is the length of the path where the light and magnetic field interact, and $\mathcal{V}$ is the Verdet constant of the material, which depends on wavelength and temperature. When light traverses through a ferromagnet, Faraday rotation can be accompanied with ellipticity generation [18].

In contrast, the Inverse Faraday effect describes the effect of light on the magnetization, rather than the effect of the magnetization on the light. An IFE is the ability of circularly polarized light to exert torques on a magnetization, which can be interpreted in terms of an effective magnetic field along its wave vector and a sign governed by its helicity. As mentioned earlier, neither FE nor IFE involves absorption of photons, which distinguishes these effects from photomagnetic effects that involve excited electrons and holes. This makes IFE potentially very fast and interesting, *e.g.* in data storage technologies.

The IFE was initially predicted by Pitaevskii in [15] and formulated in terms of the dependence of the free energy on a time-dependent electric field. After the observation of IFE by Van der Ziel *et al.* in Ref. [16], Pershan *et al.* developed a microscopic theory explaining the IFE in terms of an optically-induced splitting of degenerate spin levels, followed by thermal relaxation [19]. Their expression for the magnetization created by circularly polarized light is given as $\mathbf{M} = \mathcal{V}\lambda_0(2\pi c)^{-1}(I_R - I_L)\mathbf{e}_k$, where $I_{R(L)}$ is the intensity of the right (left) handed circularly polarized light, $\mathbf{e}_k$ is the direction of the propagation, λ_0 and C are the wavelength and speed of light, respectively.

IFE seemed to be well understood until a series of experiments in Nijmegen demonstrated that ultrashort pulses of circularly polarized light is able to excite, or even switch the magnetization on a femto-second time scale, which could not be explained by thermal relaxation anymore [2, 3, 20, 21]. Furthermore, experimental studies on a terbium gallium garnet crystal demonstrated that in the subpicosecond regime, the phenomenological models of IFE fail to explain the experimental results, and the Verdet constant for IFE deviates from the one for FE in

absorbing mediums [22]. Vahaplar *et al.* demonstrated that the values of the effective magnetic field as a result of circularly polarized light is as high as 20 Tesla, while its origin is still under debate [3].

To provide an alternative and simple understanding of IFE, Hertel followed the footsteps of plasma physicists by suggesting that the effective magnetic field in IFE is caused by circular currents in collision-less systems [23]. He assumed that in a collision-less electron plasma, a non-dissipating circular current arises in response to high frequency circularly polarized light. A plasma can be characterized by the velocity $v(r,t)$ and density $n(r,t)$, fields that can be considered as small fluctuations around their average values, and are generated by the light's electric field. The current density, $j = n(r,t)ev(r,t)$, then reads

$$\langle \boldsymbol{j} \rangle = -\frac{i}{4e\langle n\rangle\omega}\boldsymbol{\nabla}\times\left[\sigma^*\boldsymbol{E}^*\times\sigma\boldsymbol{E}\right] + \frac{1}{4e\langle n\rangle\omega}\left[\left(i\sigma^*\boldsymbol{E}\boldsymbol{\nabla}\right)(\sigma\boldsymbol{E}) + \text{c.c.}\right], \tag{1.5}$$

where $\sigma = i\langle n\rangle e^2/(m\omega)$ is the conductivity of the isotropic collision-less plasma, ω is the frequency, and $\boldsymbol{E}$ is the electric field of light. The first term is a circular current, that turns out to be relevant to IFE. The second term is the current resulting from the so called ponderomotive force, which arises from the inhomogeneity of the space (plasma), and is not relevant to the IFE. $\boldsymbol{E}^*\times\boldsymbol{E}$ vanishes for linearly polarized light, and reduces to $\pm i|\boldsymbol{E}|^2\mathbf{e}_k$ for circularly polarized light propagating in the $\mathbf{e}_k$ direction, where the sign depends on the helicity of the light. Thus, Hertel concludes that since the circular current can be written in the form of $j_m = c\bigtriangledown\times M$, we have a magnetization of

$$\boldsymbol{M} = \frac{ie\omega_{\text{p}}^2}{16\pi\omega^3 mc}\left[\boldsymbol{E}\times\boldsymbol{E}^*\right]. \tag{1.6}$$

However, the mechanism of how this magnetization is transferred to the material is not explained. A metal is not likely to withstand a current large enough to induce the 20 T magnetic field observed in experiments. Moreover, this theory cannot explain why this effect is solely observed in certain materials, and not in the others. Therefore, this theory appears to be incomplete.

A missing piece of Hertel's scenario can be sought in the spin orbit interaction (SOI). We set out to explain IFE by a light-induced circular-current mediated spin polarization in the presence of SOI. According to Eq. (1.5) a clockwise or counter-clockwise circular current flows depending on the helicity of circularly polarized light. We argue below that in the presence of spin orbit interaction, currents generate a spin polarization that in conducting magnets can actuate the magnetization.

1.2.2 SOI MEDIATED CURRENT-INDUCED SPIN TORQUE

Theoretically it has been demonstrated that currents induce torques in the presence of a Rashba SOI [24, 25]. The experimental results in Ref. [26] possibly confirm these theories. Spin orbit coupling is a relativistic effect in which the spin of a particle is coupled with its motion: the spin of a moving electron experiences the electric field as an effective magnetic field in its rest frame. This effect causes a momentum dependent spin splitting of the energy levels. The electric field can be generated by structural asymmetry or lack of inversion symmetry of the bulk material. For electrons close to the band edges of semiconductors, the former is know as Dresselhaus SOI, and the latter as Rashba SOI.

Rashba spin orbit coupling is due to an asymmetric confining potential, and usually happens in heterostructures, in which a two dimensional electron gas (2DEG) is induced e.g. by modulation doping of semiconductor bilayers. The electrons are nearly free and the spin orbit interaction is like the one in vacuum

$$H_{Rashba} = \frac{\alpha}{\hbar}\sigma \cdot \left(\mathbf{p} \times \mathbf{e}_z\right) = \frac{\alpha}{\hbar}\left(\sigma_y p_x - \sigma_x p_y\right), \tag{1.7}$$

where the spin orbit coupling constant can be strongly enhanced, σ_i and p_i are the ith component of Pauli spin matrices and momentum operator, respectively, and the electric field in the z-direction is constrained in α.

In contrast, in the case of bulk inversion asymmetry, which is caused by the lack of inversion symmetry in unit cells of e.g. III-V semiconductors, we have Dresselhaus type SO interaction. Projected to a 2DEG, the Hamiltonian reduces to

$$H_{Dresselhaus} = \frac{\beta}{\hbar}\left(\sigma_x p_x - \sigma_y p_y\right). \tag{1.8}$$

where β is Dresselhaus spin orbit coupling strength.

The current-driven intrinsic spin torque in ferromagnets was discussed by Manchon and Zhang [24, 25], who predicted a torque induced by a current in the presence of a SOI of the Rashba type, which generates an effective magnetic field perpendicular to both the inversion symmetry-breaking electric field and the current: $B_{Rashba} = -\alpha/\hbar\langle\mathbf{p}\rangle \times \mathbf{e}_z$, where $\langle\mathbf{p}\rangle$ is the average of momentum that vanishes at equilibrium, see Fig. 1.1. This effect is essentially the Edelstein effect discussed in Ref. [27] in a ferromagnetic system, i.e. a current induced spin accumulation in the 2DEG plane and normal to the current. In a ferromagnet, this spin polarization is linked to the magnetization by exchange interaction, causing an effective magnetic field, which, if not aligned with the initial magnetization, induces a spin torque on the magnetization in a conducting ferromagnet.

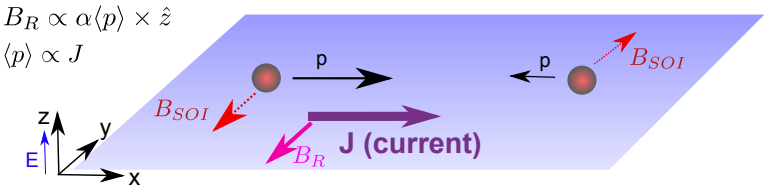

FIGURE 1.1: Schematic picture of the SO mediated current-induced effective magnetic field.

1.2.3 CURRENT INDUCED MAGNETIC DOMAIN WALL MOTION

A charge current exerts torque on noncollinear magnetization textures such as domain walls. Magnetic domains minimize the magnetostatic energy. Domain walls (DW) are the transitional space connecting adjacent domains of opposite magnetization directions with a gradual reorientation of magnetization over a finite distance, i.e. DW width, see Fig 1.2. The width of a DW is a balance between two opposing energies, i.e. magnetocrystalline anisotropy and exchange energy of the material, to minimize the total energy. The anisotropy energy is minimal when the magnetic moments are aligned with the anisotropy axes, thus tending to reduce the DW width. On the other hand, the exchange energy tends to align the neighboring magnetic moments, thereby increasing the DW width. These two compete and their balance results in a characteristic length, that is typically 100 nm for transition metal ferromagnets.

Impurity or crystal defects break the transitional symmetry and pin the DWs to energetically favorable regions. DW pinning can be induced intentionally, e.g. by a notch or antinotch in a thin magnetic wire. DWs can be depinned by sufficiently large external forces exerted by magnetic fields, or electric currents [28, 29].

In an adiabatic regime, when a current flows through a wire containing a DW, in each point the magnetization of the conducting electrons tries to align with the direction of the local magnetization. Since the local magnetization changes over the DW, the conducting electrons arrive at each point with a polarization aligned with the previous point, and slightly noncollinear with the local magnetization. Then the polarization of the electron aligns with the magnetization and the lost angular momentum is transfered to the local magnetization which, if large enough, causes DW depinning. The depinned DW then moves until it is pinned by another pinning site.

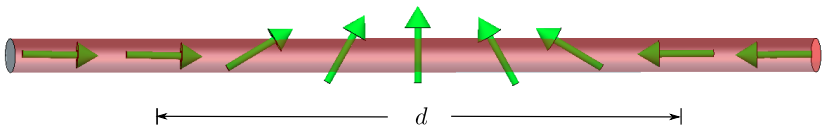

FIGURE 1.2: Schematic picture of a Domain wall with width of d.

1.3 SPIN INDUCED CURRENT (CONDUCTANCE) DYNAMICS: AHARONOV CASHER EFFECT

In Sections 1.2.2 and 1.2.3, we discussed how the current influences the spin of a system. In this Section, we discuss an opposite situation where the spins of the carriers under the effect of SOI change the conductance of the system, i.e. the Ahahronov-Casher effect.

The Aharonov-Casher (AC) effect presented in [30] is an analogue of the Aharonov-Bohm (AB) effect, but is caused by the SOI rather than by an external magnetic field. The AB effect was introduced in 1959 by Aharonov and Bohm, for a system with electrically charged particles traveling in a ring surrounding a confined magnetic field [31]. Even if the magnetic field vanishes on the ring, it nevertheless affects the phase of the wave function because the electrons feel the vector potential associated by the magnetic field. If electrons are injected into one side of the ring and collected at the other as in Fig. 1.3 (upper left), either constructive or destructive interference occurs, depending on the phase difference between the electrons passing through the upper and lower arms of the ring. This causes oscillations of conductance as a function of the magnetic field strength, as observed experimentally [32], for an illustrative example see Fig. 1.4.

Aharonov and Casher predicted in 1984 that a spin also accumulates a phase in the presence of an external electric field [30]. The situation discussed by Aharonov and Casher is similar to a single-mode ballistic ring with Rashba spin-orbit interaction, which can be understood as follows. In the ordinary AC effect, the electrons injected into a quantum ring with SOI acquire spin phases when traversing the two arms due to precession in the effective spin-orbit magnetic field. Interference of the spinor wave functions at the exit point then leads to an oscillatory conductance as a function of the spin-orbit coupling constant that in Rashba systems can be tuned by an external gate voltage. This is similar to ordinary AB effect but induced by an electric field rather than a confined magnetic field, see Fig 1.3 (upper right).

Phase interference is observable only when (half of) the circumference length

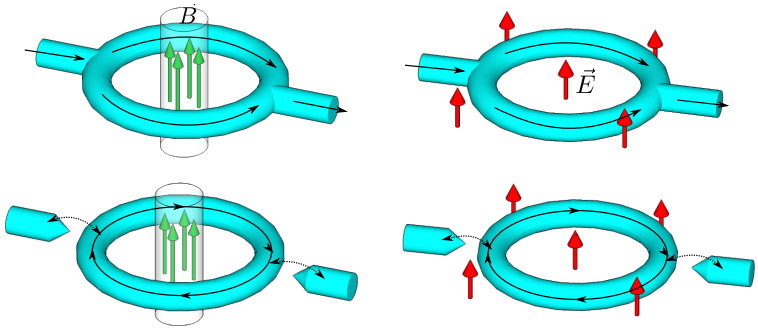

FIGURE 1.3: Schematic comparison of AC and AB effect in a quantum ring. Left side demonstrates AB effect and AC effect is demonstrated in the right side. Upper panel is the ordinary and lower panel is the bound state version of these effects.

of the ring is sufficiently smaller than the phase coherence length. The typical size of the rings in the experiments is known to be comparable with the phase coherence length [33]. Thus, this all happens assuming that the electrons exit the ring after traveling through the ring arm only once. This means that the coupling of the ring to the leads should be very strong. Thus, AC phase modulation of the conductance results in an oscillatory behavior with respect to a changing spin orbit coupling constant, which can be controlled by a gate voltage tunning the asymmetry of the potential in 2DEG. The AC effect in the ballistic 1D regime, i.e. with a single transport channel and in the absence of defect and impurity scattering was first calculated in Ref. [34]. A revision was necessary, however, since the Hamiltonian of the ring used was not Hermitian [35]. Eventually, Frustaglia *et al.* studied the AC effect in a 1D ring subjected to a low bias, computing the zero temperature conductance of the 1D Rashba ring with symmetric contacts in the spirit of the Landauer-Büttiker formalism [36]. Thus, the conductance, as a function of the Rashba spin-orbit interaction strength, α, is

$$G = \frac{e^2}{h}\left[1-\cos\left(\frac{\pi}{\cos\theta}\right)\right] = \frac{e^2}{h}\left[1-\cos\left(\pi\sqrt{1+\left(\frac{2ma\alpha}{\hbar^2}\right)^2}\right)\right], \tag{1.9}$$

where $\tan\theta = 2ma\alpha/\hbar^2$ and a is the radius of the ring.

Extensive experimental research aimed at observing such oscillatory behavior in currents has been carried out [37, 38]. However, obstacles such as making a perfectly symmetric ring, need to be overcome, since even a small asymmetry between the upper and lower arms of the ring can strongly change the phase. König

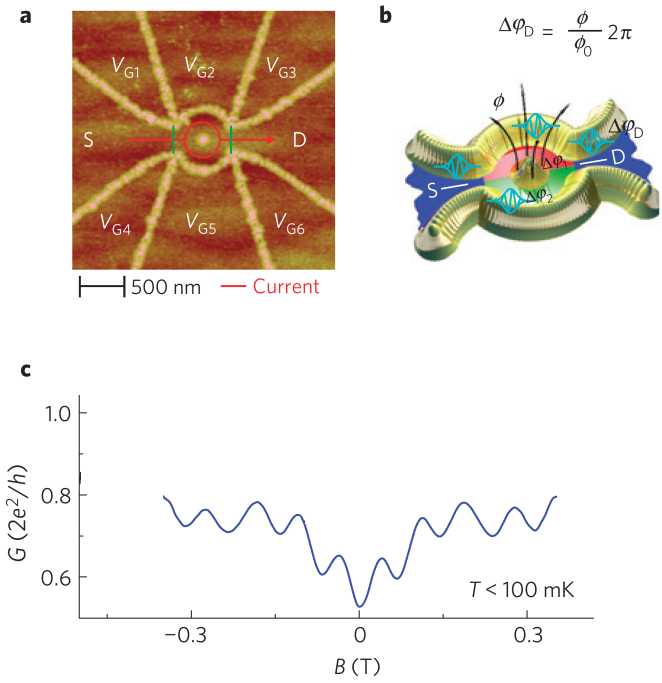

FIGURE 1.4: Aharonov-Bohm effect in a ring. (a) An example of an experimental set up measuring the oscillation of conductance due to AB effect. (b) Schematic picture of the phase interference in the ring, where Φ is magnetic flux, and $\Phi_0 = h/e$, i.e. the magnetic flux quanta. (c) An Example of experimental results of conductance oscillation due to AB effect. (Adapted by permission from Macmillan Publishers Ltd: Nature Phys. Ref. [39], copyright 2010)

et al. reported the first experimental evidence of AC effect in a single HgTe ring [37]. They measured the phase shift of the AB-type magneto-conductance oscillations caused by tuning the Rashba SO strength. However, the conductance modulation was observed only at high magnetic fields, in a regime where SO interaction has rather weak effects. In order to improve the AC signals Nitta and coworkers carried out experiments on an array of connected rings [38]. The results were in good agreement with a theory for a single-mode quantum ring symmetrically coupled to two leads [36], see Fig. 1.5.

The precise electric connection of quantum rings to the electric contact can be established by the absolute value of the conductance. In practice this is difficult to measure in the presence of parallel conductance paths through the bulk

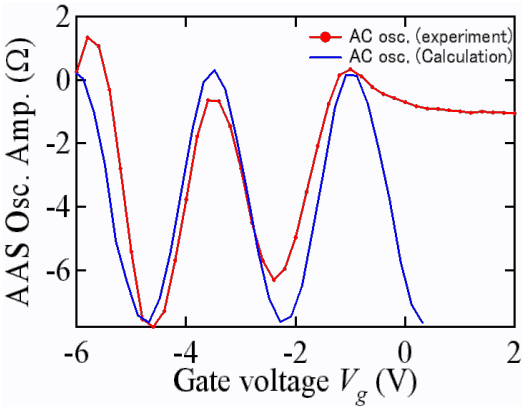

FIGURE 1.5: The oscillation in change of resistance as a result of AC effect. (Fig from Ref [33]-©2011 IEEE)

layers. Therefore, it makes sense to investigate the limit opposite to the usually assumed strong coupling. In that case, electrons confined to the ring reside in size quantized states only weakly perturbed by the contacts, i.e. the rings behave like quantum dots, see Fig. 1.3 (lower images). In the low-biased regime, an oscillatory behavior in the quantum rings can be expected. However, this is due to the discreteness of energy levels inside of the ring and not from quantum interference. The oscillations arise from shifting energy levels due to changing the spin orbit coupling constant. When an energy level is within the bias window, conductance occurs. Otherwise, the current is zero, see Fig. 1.6. As we will demonstrate in this thesis, the experiments on ring arrays can theoretically be explained by both weakly coupled ring arrays and a single ring strongly coupled to the leads equally well.

1.4 THIS THESIS

In this thesis, we study the interplay of currents and spin in nanostructures. In the first part of this thesis, we study the spin polarization generated by light-induced electric currents in quantum rings. In Chapter 2, we study the electrons and holes in non-magnetic single mode quantum rings in the presence of Rashba or Dresselhaus type SOI and light induced circular currents. In Chapter 3, we address what happens when the rings are magnetic, i.e. in the presence of an exchange potential that breaks the Kramers degeneracy. As we demonstrate in this chapter, effects can be maximized by tuning the Fermi energy into the exchange gap such that only one

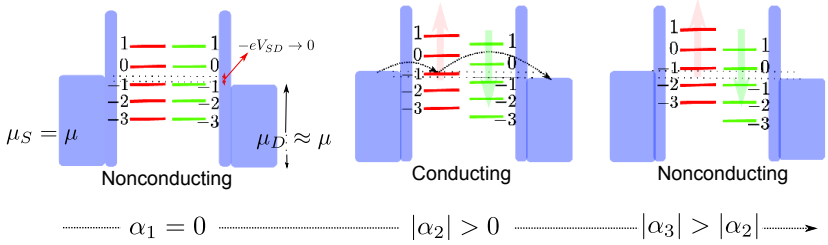

FIGURE 1.6: Schematic picture of energy levels inside a quantum ring weakly coupled to the leads. The levels are tuned with changing SO coupling strength, α. The systems conducts only when a state is in the bias window.

band is occupied. In Chapter 4, we study the current-induced motion of domain walls initially pinned by the localized magnetic fields, e.g. generated intentionally by notches in a metallic wire. We obtain the critical current needed to depin the wall.

The second part of this thesis focuses on an opposite effect, viz. control of the state of the spin by SOI on the conductance of an array of rings. We demonstrate in Chapter 5 that transport through a weakly coupled ensembles of rings oscillates as a function of a perpendicular electric field that controls the Rashba spin orbit interaction. Moreover, in this chapter we study the effect of an external in-plane magnetic field on such conductance oscillations.

REFERENCES

[1] Igor Zutic, Jaroslav Fabian, S. Das Sarma, Rev. of Mod. Phys **76**, 323 (2004).

[2] C. D. Stanciu, F. Hansteen, A.V. Kimel, A. Kirilyuk, A. Tsukamoto, A. Itoh, and Th. Rasing, Phys. Rev. Lett. **99**, 047601 (2007).

[3] K. Vahaplar, A. M. Kalashnikova, A. V. Kimel, S. Gerlach, D. Hinzke, U. Nowak, R. Chantrell, A. Tsukamoto, A. Itoh, A. Kirilyuk, and Th. Rasing, Phys. Rev. B **85**, 104402 (2012).

[4] S. D. Bader and S. S. P. Parkin, Ann. Rev. Cond. Matt. Phys. **1**, 71 (2010).

[5] D. A. Allwood, G. Xiong, C. C. Faulkner, D. Atkinson, D. Petit, and R. P. Cowburn, Science **309**, 1688 (2005).

[6] C. H. Marrows, Adv. Phys. **54**, 585 (2005).

[7] L. Berger, Phys. Rev. B **54**, 9353 (1996).

[8] G. L. Verschuur, *Hidden Attraction: The History and Mystery of Magnetism*, Oxford University Press (1993).

[9] D. J. Dunlop, Özden Özdemir, *Rock Magnetism: Fundamentals and Frontiers*, Cambridge University Press (1997).

[10] J. Slonczewski, J. Magn. Magn. Mater. **159**, L1-L7 (1996).

[11] L. Berger, Phys. Rev. B **54**, 9353 (1996).

[12] F. J. Albert, J. A. Katine, R. A. Buhrman, D. C. Ralph, Appl. Phys. Lett. **77**, 3809 (2000).

[13] A. A. Tulapurkar, T. Devolder, K. Yagami, P. Crozat, C. Chappert, A. Fukushima, Y. Suzuki, Appl. Phys. Lett. **85**, 5358 (2004).

[14] M. Nakayama, T. Kai, N. Shimomura, M. Amano, E. Kitagawa, T. Nagase, M. Yoshikawa, T. Kishi, S. Ikegawa, and H. Yoda, J. Appl. Phys. **103**, 07A710 (2008).

[15] L. P . Pitaevskii, Sov. Phys. JETP **12**, 1008 (1961).

[16] J. P. Van der Ziel, P. S. Pershan, and L. D. Malmstrom, Phys. Rev. Lett. **15**, 190 (1965).

[17] Faraday, M. Philos. Trans. R. Soc. London **26**, 2146 (1845).

[18] M. Battiato, G. Barbalinardo, and P. M. Oppeneer, Phys. Rev. B **89**, 014413 (2014).

[19] P. S. Pershan, J. P. van der Ziel, and L. D. Malmstrom, Phys. Rev. **143**, 574 (1966).

[20] A. V. Kimel, A. Kirilyuk,P. A. Usachev, R. V. Pisarev, A. M. Balbashov, and Th. Rasing, Nature **435**, 655 (2005).

[21] A. Kirilyuk, A. V. Kimel, and T. Rasing, Rev. Mod. Phys. **82**, 2731 (2010).

[22] R. V. Mikhaylovskiy, E. Hendry, and V. V. Kruglyak, Phys. Rev. B **86**, 100405 (2012).

[23] R. Hertel, J. Magn. Mag. Mat. **303**, L1-L4 (2006).

[24] A. Manchon and S. Zhang, Phys. Rev. B **78**, 212405 (2008).

[25] A. Manchon and S. Zhang, Phys. Rev. B **79**, 094422 (2009).

[26] I. M. Miron, G. Gaudin, S. Auffret, B. Rodmacq, A. Schuhl, S. Pizzini, J. Vogel and P. Gambardella, Nature Materials. **9** 230, (2010).

[27] V. M. Edelstein, Solid State Communications **73**, 233 (1990).

[28] S. Zhang and Z. Li, Phys. Rev. Lett. **93**, 127204 (2004).

[29] M. Hayashi, L. Thomas, C. Rettner, R. Moriya, X. Jiang, and S. S. P. Parkin, Phys. Rev. Lett., **97**, 207205 (2006).

[30] Y. Aharonov and A. Casher, Phys. Rev. Lett. **53**, 319 (1984).

[31] Y. Aharonov, D. Bohm, Phys. Rev. **115**, 485 (1959).

[32] R. A. Webb, S. Washburn, C. P. Umbach, R. B. Laibowitz, Phys. Rev. Lett. **54**, 2696 (1985).

[33] J. Nitta, J. Takagi, F. Nagasawa, M. Kohda, Journal of Physics: Conference Series **302**, 012002 (2011).

[34] J. Nitta, F. E. Meijer, H. Takayanagi, Appl. Phys. Lett. **75**, 695 (1999).

[35] F. E. Meijer, A. F. Morpurgo, T. M. Klapwijk, Phys. Rev. B **66**, 33107 (2002).

[36] D. Frustaglia, K. Richter, Phys. Rev. B **69**, 235310 (2004).

[37] M. Konig, A. Tschetschetkin, E. M. Hankiewicz, J. Sinova, V. Hock, V. Daumer, M. Schafer, C. R. Becker, H. Buhmann, and L. W. Molenkamp, Phys. Rev. Lett. **96**, 076804 (2006).

[38] T. Bergsten, T. Kobayashi, Y. Sekine, and J. Nitta, Phys. Rev. Lett. **97**, 196803 (2006).

[39] A. J. M. Giesbers, U. Zeitler, M. I. Katsnelson, D. Reuter, A. D.Wieck, G. Biasiol, L. Sorba, J. C. Maan, Nature Phys. **6**, 173, (2010).

2

LIGHT-INDUCED SPIN POLARIZATIONS IN NON-MAGNETIZED QUANTUM RINGS

Non-resonant circularly polarized electromagnetic radiation can exert torques on magnetization by the so-called Inverse Faraday Effect (IFE). Here we discuss the enhancement of the IFE by spin-orbit interactions (SOI). We illustrate the principle by studying a simple generic model system, i.e. the quasi 1D ring in the presence of linear/cubic Rashba and Dresselhaus interactions. We combine the classical IFE in electron plasmas that is known to cause persistent currents in the plane perpendicular to the direction of the propagation of light with the concept of current and spin-orbit induced spin transfer torques. We calculate light-induced spin polarization that in ferromagnets might give rise to magnetization switching.

2.1 INTRODUCTION

The Faraday Effect (FE) describes the rotation of the plane of linear polarized light when passing through a ferromagnet with magnetization component parallel to the light vector. It is caused by the difference of phase shifts of transmitted light in the two circular polarization states. The Inverse Faraday Effect (IFE) is the ability of circularly polarized light to exert torques on a magnetization, which can be interpreted in terms of an effective light-induced magnetic field along its wave vector with the magnitude proportional to the light intensity and the sign governed by its helicity. In contrast to other photomagnetic effects neither FE nor IFE involve the absorption of photons, which makes them potentially very fast and therefore interesting *e.g.* for data storage technologies.

The IFE was initially predicted by Pitaevskii [1] and formulated in terms of the dependence of the free energy on a time-dependent electric field. After observation of the IFE by van der Ziel *et al.* [2], Pershan *et al.* [3] developed a microscopic theory explaining the IFE in terms of an optically-induced splitting of degenerate spin levels, followed by thermal relaxation. They found a magnetization $\mathbf{M} = V\lambda_0(2\pi c)^{-1}(I_R - I_L)\mathbf{e}_k$ created by the circularly polarized light propagating in the $\mathbf{e}_k$ direction with the intensity $I_{R(L)}$ of the right (left) handed circularly polarized light component. Here V, λ_0, and c are the Verdet constant, the wavelength and the speed of the light, respectively.

Kimel *et al.* demonstrated the IFE in $DyFeO_3$ by exciting magnetization dynamics with circularly polarized laser pulses on fs time scales [4]. These and subsequent experiments as reviewed in Ref. [5] are not fully explained by the theory presented by Pershan *et al.* [3], because thermal relaxation does not occur at such short time scales. Subsequently, Stanciu *et al.* demonstrated that the perpendicular magnetization of GdFeCo thin films can be switched on subpicosecond time scale [6]. Vahaplar *et al.* [7] modeled the switching process by multiscale calculations of the magnetization dynamics [8] with effective magnetic fields of the order of 20 T. However, the microscopic origin, magnitude and material dependence of these fields remain unexplained.

The reciprocity between FE and IFE is not universally observed [9], and was found by theory to break down in the presence of absorption [10]. Taguchi *et al.* calculated the effect of terahertz electromagnetic radiation on disordered metals with SOI [11]. They found a light induced magnetization, but at the cost of light absorption. This is in contrast to the IFE phenomenology. Recently, strong effective magnetic fields were calculated for magnetic semiconductors that are caused by the spin-selective dynamical Stark effect [12].

The IFE has also been studied in classical plasmas, in which it can be explained in terms of the Ørsted magnetic fields generated by light-induced circulating DC

charge currents [13–16]. Hertel investigated this process for solid state electron plasmas [17]. He derived the eddy currents and associated magnetic fields generated by time-dependent circularly polarized light fields in a conducting metal film modeled as a collisionless electron gas. Both currents and the related magnetic fields are dissipationless and scale to second order in the electric field amplitude of the circularly polarized light, in line with the microscopic theories for the IFE. However, the effects is order of magnitudes too small to explain the light-induced magnetization switching. Yoshino discussed dissipative corrections to Hertel's theory [18].

Here, we pursue the concept that the IFE is caused by light-induced DC currents, but invoke the spin-orbit interaction (SOI) to explain the large effective fields apparently at work. This perspective of the IFE is motivated by the linear current driven intrinsic spin torque in ferromagnets predicted by Manchon and Zhang [19, 20], who demonstrated that a current in the presence of a SOI of the Rashba type produces an effective magnetic field which is perpendicular to both an inversion symmetry-breaking electric field and the current. The non-dissipative currents discussed above can be interpreted as a reactive response to a light-field, or as a ground state property of the system in the presence of the light field, quite analogous to the persistent currents or diamagnetic response to a magnetic field that can be formulated as a ground states in the presence of a vector potential [21]. The quantum mechanical ground state nature of light-induced current in a $1D$ ring has been investigated by Kibis [22]. A possible route to a theory of the IFE would be extending Kibis' approach to Hamiltonians with spin-orbit interactions. Rather than focusing on the quantum mechanics of the generation of charge currents by the light field, we concentrate here on the generation of effective magnetic fields in the presence of circulating charge currents, while using the Hertel's approach to estimate the magnitude of these currents for a given light intensity. This is allowed in the high frequency limit in which the length scale associated with the direct response is much smaller than the geometric confinement or the spin-orbit precession length.

In order to establish the principle we focus here on a non-magnetic system with spin-orbit interaction and in the presence of an electron current bias that is generated by circularly polarized light. For a magnetic sample, such a polarization can exert spin-orbit torques on magnetization. We focus on a simple yet realistic model system in which the spin-orbit interaction Hamiltonian is well known and analytical results can be achieved, *viz.* a one-dimensional (1D/single transverse mode) ring fabricated from a high-mobility two-dimensional electron/hole gas (2DEG/2DHG) with Rashba and Dresselhaus SOI interactions. A SOI in a 2DEG that is linear in the wave vector is known to be quite anomalous, causing *e.g.* a vanishing spin Hall effect by impurity scattering [23]. Here we find that the light-

induced effective fields in 1D rings with linear Rashba or Dresselhaus SOI also vanish, which can be traced to the state independence of the equilibrium spin texture. The holes of a 2DHG close to the valence band edge can also be described by Rashba and Dresselhaus SOI interactions, but with a cubic dependence on the wave vectors [24, 25]. A quantum ring containing a hole gas has an out-of-plane state-dependent spin texture that indeed generates the current-induced spin polarization. In a ferromagnet these would indeed induce torques on a magnetization, thereby confirming our working hypothesis.

The remainder of the chapter is organized as follows. We solve the problem of a ground state in the presence of a given charge current by the method of Lagrange multipliers as explained in Section 2.2. In Section 2.3, we apply this method to a simple case of rings in the absence of SOI, and discuss the difference of the ground state current induced by Lagrangian multiplier and the one induced by the magnetic field in a ring. In Section 5.1, we discuss the different SOIs in more detail. In Sections 2.4.1 and 2.4.2, we address rings consisting of electrons in the presence of a linear Rashba or Dresselhaus SOI, respectively, in which the current-induced spin polarization vanishes. In Sections 2.4.3 and 2.4.4, we continue with a p-doped quantum ring, in which a current-induced polarization is generated by the cubic Dresselhaus or Rashba SOI, respectively. We summarize our conclusions in Section 2.5.

2.2 METHOD OF LAGRANGE MULTIPLIERS

We are interested in the ground state of a conductor in the presence of currents induced by an external perturbation such as the electric field of light. Rather than diagonalizing the Hamiltonian in the presence of the electric field [22], we calculate the ground state for a given persistent current.

According to current-density-functional theory [26] the ground state energy of a system is a functional of the charge current distribution $\mathbf{j}_{\text{ext}}(\mathbf{r})$. The minimum energy of the system under the constraint of a given $\mathbf{j}_{\text{ext}}(\mathbf{r})$ can be found by the method of Lagrange multipliers. Here the Hamiltonian H_0 is augmented by the sum of the product of constraints and Lagrange multipliers that in continuous systems becomes an integral. We limit attention to non-interacting systems with single particle states $|\Psi_i\rangle$ and occupation numbers $f_i \in \{0,1\}$ with $\sum_{i=1}^{\infty} f_i = N$ for a number of N electrons. We may then express the constraint as

$$\sum_i f_i \mathbf{j}_i(\mathbf{R}) = \mathbf{j}_{\text{ext}}(\mathbf{R}), \tag{2.1}$$

where the current operator $\hat{j}(\mathbf{R})$ is defined in terms the expectation value

$$\mathbf{j}_i(\mathbf{R}) = \langle\Psi_i|\hat{j}(\mathbf{R})|\Psi_i\rangle \tag{2.2}$$

$$= \frac{e}{2}\int \Psi_i^*(\mathbf{r})\left[\mathbf{v}\delta(\mathbf{r}-\mathbf{R}) + \delta(\mathbf{r}-\mathbf{R})\mathbf{v}\right]\Psi_i(\mathbf{r})\,d\mathbf{r} \tag{2.3}$$

$$= e\,\mathrm{Re}\,\Psi_i^*(\mathbf{R})\mathbf{v}\Psi_i(\mathbf{R}) \neq e\langle\Psi_i|\mathbf{v}|\Psi_i\rangle \tag{2.4}$$

and $\mathbf{v}$ is the velocity operator. The objective functional under this constraint and the normalization condition $\langle\Psi_i|\Psi_i\rangle = 1$ is

$$F\left[\{\Psi_i\},\mathbf{j}_{\mathrm{ext}}\right] = \sum_i f_i\left(\langle\Psi_i|H_0|\Psi_i\rangle - \varepsilon_i\left(\langle\Psi_i|\Psi_i\rangle - 1\right)\right)$$
$$+\int \mathbf{A}(\mathbf{R})\cdot\left(\mathbf{j}_{\mathrm{ext}}(\mathbf{R}) - \sum_i f_i\mathbf{j}_i(\mathbf{R})\right)d\mathbf{R}\,. \tag{2.5}$$

Here $\mathbf{A}$ is the Lagrange multiplier functional. Minimizing F, i.e. $\delta F/\delta\Psi_i^* = 0$, leads to the Schrödinger equation with the eigenfunctions $|\Psi_i\rangle$ corresponding to the Hamiltonian

$$H = H_0 - \int \mathbf{A}(\mathbf{R})\cdot\hat{j}(\mathbf{R})\,d\mathbf{R}. \tag{2.6}$$

In the absence of spin-orbit interactions $\mathbf{j}_i = (e\hbar/m)\,\mathrm{Im}\,\Psi_i^*\nabla\Psi_i$ and

$$H(\mathbf{r},\mathbf{p}) \to H_0\left(\mathbf{r},\mathbf{p} - e\mathbf{A}(\mathbf{r})\right) - \frac{\hbar^2 e^2\mathbf{A}^2(\mathbf{r})}{2m} \tag{2.7}$$

When the objective current density $\mathbf{j}_{\mathrm{ext}}(\mathbf{r})$ is constant in space and time, the Lagrange function $\mathbf{A}(\mathbf{r})$ a vector potential corresponding to a constant magnetic field and the implementation of the charge current constraint is equivalent to a gauge transformation. We note the close relation with current density functional theory [26], in which effective vector and scalar potentials are introduced to construct energy functionals of charge and current densities. Finally, we observe that the time derivative of the vector potential is an electric field, $\mathbf{E} = -d\mathbf{A}/dt$. A harmonic AC electric field therefore corresponds to a vector potential in the same direction with the amplitude $A_\omega = -iE_\omega/\omega$ in frequency space. The effect of a finite A_ω in the DC limit $\omega \to 0$ is then equivalent to the transport response to an electric field that remains finite in a ballistic system. Alternatively, we can associate the vector potential to an applied magnetic field inducing a persistent ground state current, although it should be kept in mind that when the current is generated by other means, our magnetic field is a fictitious one.

2.3 SINGLE MODE QUANTUM RINGS WITHOUT SOI

In the following we focus on quantum rings fabricated from a 2DE(H)G in which the charge carriers are confined normal to the plane by a potential $V(z)$ and in the radial direction by an axially symmetric confining potential $U(r)$ centered at an effective radius $r = a$, but free to move along the azimuthal direction along the unit vector $\mathbf{e}_\varphi$. In the envelope function approximation with effective mass m for electrons or (heavy) holes:

$$H_0 = \frac{p_x^2 + p_y^2}{2m} + V(z) + U(r), \tag{2.8}$$

where $p_{x(y)}$ is the $x(y)$-component of the momentum operator. The eigenstates are then separable as $\Psi_{nlk}(r,\varphi,z) = \psi_n(\varphi) R_l(r) Z_k(z)$ normalized as $\int \left|\psi_n(\varphi)\right|^2 d\varphi = \int r|R_l(r)|^2 dr = \int |Z_k(z)|^2 dz = 1$. To simplify the problem further, we assume that the confinement is strong enough such that only the lowest subbands ($k = l = 0$) are occupied, which makes the system effectively one-dimensional (1D) in azimuthal direction. The eigenstates of Eq. (2.8) are

$$\psi_n(\varphi) = \frac{1}{\sqrt{2\pi}} e^{in\varphi} \tag{2.9}$$

with energies $\varepsilon_n = \hbar^2 n^2 / \left(2ma^2\right) + \varepsilon_0$, where ε_0 is the confinement energy of $R_0(r)$ $Z_0(z)$.

We wish to model the system in the presence of a constant persistent current. In the absence of SOI, the current operator along the ring is defined by its expectation value

$$\mathbf{j}_n^\varphi(r,z) = j_n^\varphi(r,z)\,\mathbf{e}_\varphi \tag{2.10}$$

$$= \mathbf{e}_\varphi \frac{e\hbar}{mr} |R_0(r)|^2 |Z_0(z)|^2 \operatorname{Im}\psi_n(\varphi) \frac{\partial}{\partial\varphi}\psi_n(\varphi) \tag{2.11}$$

where we used $v_\varphi = -i\hbar/(mr)\partial/\partial\varphi$, and the total current in the wire is

$$I^\varphi = \int\int dz dr\, j^\varphi(r,z) \tag{2.12}$$

$$= -\frac{e\hbar}{m} \operatorname{Im}\psi_n(\varphi) \frac{\partial}{\partial\varphi}\psi_n(\varphi) \int dr \frac{1}{r} |R_0(r)|^2 \int dz |Z_0(z)|^2 \tag{2.13}$$

$$= -\frac{e\hbar}{ma^2} \sum_n f_n \operatorname{Im}\psi_n(\varphi) \frac{\partial}{\partial\varphi}\psi_n(\varphi). \tag{2.14}$$

where $e > 0$, and we used $\int dr\, |R_0(r)|^2 / r = 1/a^2$ assuming a Gaussian R_0 [27]. The current operator Eq. (2.3) is diagonal in the basis of the states in Eq. (2.9), which

are therefore also eigenfunctions of the current carrying system. The total current density in the ring then reads:

$$I^{\varphi} = -\frac{e\hbar}{2\pi m a^2}\sum_n f_n n \tag{2.15}$$

The projected Hamiltonian $\langle Z_0 R_0 | H_0 | Z_0 R_0 \rangle$ in the presence of the Lagrange multiplier term $-A^{\varphi}\hat{I}^{\varphi}$ (parameterizing the vector potential as $A^{\varphi} = 2\pi\hbar n_\lambda / e$ where n_λ is dimensionless) is diagonal in the basis Eq. (2.9) with energies

$$\varepsilon_n = E_a n^2 - \frac{2\pi\hbar n_\lambda}{e}\frac{e\hbar}{2\pi m a^2} n + \varepsilon_0 \tag{2.16}$$

$$= E_a (n - n_\lambda)^2 + \tilde{\varepsilon}_0. \tag{2.17}$$

where $E_a = \hbar^2/(2ma^2)$ and $\tilde{\varepsilon}_0 = \varepsilon_0 - E_a n_\lambda^2$. At zero temperature $f_n = \Theta(\varepsilon_n - \epsilon_F + \tilde{\varepsilon}_0)$, where ϵ_F is the Fermi energy and Θ the step function, therefore

$$I^{\varphi} \approx \frac{2e\hbar}{\pi m a^2} n_\lambda n_F, \tag{2.18}$$

where $n_F = \sqrt{(\epsilon_F - \tilde{\varepsilon}_0)/E_a}$. We assume that the number of electrons is constant under variation of n_λ, which implies that $\tilde{\varepsilon}_0$ may be set to zero. The current constraint $I^{\varphi} = I$ determines the effective vector potential

$$n_\lambda = \frac{\pi m a^2}{2e\hbar n_F} I = \frac{\pi}{4e}\frac{\hbar}{E_a}\frac{I}{n_F}. \tag{2.19}$$

such that the spectrum (2.16) is fully determined. The current is optimally accommodated by rigidly shifting the distribution function proportional to the applied current.

A real magnetic field B_{ext} also generates persistent currents [21]. There is a difference, however. The energies of a quantum ring in the presence of a real magnetic flux $\Phi = \pi a^2 B_{\text{ext}}$ read

$$E_n = E_a\left(n - \frac{\Phi}{\Phi_0}\right)^2 \tag{2.20}$$

where $\Phi_0 = e/h$ is the flux quantum and we can identify $n_\lambda = \Phi/\Phi_0$. The total energy in the presence of a diamagnetic persistent current is

$$E' = \sum_{n_F^{(-)}}^{n_F^{(+)}} E_n \tag{2.21}$$

where $n_F^{(\pm)} = \left\lfloor \pm\sqrt{2ma^2(\epsilon_F-\epsilon_0)}/\hbar + \Phi/\Phi_0 \right\rfloor$ is the largest integer smaller of equal $\sqrt{2ma^2(\epsilon_F-\epsilon_0)}/\hbar$. $E'(\Phi)$ is periodic, since the quantum numbers of the highest occupied states jump by ±1 when two states cross the Fermi energy. The current

$$I^{\varphi\prime} = \frac{\partial}{\partial\Phi}E' = -\Phi_0 E_a \sum_{n_F^{(-)}}^{n_F^{(+)}} \left(n - \frac{\Phi}{\Phi_0}\right). \tag{2.22}$$

oscillates as a function of Φ with a maximum

$$\left|I^{\varphi\prime}\right|_{\max} = NE_a\Phi_0 = 1.5\times10^{-10}\,\mathrm{A}\,\frac{N}{1000}\left(\frac{0.1\,\mu\mathrm{m}}{a}\right)^2, \tag{2.23}$$

where $N = 2\left(n_F^{(+)} + n_F^{(-)}\right)$ is the total number of electrons.

The Lagrange multiplier on the other hand contributes the additional term $\hbar^2 n_\lambda^2/\left(2ma^2\right)$, see Eq. (2.16), which modifies the expressions to

$$\frac{E_n}{E_a} = (n-n_\lambda)^2 - n_\lambda^2 = n(n-2n_\lambda) \tag{2.24}$$

$$I^\varphi = \Phi_0\frac{\partial E}{\partial n_\lambda} = -E_a\Phi_0 \sum_{-n_F-n_\lambda}^{n_F-n_\lambda} n. \tag{2.25}$$

which agrees with Eq. (2.15).

The current is finite for any $n_\lambda \neq 0$ (except when $N=1$ and $n=0$ or $2n_\lambda$). Thus, contrary to the diamagnetic current induced by a real magnetic field, the Lagrangian method generates unbound currents. However, due to the discreteness of the energy levels the currents are quantized. see Fig. 2.1. In the following we work with a large number of electrons such that the currents are quasi-continuous.

Nevertheless, if it is taken into account that there is a maximum for magnetic-field induced currents, our method also predicts spin polarizations generated by diamagnetic currents and correspondingly enhanced paramagnetic susceptibility of quantum rings. It is instructive to compare the magnitudes of the Lagrange multipliers with the corresponding magnetic fields. With $eA^\varphi = 2\pi n_\lambda = eB_{\mathrm{ext}}a^2/(2\hbar)$

$$B_{\mathrm{ext}} = \left(\frac{\pi\hbar}{ea}\right)^2 \frac{1}{E_a}\frac{I}{n_0} = \left(\frac{\pi}{e}\right)^2 \frac{2m}{n_0} I \tag{2.26}$$

$$\approx 0.1\,\mathrm{mT}\,\frac{1000}{n_0}\,\frac{I}{\mathrm{nA}}, \tag{2.27}$$

which does not depend on the size of the ring.

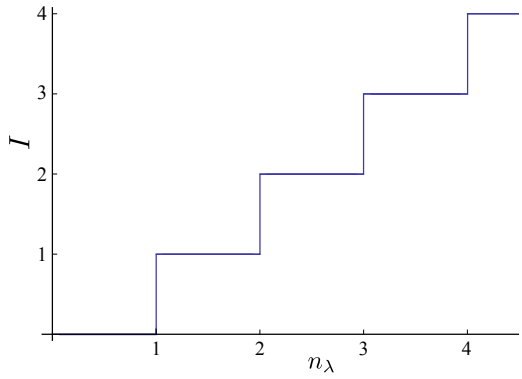

FIGURE 2.1: Current versus n_λ. The current axis is scaled in units of $I_0 = 2e\hbar n_F/(\pi m a^2)$.

2.4 SINGLE MODE RINGS IN THE PRESENCE OF SOI

In the weakly relativistic limit a particle spin experiences SOI, i.e. an effective magnetic field that scales with the particle velocity. It requires inversion symmetry breaking induced either by space charges or asymmetric heterostructures or by a unit cell without inversion symmetry, as is the case for the zinkblende structure. The Rashba SOI in the quasi-two-dimensional electron gas (2DEG) is a simple realization of the former [28, 29], while the Dresselhaus [30] SOI represents the latter type. For a 2DEG in the x, y-plane the Hamiltonian (2.8) is then augmented by

$$H_{SO}^{e} = \frac{\alpha_e}{\hbar}\left(\sigma_y p_x - \sigma_x p_y\right) + \frac{\beta_e}{\hbar}\left(\sigma_x p_x - \sigma_y p_y\right), \tag{2.28}$$

where $\sigma_{x(y)}$ are the $x(y)$-components of the momentum operator for electrons and vector of Pauli matrices, respectively. In a two-dimensional hole gas (2DHG), on the other hand [31–33],

$$H_{SO}^{h} = \left(i\frac{\alpha_h}{\hbar^3}p_-^3 + \frac{\beta_h}{\hbar^3}p_- p_+ p_-\right)\sigma_+ + \text{h.c.}, \tag{2.29}$$

and $O_\pm = O_x \pm iO_y$, where $\mathbf{O} \equiv \mathbf{p}, \boldsymbol{\sigma}$, are the momentum operator and Pauli spin matrix vectors, respectively. $\alpha_{e(h)}$ and $\beta_{e(h)}$ parameterize the linear (cubic) Rashba and linear (cubic) Dresselhaus SOI. The canonical velocity operators are modified by the spin-orbit interaction since they do not commute with the Hamiltonian.

Dropping the index for electrons and holes

$$\mathbf{v} = \dot{\mathbf{r}} = \frac{1}{i\hbar}[\mathbf{r}, H] \tag{2.30}$$

$$= \mathbf{v}_0 + \mathbf{v}_{SO} = \frac{\hbar}{im}\boldsymbol{\nabla} + \frac{1}{i\hbar}[\mathbf{r}, H_{SO}]\ . \tag{2.31}$$

where $\mathbf{v}_{SO}$ is the anomalous velocity. The current operators are modified analogously.

As before, we add an axially symmetric confinement potential to the 2DE(H)G and consider the electric quantum confinement (1D) limit. Here, we separately discuss electrons and holes in such quantum rings in the presence of a circular current, and calculate the current-induced spin polarization in each system.

2.4.1 ELECTRONS WITH RASHBA SOI

For electrons in the 1D quantum ring the projection of the full Hamiltonian H onto the azimuthal subspace, leads to [27]

$$\begin{aligned} H(\varphi) = \langle Z_0 R_0 | H_0 + H_{SO} | Z_0 R_0 \rangle = &-\frac{\hbar^2}{2ma^2}\partial_\varphi^2 \\ &- i\frac{\alpha}{a}\left\{(\sigma_x\cos\varphi + \sigma_y\sin\varphi)\partial_\varphi + \frac{1}{2}(\sigma_y\cos\varphi - \sigma_x\sin\varphi)\right\} \\ &- i\frac{\beta}{a}\left\{(\sigma_x\sin\varphi + \sigma_y\cos\varphi)\partial_\varphi + \frac{1}{2}(\sigma_x\cos\varphi - \sigma_y\sin\varphi)\right\}. \end{aligned} \tag{2.32}$$

Let us first focus on the Rashba spin-orbit interaction, i.e. $\beta = 0$. The eigenstates of the system are

$$\psi^R_{n+}(\varphi) = \frac{1}{\sqrt{2\pi}} e^{in\varphi} \begin{pmatrix} \cos\frac{\theta_R}{2} \\ \sin\frac{\theta_R}{2} e^{i\varphi} \end{pmatrix}; \tag{2.33}$$

$$\psi^R_{n-}(\varphi) = \frac{1}{\sqrt{2\pi}} e^{in\varphi} \begin{pmatrix} -\sin\frac{\theta_R}{2} \\ \cos\frac{\theta_R}{2} e^{i\varphi} \end{pmatrix}, \tag{2.34}$$

where n is an integer, with energies

$$\frac{E_{n\sigma}}{E_a} = \left(n + \frac{1}{2}\right)^2 + \sigma\left(n + \frac{1}{2}\right)\sec\theta_R + \frac{1}{4}, \tag{2.35}$$

where $\tan\theta_R = 2ma\alpha/\hbar^2$, and the velocity operator in this system reads

$$v_\varphi = -\frac{i\hbar}{ma}\partial_\varphi + \frac{\alpha}{\hbar}\sigma_r. \tag{2.36}$$

and current is $\langle I^{\varphi}\rangle = \sum_{n\sigma} f_{n\sigma} I^{\varphi}_{n\sigma} = I$. The current operator is diagonal in the $n\sigma$ basis (Eqs. (2.33-2.34), but acquires a spin-dependence

$$I^{\varphi}_{n\sigma} = -\frac{e\hbar}{2\pi m a^2} n - \sigma \frac{e\alpha}{2\pi\hbar a}\sin\theta - \frac{e\hbar}{2\pi m a^2}\left(\delta_{\sigma,+1}\cos^2\frac{\theta}{2} + \delta_{\sigma,-1}\sin^2\frac{\theta}{2}\right), \tag{2.37}$$

The projected Hamiltonian in the presence of the Lagrange multiplier term (parameterizing the vector potential as $A^{\varphi} = \hbar n_\lambda / e$ where n_λ is dimensionless) is diagonal in the basis Eq. (2.9) with energies

$$\begin{aligned}\frac{E_{n\sigma}}{E_a} &= \left(n+\frac{1}{2}\right)^2 + \sigma\,(n+1/2)\sec\theta_R + \frac{1}{4} \\ &\quad - \frac{2\pi\hbar n_\lambda}{e}\frac{2ma^2}{\hbar^2}\left[\frac{e\hbar}{2\pi m a^2} n + \sigma\frac{e\alpha}{2\pi\hbar a}\sin\theta_R \right. \\ &\quad \left. + \frac{e\hbar}{2\pi m a^2}\left(\delta_{\sigma,+1}\cos^2\frac{\theta_R}{2} + \delta_{\sigma,-1}\sin^2\frac{\theta_R}{2}\right)\right] \qquad (2.38) \\ &= \left(n - n_\lambda + \frac{1}{2}\right)^2 + \sigma\left(n - n_\lambda + \frac{1}{2}\right)\sec\theta_R + \frac{1}{4} - n_\lambda^2 \qquad (2.39)\end{aligned}$$

At zero temperature:

$$I = \sum_{n\sigma} f_{n\sigma} I^{\varphi}_{n\sigma} = \sum_{\sigma} \sum_{-n_r + n_{\lambda\lambda} - \sigma\sec\theta_R - 1/2}^{n_r + n_{\lambda\lambda} - \sigma\sec\theta_R - 1/2} I^{\varphi}_{n\sigma} = \frac{2e\hbar}{\pi m a^2} n_\lambda n_r \tag{2.40}$$

where $n_r \equiv \sqrt{\epsilon_F / E_a + \sec^2\theta_R/4}$ and we substituted Eq. (2.37). The leading term is therefore the same as in the absence of spin-orbit interaction:

$$n_\lambda = \frac{\pi}{4e}\frac{\hbar}{E_a}\frac{I}{n_r}. \tag{2.41}$$

Since the system is not magnetic, the system is not spin polarized at equilibrium. The spin polarization of the current-carrying ground state reads

$$\langle\sigma_z\rangle^R_I = \sum_{n\sigma}\left\langle\psi^R_{n\sigma}\left|\sigma_z\right|\psi^R_{n\sigma}\right\rangle_I = \sum_{n\sigma} f_{n\sigma}\sigma\cos\theta_R.$$

and $\langle\sigma_y\rangle^R_I = \langle\sigma_x\rangle^R_I = 0$. In the absence of current the energy bands are equally filled for both spins in the negative and positive directions, and we do not have unpaired

electrons. Thus:

$$\langle\sigma_z\rangle_{I=0}^{R} = \cos\theta_R \sum_{n\sigma} \sigma\Theta(\epsilon_F - E_{n\sigma}) \tag{2.42}$$

$$= \cos\theta_R \sum_{\sigma} \sum_{-n_r+n_\lambda-\sigma\sec\theta_R-1/2}^{n_r+n_\lambda-\sigma\sec\theta_R-1/2} \sigma = 0. \tag{2.43}$$

In the presence of the current bias the electron distribution is shifted in reciprocal space around the Fermi level by n_λ. The spinors Eqs. (2.33, 2.34) that determine the spin texture do not depend on n. Furthermore, the relative occupation of the two spin bands also remains the same. Therefore, an induced current does not generate a spin polarization and $\langle\sigma_z\rangle_I^R = 0$ for all current levels. The conclusion that there is no current-induced spin accumulation in the Rashba systems holds also for 1D wires. The vanishing of the spin accumulation is caused by the compensating effect of the two subbands. This can be suppressed when a gap is induced at $k = 0$ by a Zeeman field or exchange interaction and a Fermi energy that is tuned to fall into this gap [34]. We also note that the linear current-induced spin accumulation does not vanish in the two-dimensional electron gas either [35].

2.4.2 ELECTRONS WITH DRESSELHAUS SOI

A similar situation arises for a ring with only a linear Dresselhaus interaction, i.e. $\alpha = 0$ in Eq. (2.32). Its eigenstates are [36]

$$\psi_{n+}^{D}(\varphi) = \frac{1}{\sqrt{2\pi}} e^{in\varphi} \begin{pmatrix} -\sin\frac{\theta_D}{2} \\ i\cos\frac{\theta_D}{2} e^{-i\varphi} \end{pmatrix}; \tag{2.44}$$

$$\psi_{n-}^{D}(\varphi) = \frac{1}{\sqrt{2\pi}} e^{in\varphi} \begin{pmatrix} \cos\frac{\theta_D}{2} \\ i\sin\frac{\theta_D}{2} e^{-i\varphi} \end{pmatrix}, \tag{2.45}$$

with energies identical to those for the Rashba ring

$$\frac{E_{n\sigma}}{E_a} = \left(n+\frac{1}{2}\right)^2 + \sigma\left(n+\frac{1}{2}\right)\sec\theta_D + \frac{1}{4}, \tag{2.46}$$

but $\tan\theta_D = 2ma\beta/\hbar^2$. Thus, the spin texture does not depend on the angular momentum. This means that shifting a distribution function rigidly does not change the balance of the spin states, and as in the Rashba case, there is no current-induced spin polarization.

2.4.3 HOLES WITH DRESSELHAUS SOI

Stepanenko *et al.*[37] derived an effective low energy Hamiltonian for heavy holes from the Luttinger Hamiltonian that includes Dresselhaus and Rashba like SOI that

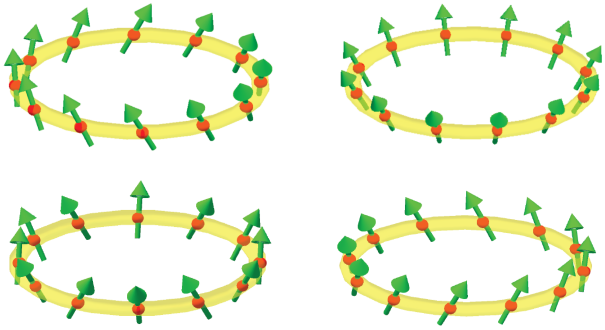

FIGURE 2.2: Top: Electrons spin texture in the presence of linear Dresselhaus (left) or Rashba (right) interaction. The angle of the spin with the ring in this case only depends to the SO coupling strength and not the angular momentum.
Bottom: The hole spin texture in the presence of cubic Dresselhaus (left) or Rashba (right) spin-orbit interaction. The direction the spins in both cases dependents on the angular velocity of the holes and on the SO coupling strength.
Here, the particles orbit counterclockwise. The clockwise movement induces spin texture which is mirrored with respect to the plane containing the ring.

are cubic in the angular momenta. Simple analytical solutions were obtained in two limits, representing the Dresselhaus-only interaction ($\alpha_h = 0$) and the Rashba-only SOI ($\beta_h = 0$). The spin textures in these two limits are shown in Fig. 2.2. In contrast to the electron case, both spinors include terms quadratic in the angular momentum. Here, we show that these do generate a current-induced spin accumulation.

The heavy-hole Hamiltonian for a 1D ring with Dresselhaus SOI is [37]

$$\begin{aligned} H_0^{cD} = &-\frac{\hbar^2}{2m_{hh}a^2}\partial_\varphi^2 \\ &+ \beta_h e^{i\varphi}\left(G_0 + G_1\partial_\varphi + G_2\partial_\varphi^2 + G_3\partial_\varphi^3\right)\sigma_- \\ &+ \beta_h e^{-i\varphi}\left(G_0 - G_1\partial_\varphi + G_2\partial_\varphi^2 - G_3\partial_\varphi^3\right)\sigma_+ , \end{aligned} \tag{2.47}$$

where $G_0 = i(R_0 + R_1 - R_2)$, $G_1 = -(R_1 + R_2)$, $G_2 = i(R_2 - 2R_3)$, and $G_3 = -R_3$, and the coefficients $R_j = \left\langle r^{-j}\partial_r^{3-j}\right\rangle_{\text{radial}}$ depend on the ground state radial confinement wave function. For a ring with radius a and width w, $R_2 = R_3/2 = 1/(2a^3)$ and $R_1 = -2/3R_0 = -1/(aw^2)$[38]. $m_{hh} = m_0/(\gamma_1 + \tilde{\gamma})$, where $\tilde{\gamma} = \gamma_2$ for the [001] ($\tilde{\gamma} = \gamma_3$ for [111]) growth direction and γ_i are the standard Luttinger parameters for the

valence band of III-V semiconductors. The eigenfunctions of the system are

$$\psi^{cD}_{l,+} = \frac{1}{\sqrt{2\pi}} e^{il\varphi} \begin{pmatrix} i\cos\frac{\theta^{cD}(l)}{2} e^{-i\varphi/2} \\ -\sin\frac{\theta^{cD}(l)}{2} e^{i\varphi/2} \end{pmatrix}; \tag{2.48}$$

$$\psi^{cD}_{l,-} = \frac{1}{\sqrt{2\pi}} e^{il\varphi} \begin{pmatrix} i\sin\frac{\theta^{cD}(l)}{2} e^{-i\varphi/2} \\ \cos\frac{\theta^{cD}(l)}{2} e^{i\varphi/2} \end{pmatrix}, \tag{2.49}$$

where $l = n + 1/2$, and the texture angle $\theta^{cD}(l)$ is

$$\theta^{cD}(l) = \tan^{-1}\left[\frac{2m_{hh}\beta_h}{\hbar^2 R_3^{2/3}}\left(\frac{2}{3}R_0 + \left(l^2 - \frac{5}{4}\right)R_3\right)\right], \tag{2.50}$$

with energies

$$E_{l\sigma} = E_a^h\left(l^2 + \frac{1}{4} + \sigma l \sec\theta^{cD}(l)\right),$$

where $E_a^h = \hbar^2/(2m_{hh}a^2)$. In terms of the velocity operator

$$\begin{aligned} v_\varphi = &-\frac{i\hbar}{m_{hh}a}\partial_\varphi + \frac{ia\beta_h}{\hbar}e^{i\varphi}\left(G_1 + 2G_2\partial_\varphi + 3G_3\partial_\varphi^2\right)\sigma_- \\ &+ \frac{ia\beta_h}{\hbar}e^{-i\varphi}\left(-G_1 + 2G_2\partial_\varphi - 3G_3\partial_\varphi^2\right)\sigma_+, \end{aligned} \tag{2.51}$$

the current operator reads

$$\hat{I}^{\varphi}_{l\sigma\sigma'} = \frac{e}{a}\,\mathrm{Re}\,\psi^\dagger_{l\sigma}(\varphi)\, v_\varphi \psi_{l\sigma'}(\varphi). \tag{2.52}$$

Both the Hamiltonian and current operators are diagonal in the orbital angular momentum, which allows us to introduce 2×2 operators in spin space calculation of the expectation values in position space:

$$\begin{aligned} -\frac{\hat{I}^{\varphi}_l}{e} =& 2E_a^h(l_-\sigma_1 + l_+\sigma_2) \\ &+ \frac{\beta_h}{\hbar}\left(G_1 + 2iG_2 l_- + 3G_3 l_-^2\right)\sigma_- \\ &+ \frac{\beta_h}{\hbar}\left(G_1 - 2iG_2 l_+ + 3G_3 l_+^2\right)\sigma_+, \end{aligned} \tag{2.53}$$

where σ_1, and σ_2 are 2×2 matrices with all elements zero except for the first and second diagonal one, respectively, and $l_\pm = l \pm 1/2$. Thus, the Hamiltonian H^{cD} +

$\lambda \langle I^{\varphi} \rangle$ in spin space reads

$$\begin{aligned} H_l^{cD} = & E_a^h \left[\left(l_-^2 - n_\lambda l_- \right) \sigma_1 + \left(l_+^2 - n_\lambda l^+ \right) \sigma_2 \right] \\ & - \beta_h \left(G_0 + G_1 l_- + G_2 l_-^2 + G_3 l_-^3 \right) \sigma_- \\ & - \beta_h \left(G_0 - G_1 l_+ + G_2 l_+^2 - G_3 l_+^3 \right) \sigma_+ \\ & + n_\lambda \beta_h \left(G_1 + 2G_2 l_- + 3G_3 l_-^2 \right) \sigma_- \\ & + n_\lambda \beta_h \left(-G_1 + 2G_2 l_+ - 3G_3 l_+^2 \right) \sigma_+ \, . \end{aligned} \tag{2.54}$$

The eigenstates in the presence of a current now read

$$\psi^{cD}_{(l,n_\lambda),+} = \frac{1}{\sqrt{2\pi}} e^{il\varphi} \begin{pmatrix} \cos \frac{\theta^{cD}(l,n_\lambda)}{2} e^{-(i/2)(\varphi+\pi/2)} \\ \sin \frac{\theta^{cD}(l,n_\lambda)}{2} e^{(i/2)(\varphi+\pi/2)} \end{pmatrix}; \tag{2.55}$$

$$\psi^{cD}_{(l,n_\lambda),-} = \frac{1}{\sqrt{2\pi}} e^{il\varphi} \begin{pmatrix} -\sin \frac{\theta^{cD}(l,n_\lambda)}{2} e^{-(i/2)(\varphi+\pi/2)} \\ \cos \frac{\theta^{cD}(l,n_\lambda)}{2} e^{(i/2)(\varphi+\pi/2)} \end{pmatrix}, \tag{2.56}$$

with spin texture

$$\begin{aligned} \theta^{cD}(l,n_\lambda) = & \arctan \\ & \left[\frac{2m_{hh}\beta_h}{\hbar^2 R_3^{2/3}} \left(\frac{2}{3} R_0 + \left(l^2 - \frac{5}{4} - 3n_\lambda^2 + 2\frac{n_\lambda^3}{l} \right) R_3 \right) \right] , \end{aligned} \tag{2.57}$$

and energies

$$E_{l\sigma} = E_a \left((l - n_\lambda)^2 + \frac{1}{4} + \sigma \frac{(l-n_\lambda)}{\cos\theta^{cD}\left((l-n_\lambda), n_\lambda\right)} \right).$$

We can obtain n_λ from the current constraint by noting that the state $l\sigma$ carries the current

$$\begin{aligned} I^{\varphi}_{l\sigma} = & -\frac{e}{2\pi} \left\{ \frac{\hbar}{ma^2} l - \sigma \frac{\hbar}{2ma^2} \cos\theta^{cD}(l) \right. \\ & \left. + \sigma \frac{\beta_h}{\hbar} \left(G_1 - iG_2 - 3G_3 \left[l^2 + \frac{1}{4} \right] \right) \sin\theta^{cD}(l) \right\}. \end{aligned} \tag{2.58}$$

We now derive analytical expressions for n_λ in the weak spin-orbit coupling limit, i.e. for small θ^{cD}. Subsequently, we also present numerical results for larger SOI strengths. For small angles θ^{cD}, the expectation value of the current reduces

to

$$I_{l\sigma}^{\varphi} \approx -\frac{e}{2\pi}\left\{\frac{\hbar}{ma^2}l - \sigma\frac{\hbar}{2ma^2} + \sigma\frac{\beta_h^2}{\hbar E_a^h}\left(G_1 - iG_2 - 3G_3\left[l^2+\frac{1}{4}\right]\right)\times \left(\frac{2}{3}R_0 + \left(l^2 - \frac{5}{4} - 3n_\lambda^2 + 2\frac{n_\lambda^3}{l}\right)R_3\right)\right\}. \tag{2.59}$$

At zero temperature

$$I_\varphi = \sum_{\sigma=\pm1}\sum_{-n_r+n_\lambda-\sigma/2}^{n_r+n_\lambda-\sigma/2} I_{l\sigma}^{\varphi} = I, \tag{2.60}$$

where $n_r \approx \sqrt{\epsilon_F/E_a^h}$ and ϵ_F is the Fermi energy in the absence of current. Taking $\cos\theta^{cD} \approx 1$ in the boundaries of the summation,

$$n_\lambda \approx \frac{\hbar}{4E_a^h}\frac{\pi}{e}\frac{I}{n_r}\left(1+3\left(\frac{\beta_h R_3 n_r}{E_a}\right)^2\right) \approx \frac{\pi\hbar}{4eE_a^h}\frac{I}{n_r}. \tag{2.61}$$

which in the limit of weak SOI does not depend on β_h. We find that the system is now spin-polarized in the z-direction. With

$$\begin{aligned}\langle\sigma_z\rangle_{l\sigma} &= \langle\psi^{cD}_{(l,n_\lambda)\sigma}|\sigma_z|\psi^{cD}_{(l,n_\lambda)\sigma}\rangle \\ &= \sigma\cos\theta^{cD}(l,n_\lambda) \approx \sigma\left(1-\theta^{cD}(l,n_\lambda)^2\right),\end{aligned} \tag{2.62}$$

the total spin polarization is

$$\begin{aligned}\langle\sigma_z\rangle_I^{cD} &= \sum_{n\sigma}\sigma f_{n\sigma}\cos\theta^{cD}(l,n_\lambda) \\ &\approx \sum_{\sigma=\pm1}\sum_{n=-n_r-n_\lambda+\sigma/2}^{n_r-n_\lambda+\sigma/2}\sigma\left(1-\left(\theta^{cD}(l,n_\lambda)\right)^2\right).\end{aligned} \tag{2.63}$$

This leads to

$$\begin{aligned}\langle\sigma_z\rangle_I^{cD} = \frac{\beta_h^2}{\left(E_a^h\right)^2 a^6}\Bigg\{&-4n_\lambda^3 n_r + 64\frac{n_\lambda^6}{n_r^3}\left(n_\lambda - \frac{1}{2}\right) \\ &+ 2n_r n_\lambda\left(4n_\lambda^2 + 1 + (n_r+1)(2n_r+1)\right) \\ &-\left(\frac{a^2}{w^2} - \left(\frac{5}{4}+3n_\lambda^2\right)\right)\left(-4n_\lambda n_r - 16\frac{n_\lambda^4}{n_r^2}\right)\Bigg\}.\end{aligned} \tag{2.64}$$

To leading order in the current n_λ:

$$\langle\sigma_z\rangle_I^{cD} \to \frac{2\beta_h^2}{\left(E_a^h\right)^2}\frac{n_r n_\lambda}{a^6} \left[1+(n_r+1)(2n_r+1)+\frac{2a^2}{w^2}-\frac{5}{2}\right]. \tag{2.65}$$

The total number of electrons

$$N=\sum_{n\sigma} f_{n\sigma} \approx \sum_{\sigma=\pm 1}\sum_{-n_r+n_\lambda-\sigma/2}^{n_r+n_\lambda-\sigma/2} 1 = 4n_r. \tag{2.66}$$

For $n_r \gg a/w$ the term proportional to $2n_r^3$ dominates and the spin polarization simplifies to

$$\langle\sigma_z\rangle_I^{cD} \approx \frac{4\beta_h^2}{E_a^{h2}} R_3^2 n_r^3 n_\lambda = \frac{\epsilon_F}{E_a^h}\frac{\pi\hbar\beta_h^2}{\left(E_a^h a^2\right)^3}\frac{I}{e}, \tag{2.67}$$

while in the limit of a wide and narrow ring

$$\langle\sigma_z\rangle_I^{cD} \approx \frac{4\beta_h^2}{\left(E_a^h a^2\right)^2}\frac{n_r n_\lambda}{w^2} = \frac{a^2}{w^2}\frac{\pi\hbar\beta_h^2}{\left(E_a^h a^2\right)^3}\frac{I}{e}. \tag{2.68}$$

The spin polarization is in both cases proportional to the current and the squared amplitude of the SOI interaction, which is expected. The proportionality with Fermi energy when $n_r \gg a/w$ reflects the increasing spin texture angle θ^{cD} with energy. This implies a scaling with the squared number of particles as well as the area of the ring. In the opposite limit, we find that the spin polarization increases when tightening the laterally quantized subband, because this increases the SOI matrix elements. For realistic and currently experimentally feasible dimensions, the first approximation seems more appropriate, and thus, we focus on this limit henceforth. One can estimate the the spin polarization in this regime from Eq. (2.67) and the Dresselhaus coupling constant for GaAs [39] $\beta_h = 30$ eVÅ^3 as:

$$\langle\sigma_z\rangle_{I_\varphi}^{cD} \approx 0.2\left(\frac{\epsilon_F}{10\,\mathrm{meV}}\right)\left(\frac{a}{1\mu\mathrm{m}}\right)^2\left(\frac{I}{\mathrm{nA}}\right)\left(\frac{\beta_h}{30\,\mathrm{eV\AA}^3}\right)^2. \tag{2.69}$$

For a better understanding we can derive an equivalent effective magnetic field that would generate the same spin polarization (2.67) in the absence of SOI. Consider the Hamiltonian $H_B = p^2/(2m_{hh})\hat{1} - \Delta\sigma_z$, with the Zeeman energy $\Delta = \hbar e g_h$

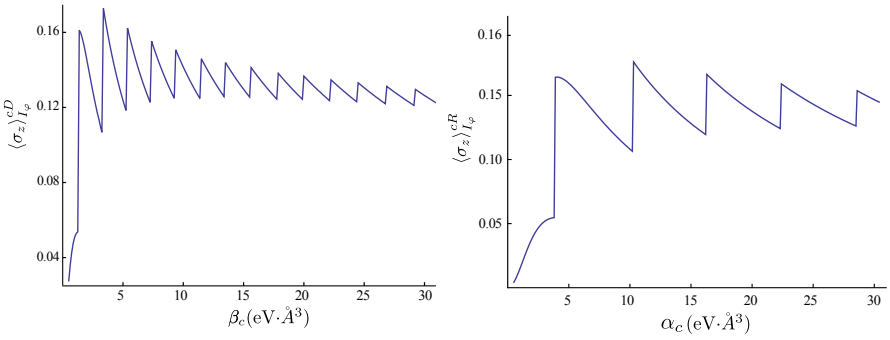

FIGURE 2.3: The current-induced spin polarization of heavy holes in a quantum ring subject to the cubic Dresselhaus (Rashba) SOI, plotted in the left (right) side. The plots are shown as a function of the SOI parameters and $m_{hh} = 0.45m_0$, $N = 1144$, which in the absence of current is equivalent to $\epsilon_F = 10$ meV, a radius of $a = 1$ μm, and width of $w = 50$ nm. Here, we assumed a current of $I = 35$ nA, which is equivalent to circularly polarized light with the frequency of $\omega = 2\times10^{14}\mathrm{s}^{-1}$, and electric field amplitude of $|E_0| = \sqrt{60}\times10^7\mathrm{Vm}^{-1}$, see appendix 2.6.1.

$B_{\mathrm{eff}}/(4m_{hh})$, where g_h is the gyromagnetic ratio. Clearly such a system is spin polarized and in the limit of $\Delta/\epsilon_F \ll 1$:

$$\langle\sigma_z\rangle_Z \approx \frac{\hbar}{2}\frac{eg_hB_{\mathrm{eff}}}{m_{hh}}\frac{1}{\sqrt{E_a^h\epsilon_F}}. \tag{2.70}$$

The $\epsilon_F^{-1/2}$ dependence reflects the 1D density of states that decreases with energy. Comparison of Eqs. (2.70) and (2.67) gives an equivalent effective field of

$$B_{\mathrm{eff}} = \frac{32\pi}{\sqrt{2}}\frac{m_{hh}^{9/2}a}{e\hbar^7 g_h}\epsilon_F^{3/2}\beta_h^2\frac{I}{e},$$

where we assume the g-factor $g_h = -0.5$ [40]. Inserting parameters

$$B_{\mathrm{eff}} = 1.3\left(\frac{\epsilon_F}{10\,\mathrm{meV}}\right)^{3/2}\frac{a}{1\,\mu\mathrm{m}}\frac{I}{\mathrm{nA}}\left(\frac{\beta_h}{30\,\mathrm{eV\mathring{A}}^3}\right)^2\mathrm{mT}, \tag{2.71}$$

we find that a light-induced current of the order of 10 nA (see Appendix) generates an effective field of roughly 10 mT.

Keeping in mind that the current is quantized in steps as function of the system parameters as discussed above, the spin polarization computed numerically

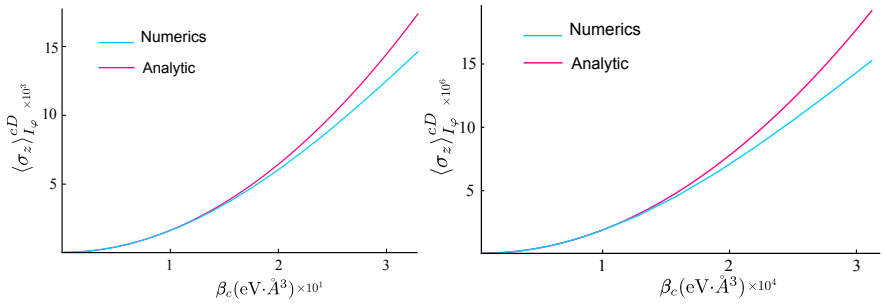

FIGURE 2.4: Comparison of analytical and numerical results in the regime of small Dresselhaus SOI for holes orbiting in a ring. Left: $n_r^2 \gg a^2/w^2$. The parameters are the same as in Fig. 2.3 in this limit. Right: Limit of $n_r^2 \ll a^2/w^2$ with $w = 1$ nm. The other parameters are the same as in Fig. 2.3.

increases linearly with the current level up to $I = 100$ nA, in agreement with the analytic result. The deviations from perturbation theory are quite large for the spin-orbit interaction parameter for GaAs used above. The non-perturbative numerical results for the spin polarization are plotted as a function of SOI strengths for constant electron numbers in Fig. 2.3. We observe that at small β_h the spin polarization increases quadratically with SOI as found in the weak SOI limit above but a saturation at higher values. We also observe saw-tooth like behavior on top of this trend that is caused by a repopulation of states: The SOI induces a spin polarization when the current bias shifts the occupation numbers around the Fermi level. For small but increasing β_h we expect an increasing spin polarization with SOI at constant current since the state dependence of the spin texture increases. At large β_h, on the other hand, the angle of the spin with respect to the z-axis $\theta^{cD}(l, n_\lambda)$ can be large, corresponding to smaller values of the z-component of the spin. Thus, by further increasing β_h, the overall polarization saturates and even slightly decreases. The jumps reflect level crossings with increasing β_h. In these calculations the number of electrons is kept constant. At such a discontinuity an electron vacates a high angular momentum state in favor of a smaller one, which reduces the total spin polarization. In the regime of small SOI, the numerical and analytical results for the current induced spin polarization agree well, see Fig. 2.4.

2.4.4 HOLES WITH RASHBA SOI

The Hamiltonian of holes in the presence of the Dresselhaus SOI is [37]:

$$\begin{aligned} H_0^{cR} =& -\frac{\hbar^2}{2m_{hh}a^2}\partial_\varphi^2 \\ &+ i\alpha_h e^{3i\varphi}\left(F_0 + F_1\partial_\varphi + F_2\partial_\varphi^2 + F_3\partial_\varphi^3\right)\sigma_- \\ &- i\alpha_h e^{-3i\varphi}\left(F_0 - F_1\partial_\varphi + F_2\partial_\varphi^2 - F_3\partial_\varphi^3\right)\sigma_+, \end{aligned} \tag{2.72}$$

where $F_0 = i(R_0 - 3R_1 + 3R_2)$, $F_1 = -3R_1 + 9R_2 - 8R_3$, $F_2 = i(-3R_2 + 6R_3)$, and $F_3 = R_3$. The R_is depend on the radial confinement, and are defined in Section 2.4.3.

The current operator in spin space is:

$$\begin{aligned} \frac{\hat{I}_l^\varphi}{e} =& 2E_a^h\left(l'_-\sigma_1 + l'_+\sigma_2\right) \\ &- \frac{\alpha_h}{\hbar}\left(F_1 + 2iF_2 l'_- + 3F_3 {l'_-}^2\right)\sigma_- \\ &- \frac{\alpha_h}{\hbar}\left(F_1 - 2iF_2 l'_+ + 3F_3 {l'_+}^2\right)\sigma_+, \end{aligned} \tag{2.73}$$

where $l'_+ = l+1$, and $l'_- = l-2$. Thus, the same procedure as before, leads to the Hamiltonian carrying a ground state current. In spin space:

$$\begin{aligned} H^{cR} =& H_0^{cR}(l - n_\lambda)|_{\bar{F}_1 \to F_1, \bar{F}_0 \to F_0} \\ &- 2\alpha_h e^{i\varphi} F_3 n_\lambda^3 \sigma_- + 2\alpha_h F_3 n_\lambda^3 e^{-i\varphi}\sigma_+, \end{aligned} \tag{2.74}$$

where $\bar{F}_1 = F_1 + 3F_3 n_\lambda^2$, and $\bar{F}_0 = F_0 - F_2 n_\lambda^2$, and we neglect a constant shift of $-\hbar^2 n_\lambda^2/(2m_{hh}a^2)$ in the Hamiltonian. Eigenstates are now:

$$\psi^{cR}_{(l,n_\lambda),+} = e^{il\varphi}\begin{pmatrix} \cos\frac{\theta^{cR}(l,n_\lambda)}{2}e^{-(3i/2)(\varphi)} \\ \sin\frac{\theta^{cR}(l,n_\lambda)}{2}e^{(3i/2)(\varphi)} \end{pmatrix}; \tag{2.75}$$

$$\psi^{cR}_{(l,n_\lambda),-} = e^{il\varphi}\begin{pmatrix} -\sin\frac{\theta^{cR}(l,n_\lambda)}{2}e^{-(3i/2)(\varphi)} \\ \cos\frac{\theta^{cR}(l,n_\lambda)}{2}e^{(3i/2)(\varphi)} \end{pmatrix}, \tag{2.76}$$

where the texture angle $\theta^{cR}(l,n_\lambda)$ is

$$\theta^{cR}(l,n_\lambda) = \tan^{-1}\left[\tilde{\alpha}_h\left(\frac{2}{3}R_0 + \left(\frac{13}{12} - \frac{1}{3}l^2 + n_\lambda^2 - \frac{2}{3}\frac{n_\lambda^3}{l}\right)R_3\right)\right], \tag{2.77}$$

with $\tilde{\alpha}_h = 2m_{hh}\alpha_h/(\hbar^2 R_3^{2/3})$ and energies

$$E_{k,\sigma} = E_a\left((l-n_\lambda)^2 + \frac{1}{4} + \sigma\frac{(l-n_\lambda)}{\cos\left[\theta^{cR}\left((l-n_\lambda),n_\lambda\right)\right]}\right).$$

For small θ^{cR} we find, as above,

$$n_\lambda \approx -\frac{\hbar}{4E_a^h}\frac{\pi}{e}\frac{I}{n_r}. \tag{2.78}$$

and a spin polarization in the z-direction:

$$\langle\sigma_z\rangle_{I_\varphi}^{cR} \approx -\frac{\epsilon_F}{E_a^h}\frac{\pi\hbar\alpha_h^2}{9\left(E_a^h a^2\right)^3}\frac{I}{e}. \tag{2.79}$$

very similar to the Dresselhaus limit, but with a prefactor 1/9. Therefore above discussions for the small SOI limit hold for the cubic Rasba Hamiltonian as well. In the lower part of Fig. 2.3, we plotted numerical results for larger values of α_h. The values of the SO coupling used in this figure can be experimentally achieved (e.g. Ref. [42]), by an external gate voltage.

2.5 CONCLUSION

The IFE allows in principle ultrafast and non-dissipative actuation and eventual switching of magnetization. We investigated the impact of the SOI on this non-absorbing 'Opto-Spin' phenomena. We provided a proof of principle for a mechanism that is based on the current-induced generation of a spin polarization that would generate torques in a magnetic sample. The current bias can be generated by the Lagrange multiplier method inspired by current-density functional theory. For electrons moving in quantum rings in the presence of Rashba and Dresselhaus SOIs, the effect vanishes. It becomes non-zero only when the Kramer's degeneracy is broken by an exchange potential or applied magnetic field, but the effects are still small [34]. On the other hand, holes in a ring with cubic Dresselhaus and Rashba SOI display a spin polarization under a current bias. This polarization is a competition between two effects. On one hand, with increasing SOI the band splitting increases, which amplifies the magnitude of the polarization. Simultaneously, however, the z-component of the spin of holes with energies near to the Fermi level decreases, and therefore the net polarization decreases. These two might enhance the effect rather than canceling each other when the spin texture would push the spin out of the plane. This can be achieved in a ring with an asymmetric potential in the radial direction, such as a thin slice of GaAs|p-doped GaAlAs core/shell

nanowire. The second Rashba SOI would pull the spin toward the z-direction and lead to monotonic increase of current-induced spin polarization with SOI.

Induced polarization in the z-direction, calculated in this section, could be either parallel or anti-parallel to the z-axis depending on the direction of the current. This is consistent with the IFE in which the effective magnetic field changes sign with the helicity of light. Here, we focused on the spin polarization induced by current in a material which is nonmagnetic. This spin polarization can be measured directly by pump and Kerr rotation probe measurements. GaMnAs in the ferromagnetic state is a hole conductor. Here the current-induced spin polarization would induce torques on the magnetic order parameter, eventually causing magnetization switching. The spin-dependent dynamic Stark effect also induces torques by circularly polarized light [12]. The two processes are independent and should be added. They can be distinguished by tuning the light frequency close to the energy gap, where the dynamic Stark effect is resonantly enhanced.

The currents generated by non-resonant light are persistent, analogous to the diamagnetic currents in conducting rings induced by dc magnetic fields [21]. While this issue has not been central to our study, our results imply that the spin-orbit interaction can induce large paramagnetic corrections to the diamagnetic response. Cantilever-based torsional magnetometers with integrated mesoscopic rings allow very sensitive measurements of magnetic susceptibilities [43]. We suggest that quantum ring arrays made from 2DHGs would be interesting subjects for such experiments.

2.6 APPENDIX

2.6.1 LIGHT INDUCED CURRENTS

Here we show how to use the collisionless plasma model by Hertel [17] to obtain the light-induced current in a quantum ring. This model can be used for the present system in the high-frequency limit, in which the path an electron traverses under a half-cycle of the oscillating light electric field is much smaller than the characteristic length scales such as the finite radial thickness or the spin-orbit precession length.

Hertel finds a circular current as a result of the circularly polarized light in the form of

$$\mathbf{j}_\varphi = -\frac{i}{4e\langle n\rangle\omega}\boldsymbol{\nabla}\times\left[\sigma^*\mathbf{E}^*\times\sigma\mathbf{E}\right] \tag{2.80}$$

where $\mathbf{E}$ is the electric field of the light, and

$$\sigma = \frac{i\langle n\rangle e^2}{m\omega}, \tag{2.81}$$

is the conductivity of a collisionless plasma in a high frequency regime, $\langle n\rangle$ is the volume density of the electrons and ω is the light frequency. For circularly polarized light with helicity $\Lambda = \pm$

$$\mathbf{E}\times\mathbf{E}^* = \Lambda i\,|E|^2\cdot\mathbf{e}_z$$

Thus,

$$\mathbf{j}_\varphi(r) = \Lambda\frac{\langle n\rangle e^3}{4m^2\omega^3}\boldsymbol{\nabla}\times\left(|E(r)|^2\,\mathbf{e}_z\right) \tag{2.82}$$

$$= -\Lambda\frac{\langle n\rangle e^3}{4m^2\omega^3}\left(\frac{\partial|E(r)|^2}{\partial r}\right)\mathbf{e}_\varphi \tag{2.83}$$

Since this result does not depend on the z-coordinate, it holds for a 2DEG and normally incident light.

In a ring we can project the current to one dimension by writing the current density

$$\mathbf{j}_\varphi = j_{ext}^{1D}\mathbf{e}_\varphi, \tag{2.84}$$

where

$$j_{ext}^{1D} = \langle R_0(r)Z_0(z)|\,j_{ext}(r)\,|Z_0(z)R_0(r)\rangle \tag{2.85}$$

$$= -\Lambda\frac{\langle n\rangle e^3}{4m^2\omega^3}\int dr\,|R_0(r)|^2\,\frac{\partial|E(r)|^2}{\partial r}. \tag{2.86}$$

We consider a laser spot with Gaussian spatial distribution:

$$\mathbf{E}(r) = (\mathbf{e}_x + \Lambda i\mathbf{e}_y)E_0\exp\left(-\frac{\gamma r^2}{2}\right), \tag{2.87}$$

$$|E|^2 = E_0^2\exp\left(-\gamma r^2\right), \tag{2.88}$$

where E_0 is the maximum value of the electric field in the spot center. Thus, the total current in the ring with radius a then becomes

$$I = \int\int dz dr\, j_{ext}^{1D} = \Lambda\gamma E_0^2\exp\left(-a^2\gamma\right)\frac{Ne^3}{4\pi m^2\omega^3}. \tag{2.89}$$

where we used $\int dr\int dz\langle n\rangle = N/(2\pi a)$, the linear density of a ring with N electrons. The above current has dimension of Ampere. The result is also valid for the holes (with modified mass and opposite current direction). The light intensity reads in terms of the electric field

$$\text{Intensity} = \frac{cn'\epsilon}{2}\,|E|^2, \tag{2.90}$$

where c is the velocity of light in vacuum, ϵ is the dielectric constant , and n' the index of refraction. We estimate the current by assuming $\epsilon \approx 10\epsilon_0$, $n' \approx 3$. At a typical laser intensity of $10^{13}\,\mathrm{W m^{-2}}$, or equivalently $|E_0|^2 \approx 3\times 10^{15}\,\mathrm{V^2 m^{-2}}$, and wave length/frequency $\lambda' = 12\pi\,\mu\mathrm{m}\,/\,\omega = 2\times 10^{14}\mathrm{s^{-1}}$ used in all-optical switching [41], we find for the current in a 2DHG ring:

$$|I| = 16\,\mathrm{nA}\frac{E_0^2}{3\times 10^{15}\mathrm{V^2 m^{-2}}}\frac{\gamma\exp\left(-a^2\gamma\right)}{10^{12}\exp(-1)\mathrm{m^{-2}}}\frac{N}{1000} \tag{2.91}$$

$$\times\left(\frac{0.45m_0}{m}\right)^2\left(\frac{2\times 10^{14}\mathrm{s^{-1}}}{\omega}\right)^3 \tag{2.92}$$

REFERENCES

[1] L. P . Pitaevskii, Sov. Phys. JETP **12**, 1008 (1961).

[2] J. P. Van der Ziel, P. S. Pershan, and L. D. Malmstrom, Phys. Rev. Lett. **15**, 190 (1965).

[3] P. S. Pershan, J. P. van der Ziel, and L. D. Malmstrom, Phys. Rev. **143**, 574 (1966).

[4] A. V. Kimel, A. Kirilyuk, P. A. Usachev, R. V. Pisarev, A. M. Balbashov, and Th. Rasing, Nature **435**, 655 (2005).

[5] A. Kirilyuk, A. V. Kimel, and T. Rasing, Rev. Mod. Phys. **82**, 2731 (2010).

[6] C. D. Stanciu, F. Hansteen, A.V. Kimel, A. Kirilyuk, A. Tsukamoto, A. Itoh, and Th. Rasing, Phys. Rev. Lett. **99**, 047601 (2007).

[7] K. Vahaplar, A. M. Kalashnikova, A. V. Kimel, S. Gerlach, D. Hinzke, U. Nowak, R. Chantrell, A. Tsukamoto, A. Itoh, A. Kirilyuk, and Th. Rasing, Phys. Rev. B **85**, 104402 (2012).

[8] N. Kazantseva, D. Hinzke, U. Nowak, R. W. Chantrell, U. Atxitia, and O. Chubykalo-Fesenko, Phys. Rev B **77**, 184428 (2008).

[9] R. V. Mikhaylovskiy, E. Hendry, and V. V. Kruglyak, Phys. Rev. B **86**, 100405 (2012).

[10] M. Battiato, G. Barbalinardo, and P. M. Oppeneer, Phys. Rev. B **89**, 014413 (2014).

[11] K. Taguchi and G. Tatara, Phys. Rev. B **84**, 174433 (2011).

[12] A. Qaiumzadeh, G. E. W. Bauer, and A. Brataas, Phys. Rev. B **88**, 064416 (2013).

[13] V. I. Karpman and A. G. Shagalov, J. Plasma. Phys. **27**, 215 (1982).

[14] V. Tsytovich, Comm. Plasma Phys. Cont. Fusion **4**, 81 (1978).

[15] S. A. Belkov and V. N. Tsytovich, Sov. Phys. JETP. **49**, 656 (1979).

[16] M. Kono, M. M. Skoric, and D. Ter Haar, J. Plasma Phys. **26**, 123 (1981).

[17] R. Hertel, J. Magn. Mag. Mat. **303**, L1-L4 (2006).

[18] T. Yoshino, J. Magn. Magn. Mat. **323**, 2531 (2011).

[19] A. Manchon and S. Zhang, Phys. Rev. B **78**, 212405 (2008).

[20] A. Manchon and S. Zhang, Phys. Rev. B **79**, 094422 (2009).

[21] M. Büttiker, Y. Imry, R. Landauer, Phys. Lett. A **96**, 365 (1983).

[22] O.V. Kibis, Phys. Rev. Lett. **107**, 106802 (2011).

[23] J. Inoue, T. Kato, G. E. W. Bauer, and L. W. Molenkamp, Semicond. Sci. Technol. **24**, 064003 (2009).

[24] X. C. Zhang, A. Pfeuffer-Jeschke, K. Ortner, V. Hock, H. Buhmann, C. R. Becker, and G. Landweh, Phys. Rev. B **63**, 245305 (2001).

[25] R. Winkler, Phys. Rev. B **62**, 4245 (2000).

[26] G.Vignale, Phys. Rev. B **70**, 201102(R) (2004).

[27] F. E. Meijer, A. F. Morpurgo, and T. M. Klapwijk, Phys. Rev. B **66**, 33107 (2002).

[28] F.J. Ohkawa and Y. Uemura, J. Phys. Soc. Jpn. **37**, 1325 (1974).

[29] Y.A. Bychkov and E.I. Rashba, J. Phys. C: Solid State Phys. **17**, 6039 (1984).

[30] G. Dresselhaus, Phys. Rev. **100**, 580 (1955).

[31] R. Winkler, Phys. Rev. B **62**, 4245 (2000).

[32] R. Winkler, H. Noh, E. Tutuc, and M. Shayegan, Phys. Rev. B **65**, 155303 (2002).

[33] D. V. Bulaev and D. Loss, Phys. Rev. Lett. **95**, 076805 (2005).

[34] F. Joibari, Chapter 3 of this thesis.

[35] M. Edelstein, Solid State Commun. **73**, 233 (1990).

[36] B. Berche, C. Chatelain and E. Medina, Eur. J. Phys. **31**, 1267 (2010).

[37] D. Stepanenko, M. Lee, G. Burkard, and D. Loss, Phys. Rev. B **79**, 235301 (2009).

[38] A. A. Kovalev, M. F. Borunda, T. Jungwirth, L. W. Molenkamp, and J. Sinova, Phys. Rev. B **76**, 125307 (2007).

[39] J. B. Miller, D.M. Zumbuhl, C.M. Marcus, Y. B. Lyanda-Geller, D. Goldhaber-Gordon, K. Campman, and A. C. Gossard, Phys. Rev. Lett. **90**, 076807 (2003).

[40] M. Rubinstein, A. Hanbicki, P. Lubitz, M. Osofsky, J.J. Krebs, B. Jonker, Journal of Mag. Mag. Mat. **250**, 164 (2002).

[41] K. Vahaplar, A. M. Kalashnikova, A. V. Kimel, D. Hinzke, U. Nowak, R. Chantrell, A. Tsukamoto, A. Itoh, A. Kirilyuk, and Th. Rasing, Phys. Rev. Lett. **103**, 117201 (2009).

[42] X. C. Zhang, A. Pfeuffer-Jeschke, K. Ortner, V. Hock, H. Buhmann, C. R. Becker, and G. Landwehr, Phys. Rev. B **63**, 245305 (2001).

[43] A. C. B. Jayich, W. E. Shanks, B. Peaudecerf, E. Ginossar, F. von Oppen, L. Glazman, and J. G. E. Harris, Science, **326**, 272 (2009).

3

CHANGE IN SPIN POLARIZATION OF ELECTRONS IN MAGNETIZED QUANTUM RINGS FROM LIGHT-INDUCED CURRENTS

In Chapter 2, we have shown that electrons orbiting Rashba/ Dresselhaus quantum rings in the presence of light-induced current cannot accumulate spin polarization. This situation can be different if an exchange energy is present, i.e. the ring is initially magnetized. To illustrate this situation, we investigate a quantum ring in the presence of Rashba SOI and a ground state current. We demonstrate that the spin polarization of the conducting electrons can be changed by a circular current.

3.1 1D RING IN THE PRESENCE OF A SMALL EXCHANGE GAP

In Chapter 2, it was shown that in 1D rings the shift in the distributions of the two spin bands cause effects that exactly cancel each other. If the expectation value of spin would be angular momentum dependent, these effects would not cancel each other. This situation arises when exchange energy is present. For simplicity, let's first consider the Fermi energy to be exactly at the crossing point of two spin bands at $l = 0$, where only the first energy band is occupied, and we consider a small exchange energy to separate these two bands, see Fig 3.1. A small exchange energy mainly affects the degeneracy point, and one could neglect the change of high-momentum states at the Fermi energy. Thus, the energies around the Fermi level remain as:

$$E = E_a\left(l^2 + \sigma l \sec\theta_R\right) + \epsilon_0. \tag{3.1}$$

ϵ_0 is a constant energy caused by the confinement energies in the z and r directions, and can be assumed zero without affecting the generality of the calculations. Thus, at the crossing point $\epsilon_F = 0$, the Fermi wave numbers reduce to $l_{F,\sigma,\max(\min)} = -\sigma\sec\theta_R/2 + (-)\sec\theta_R/2$. Moreover, we assume that the low momentum states do not contribute to the current-induced spin accumulation, because the levels near to the Fermi energy are the ones mostly influenced by current. Thus, the expectation value of the z-component of spin near to the Fermi energy remains $\langle l,\sigma|\hat{\sigma}_z|\,l,\sigma\rangle = -\sigma\cos\theta_R$, and hence the spin polarization is:

$$\langle\hat{\sigma}_z\rangle = \sum_{\sigma,l} f_{\sigma,l}\left\langle\Psi_{l,\sigma}|\hat{\sigma}_z|\,\Psi_{l,\sigma}\right\rangle \tag{3.2}$$

$$= \sum_{0}^{l_{F,-,\max}+n_\lambda}\langle l,-|\hat{\sigma}_z|\,l,-\rangle + \sum_{l_{F,-,\min}-n_\lambda}^{0}\langle l,+|\hat{\sigma}_z|\,l,+\rangle = 2n_\lambda\cos\theta_R. \tag{3.3}$$

Where we consider only the lowest band in the presence of the exchange energy to be occupied, with the spin band $\sigma = +$ for $l < 0$, and $\sigma = -$ for $l > 0$. Satisfying the Lagrange multiplier constraint, the same approach taken in Chapter 2, one obtains n_λ as following:

$$n_\lambda = -\frac{\pi\hbar}{eE_a}\cos\theta_R I_\varphi. \tag{3.4}$$

Thus:

$$\langle\hat{\sigma}_z\rangle_I = \frac{2\pi\hbar}{eE_a}\cos^2\theta_R I_\varphi. \tag{3.5}$$

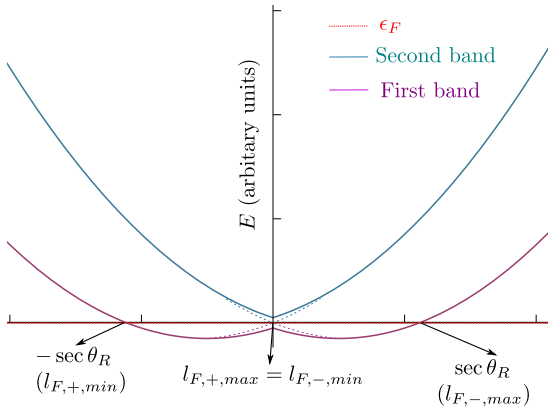

FIGURE 3.1: Schematic picture of energy bands for a 1D system in the presence of a small exchange energy. The band gap is exaggerated to be more illustrative. The solid violet and blue lines are the energies in the presence of the exchange energy. The dashed lines, in the same color, represent the energies in the absence of the exchange interaction. For the case of a ring, the energies are quantized values on each curve.

Since we assume that the Fermi energy passes the crossing point of the energy bands, one should note that the number of allowed energy levels, and therefore the number of electrons in the system is directly dependent to SOI via $N = 2/\cos\theta_R$. Thus, at zero temperature, vanishing SOI means zero particles in the system and the above result is no longer valid. We can identify a theoretical upper bound for the spin polarization as

$$\langle\hat{\sigma}_z\rangle = \frac{2\pi\hbar}{eE_a} I_\varphi. \tag{3.6}$$

If we consider quantities for Au, $\alpha = 0.6\times10^{-10}$ eV. m, $m_{\text{eff}} \approx m_0 \approx 9.1\times10^{-31}$ kg, $g \approx 2$, the above spin polarization is equivalent to a magnetic field of:

$$\rightarrow B_{\text{eff}} \approx 3\times10^4 \left[\frac{I_\varphi}{A}\right] \text{T}. \tag{3.7}$$

where we assume a ring with radius $a = 10\ \mu$m.

3.2 1D RING WITH A BROADER RANGE OF EXCHANGE ENERGY

In order to obtain a more general result for the change in spin polarization in the presence of light induced current, here we use numerical approaches.

3.2.1 NUMERICAL RESULTS OF SPIN POLARIZATION

The Hamiltonian for a ring in the presence of the Zeeman field reads [1]

$$\hat{H}_{1D} = \frac{\hbar^2}{2ma^2}\left(i\frac{\partial}{\partial\varphi}\right)^2 - \frac{\alpha}{a}\left(\cos\varphi\hat{\sigma}_x + \sin\varphi\hat{\sigma}_y\right)\left(i\frac{\partial}{\partial\varphi}\right) - i\frac{\alpha}{2a}\left(\cos\varphi\hat{\sigma}_y - \sin\varphi\hat{\sigma}_x\right) + \Delta\hat{\sigma}_z, \tag{3.8}$$

where a is the radius of the ring, α the spin-orbit coupling constant, and Δ is the exchange energy. Its eigenfunctions are

$$\psi_{n,\sigma}(\varphi) = \frac{1}{\sqrt{2\pi\left(A_{n,\sigma}^2 + B_{n,\sigma}^2\right)}} e^{in\varphi}\begin{pmatrix} A_{n,\sigma} \\ B_{n,\sigma}e^{i\varphi} \end{pmatrix}, \tag{3.9}$$

and the energies read

$$\frac{E_{(\sigma=\pm)}}{E_a} = l^2 + \frac{1}{4} + \sigma\sqrt{(l-\delta)^2 + l^2\tan^2\theta_R}, \tag{3.10}$$

where $\delta = \Delta/E_a$, and for $\theta_R \neq 0$:

$$A_{n,\sigma} = \frac{l\tan\theta_R}{\sqrt{\left(\delta - l - \sigma\sqrt{(\delta-l)^2 + l^2\tan\theta_R^2}\right)^2 + (l\tan\theta_R)^2}} \tag{3.11}$$

$$B_{n,\sigma} = \frac{\delta - l - \sigma\sqrt{(\delta-l)^2 + l^2\tan\theta_R^2}}{\sqrt{\left(\delta - l - \sigma\sqrt{(\delta-l)^2 + l^2\tan\theta_R^2}\right)^2 + (l\tan\theta_R)^2}}. \tag{3.12}$$

Thus, the expectation value of the z component of the spin reads:

$$\langle\psi_{l,\sigma}|\hat{\sigma}_z|\psi_{l,\sigma}\rangle = A_{n,\sigma}^2 - B_{n,\sigma}^2, \tag{3.13}$$

and for the expectation value of the current we have:

$$\langle\psi_{l,\sigma}|\hat{I}_\varphi|\psi_{l,\sigma}\rangle = \frac{1}{2\pi a}\left(-\frac{e\hbar}{ma}n - 2\frac{e\alpha}{\hbar}A_{n,\sigma}B_{n,\sigma}\right). \tag{3.14}$$

Using Eq. (3.10), one can find the Fermi wave numbers numerically and use them to calculate the total spin polarization. The effect of the ground state current is a constant shift of the wave numbers which is equivalent to a shift in the Fermi wave numbers used in Eq. (3.10). This constant shift n_λ can be obtained numerically using the constraint, i.e. $\sum_i f_i \hat{I}_i^\varphi = I$.

Due to the exchange energy, this system is initially spin polarized. Our goal is to calculate the percentage of polarization that changes as a function of the current.

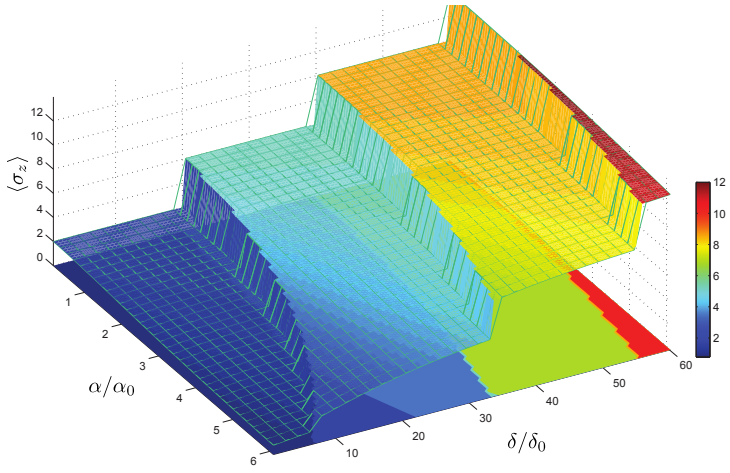

FIGURE 3.2: Total spin polarization as a function of normalized exchange energy δ/δ_0, and normalized SO coupling constant, α/α_0. The normalization constants are $\alpha_0 = 6.25 \times 10^{11}$eV.m, $\delta_0 = 2.5 \times 10^{-4}$. The parameters used in this plots are: $N = 10^4$, $E_F = 3$eV, $a = 5\mu$m, and the current is $I = 1\mu$A. These are conventions that we will henceforth use in the figures of this chapter.

Therefore, we calculate both the total spin polarization and the change in the spin polarization caused by the ground state current. These quantities are functions of the SOI constant and exchange energy.

Fig. 3.2 shows increasing spin polarization with increasing exchange energy, as we expect. However, this increase is a combination of two different effects: First, we see a gradual increase in the spin polarization. This is the consequence of the exchange energy dominating the SO energy, which encourages the spin to tilt in the plane of the motion. The second behavior is a sharp jump in the spin polarization, which occurs when the exchange energy increases enough to redistribute two electrons from one band to the other band. This effect is similar to Pauli paramagnetism.

The numerical result for the change in spin polarization in the presence of a ground state current has been demonstrated in Fig. 3.3. In Appendix 3.3, this result has been compared with the analytical results in the regime of small exchange energy. As we see in Fig. 3.3, for constant α and increasing δ, it becomes more difficult to change the spin polarization. Therefore, as we expect, we need larger currents to change the polarization for higher values of exchange energy. For a constant exchange energy, we observe an initial increase in the change of polarization from the increasing SOI. Gradually, we observe a secondary decrease in

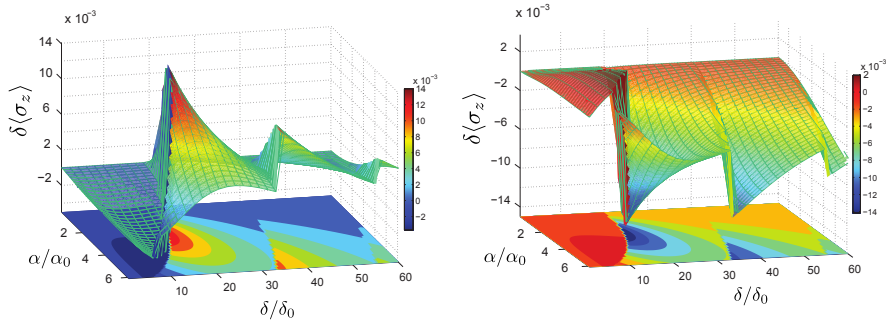

FIGURE 3.3: Change in spin polarization in the presence of a positive (right figure) and a negative (left figure) current. Comparing the figures in the left and right side, we show that for different directions of the current, which is a result of different helicities of the light, the change in spin polarization has the same behavior but in opposite directions. The color bar in this figures indicates the value of $\delta\langle\sigma_z\rangle$.

the change of polarization. The other outstanding features in these figures are the jumps that occur at the same values of the exchange energy observed in Fig. 3.2. These jumps are caused by an extra current that arises from the Pauli paramagnetism redistribution. This redistribution amplifies the effect of the current and the change in spin polarization becomes higher at these values. Thus, the overall behavior is similar to the current induced spin polarization of holes in the absence of the exchange energy, and can be understood similarly to what is discussed in Chapter 2.

As we see in Fig. 3.3, the sign of the change in polarization depends on the direction of the current; opposite currents induce equal spin polarizations but with the opposite sign. This means that the total spin polarization increases or decreases depending on the direction of the current. This is qualitatively in agreement with experiments that show opposite helicities of circularly polarized light induce magnetic fields in opposite directions [2]. One should note that opposite helicities also induce currents in opposite directions [3].

We can calculate the percentage of the change in polarization by considering the ratio of the change to the total polarization. As we can see in Figs. 3.3, and 3.2, the maximum change in polarization is $\delta\langle\hat{\sigma}_z\rangle \approx 1.5\times10^{-2}$, which happens at $\alpha \approx 3\alpha_0$, and $\delta \approx 10\delta_0$, with a total polarization of $\langle\hat{\sigma}_z\rangle \approx 4$, resulting in a change in polarization of about 4%. Even though it is nonzero, the effect of light induced circular currents on electrons in the presence of Rashba SOI is small.

In this chapter, we have demonstrate that in principle the circular-current induced spin polarization for electrons rotating in a Rashba ring in the presence of

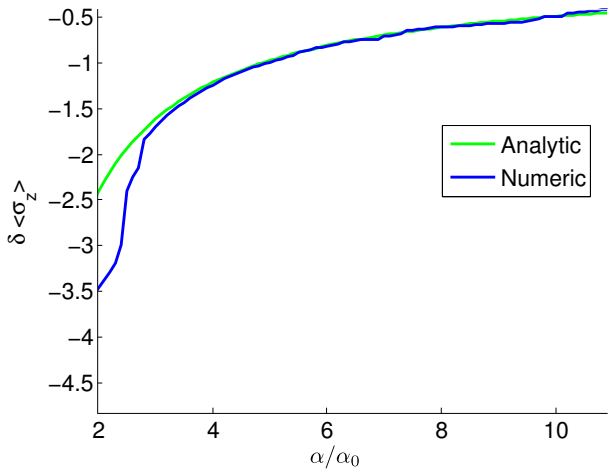

FIGURE 3.4: This figure compares the analytical and numerical results in the limit of small exchange energy while only one band is occupied.

exchange energy is nonzero. However, the effect seems to be small in this system. As we have demonstrated in this chapter, the change in the spin polarization can be maximized by tunning the Fermi energy in the exchange gap, in such a way that only one band is occupied.

3.3 APPENDIX

COMPARISON OF NUMERICAL AND ANALYTICAL RESULTS

Here, we compare our numerical result with the analytical solution for two cases in the regime of small exchange energy: First, the result of Section 3.1 with only the lowest band occupied, and second when both bands are occupied.

Fig. 3.4 presents a comparison of the analytical and numerical results for the first case. As we discussed in Section 3.1, the result is only valid when α is not too small. Accordingly, for larger values of the SO coupling constant, the analytical and numerical results in this figure are in a good agreement. For the second case, we calculate the change in spin polarization in the limit of small exchange, assuming that both energy bands are filled. The change in spin polarization in this case is:

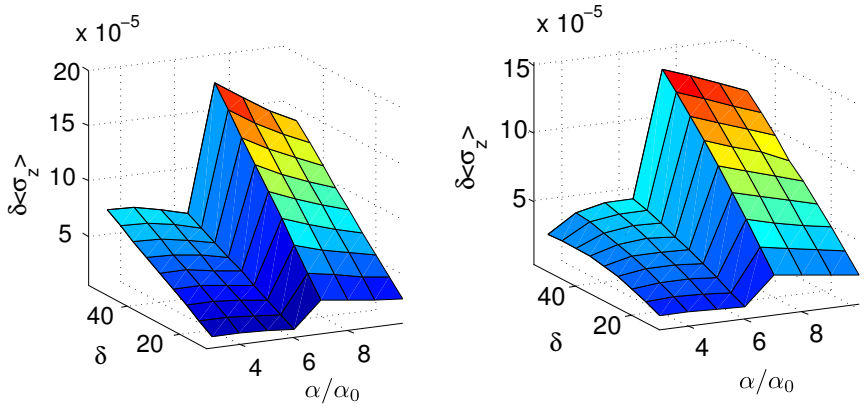

FIGURE 3.5: Analytical (right) and numerical (left) calculations on the spin polarization as a function of α and δ in the limit of small exchange energy. In this case both bands are occupied.

$$\begin{aligned}\delta\langle\hat{\sigma}_z\rangle &= \sum_{\sigma}\left[\sum_{n_{\min,\sigma}+n_\lambda}^{n_{\max,\sigma}+n_\lambda}\langle\hat{\sigma}_z\rangle_{n,\sigma} - \sum_{n_{\min,\sigma}}^{n_{\max,\sigma}}\langle\hat{\sigma}_z\rangle_{n,\sigma}\right] \\ &= \sum_{\sigma}\left[-\sum_{n_{\min,\sigma}+n_\lambda}^{n_{\min,\sigma}}\langle\hat{\sigma}_z\rangle_{n,\sigma} + \sum_{n_{\max,\sigma}}^{n_{\max,\sigma}+n_\lambda}\langle\hat{\sigma}_z\rangle_{n,\sigma}\right] \end{aligned} \tag{3.15}$$

With typical parameters used in this calculation, even for large values of current densities, $n_\lambda \ll n_{F,\sigma}$. Thus, in the regime of the small exchange energy, $\delta \ll n_{F,\sigma}$, one obtains:

$$\langle\hat{\sigma}_z\rangle_{n,\sigma} = \sigma\left(-\cos\theta_R + \frac{\delta}{n}\cos\theta_R\sin^2\theta_R\right). \tag{3.16}$$

Therefore:

$$\delta\langle\hat{\sigma}_z\rangle = \delta\cos\theta_R\sin^2\theta_R\sum_{\sigma}\sigma\left[-\sum_{n_{\min,\sigma}+n_\lambda}^{n_{\min,\sigma}}\frac{1}{n} + \sum_{n_{\max,\sigma}}^{n_{\max,\sigma}+n_\lambda}\frac{1}{n}\right] \tag{3.17}$$

For a typical quantum ring we have $1 \ll n_F$ at the Fermi level, therefore:

$$\sum_{\sigma}\sigma\left[-\sum_{n_{\min,\sigma}+n_\lambda}^{n_{\min,\sigma}}\frac{1}{n} + \sum_{n_{\max,\sigma}}^{n_{\max,\sigma}+n_\lambda}\frac{1}{n}\right] \approx n_\lambda\frac{N_{\sigma=+} - N_{\sigma=-}}{N^2} \tag{3.18}$$

where $N_\sigma = 2\sigma\cos\theta_R$ and $N = 4\sqrt{\epsilon_F/E_a}$. Thus, the change in spin polarization reduces to:

$$\delta\langle\hat{\sigma}_z\rangle = n_\lambda\delta^2\cos^2\theta_R\sin^2\theta_R\frac{E_a}{\epsilon_F} \tag{3.19}$$

Fig. 3.5 demonstrates that the above analytical expression and the numerical calculations are in a good agreement.

REFERENCES

[1] F. E. Meijer, A. F. Morpurgo, and T. M. Klapwijk, Phys. Rev. B **66**, 33107 (2002).

[2] C. D. Stanciu, F. Hansteen, A.V. Kimel, A. Kirilyuk, A. Tsukamoto, A. Itoh, and Th. Rasing, Phys. Rev. Lett. **99**, 047601 (2007).

[3] R. Hertel, J. Magn. Mag. Mat. **303,** L1-L*4* (2006).

4

CURRENT DRIVEN DOMAIN WALL DEPINNING IN A FERROMAGNETIC WIRE

Electric currents can move domain walls (DWs), which are initially pinned. Here, we study the current induced depinning of a DW pinned by a local magnetic field at the center of the wall, possibly caused by notches/anti-notches. We use Lagrange multiplier method to calculate the Hamiltonian of the system in the presence of the current in a ballistic regime. Using the energy considerations, we obtain the minimum current needed to depin such a DW as a function of the pinning magnetic field. In addition, we present a quantitative result for the local magnetic field by a simple model of notch/antinotch in a dipole magnetic moment scheme. We also demonstrate that for spin spiral magnetic texture in a ballistic regime, the current induced torque obtained by quantum mechanical methods agrees with the adiabatic torque obtained phenomenologically by Zhang et al. in Ref. [11]. Moreover, our results agree with that by solving the dynamical Landau-Lifshitz-Gilbert equation in the presence of a adiabatic spin transfer torque.

4.1 INTRODUCTION

Understanding the physics of magnetic domain walls (DWs) in ferromagnets is important for potential applications in, e.g., data storage and computer logics [1–3]. DW motion driven by applied magnetic fields has been studied extensively in the late 1970s [4]. Schryer and Walker [5] pioneered the collective coordinate approach of rigid DW motion in magnetic wires. The DW race-track shift register [6, 7], on the other hand, operates by current-induced DW motion [8–12]. The spacing between consecutive DWs is controlled by pinning sites fabricated by patterning "notches" along the edges of the track or modulating the track's size and material properties. The pinning sites define the bit length and provide DW stability against thermal fluctuations or stray magnetic fields natural imperfections. The geometrically induced pinning dominates when natural imperfections are sufficiently suppressed. The depinning field in nanostructures with constrictions can be adjusted over a wide range of values by changing the notch geometry. The strength and width of the pinning potential are crucial parameters in designing memory devices with low power consumption, which can be parameterized by the depinning threshold current j_{th}. Several experiments report the pinning of domain walls by artificial notches in magnetic nanowires [13–18]. Tatara and Kohno [9] showed that in the presence of the imperfections of material such as edge roughness, j_{th} is entirely determined by the pinning potential rather than the magnetization parameters such as its anisotropy. Due to the complexity of the problem, the most theoretical studies on the pinning by constrictions or notches are limited to micromagnetic simulations [19, 20].

The physics of the present problem is rather well understood, at least in the absence of interface spin transfer torques caused by the spin-orbit coupling, and micromagnetic solvers can produce quantitative results. However, there is still the need for simple models and calculations that give direct physical insights in parameter dependences etc. The wide spread belief, that the problem cannot be formulated as a minimum principle [21], severely limits the possible approaches. Here, we demonstrate that current-induced magnetic texture depinning can be formulated as a minimum principle by current-density functional theory [22].

In order to demonstrate the principle, we focus here on a very simple problem, viz. the current induced magnetization texture of a Walker-type rigid domain wall in a thin-film wire trapped by a pinning site and in the absence of dissipation. At current below the critical value the magnetization is static and can be obtained by minimizing the energy of the wire under a current constraint. The critical value at which there is no static solution anymore then corresponds to the depinning current. We model a notch by its pinning magnetic field induced by the modified demagnetization field. We assume a system of free electrons that carry the cur-

rent and are coupled to the ferromagnetic domain wall in an otherwise ballistic wire by a constant exchange interaction. We study the effect of a current on the pinned domain wall texture and the critical current at which the transfer torque overcomes the pinning. These results agree with that obtained by conventional methods, thereby illustrating that we can treat more complex problems beyond the simple Walker ansatz. Since the basic torque calculation is based on quantum mechanics, we expect that our method can be easily calculated by first principles and in the presence of spin-orbit torques.

This chapter is organized as follows. In Section 4.2, we introduce the Lagrange multiplier method for a magnetic wire. We use this method in Section 4.3 to study the ground state of a DW in a magnetic nanowire in the presence of an external current. In this section, we obtain and solve the Hamiltonian of the conducting electrons in the presence of the current. We use energy minimization considerations, and obtain a critical current where beyond that the minimization fails, and therefore domain wall depins. The results on critical current is discussed in Section 4.4. We eventually conclude in Section 4.5.

4.2 LAGRANGE MULTIPLIER METHOD

We can study the effects of an electric current in an inhomogeneous electron gas by current density-functional theory, which assures us that the ground state energy is the minimum of an energy functional of the electron current and density distribution [22]. Essential here is the method of Lagrange multipliers, which is a mathematical method to find the extremum of a function subject to boundary conditions expressed as equality constraints. Let us consider a system, in our case a metallic ferromagnet, be described by a Hamiltonian $\mathscr{H}$. We can then calculate $\mathscr{F}_0[\mathbf{M}]$, the ground state energy as a functional of the magnetization texture $\mathbf{M}(\mathbf{r})$ with $\delta\mathscr{F}_0[\mathbf{M}]/\delta\mathbf{M}(\mathbf{r}) = 0$. If we subject the sample to a current density distribution $\mathbf{j}_{ext}(\mathbf{r})$ we can set-up the new functional

$$\mathscr{F}[\mathbf{M},\mathbf{j}] = \mathscr{F}_0[\mathbf{M},\mathbf{j}] + \int \mathbf{A}(\mathbf{r}) \cdot \left(\mathbf{j}(\mathbf{r}) - \mathbf{j}_{ext}(\mathbf{r})\right) d\mathbf{r}, \tag{4.1}$$

where $\mathbf{A}(\mathbf{r})$ is a Lagrange multiplier function, which can be interpreted as an effective vector potential. We have to minimize this functional with respect to $\mathbf{M}$ and $\mathbf{A}$. The variation

$$\frac{\delta\mathscr{F}[\mathbf{M},\mathbf{j}]}{\delta\mathbf{A}(\mathbf{r})} = \mathbf{j}(\mathbf{r}) - \mathbf{j}_{ext}(\mathbf{r}), \tag{4.2}$$

should vanish when the real and object current distribution are the same. We can then compute the conditional ground state energy and current-induced magneti-

zation texture as

$$\frac{\delta \mathscr{F}\left[\mathbf{M},\mathbf{j}\right]}{\delta \mathbf{M}\left(\mathbf{r}\right)}=0. \tag{4.3}$$

This functional derivative can be interpreted as an effective magnetic field that has to vanish for a stable ground state. In the presence of several contributions to the energy, Eq. (4.3) implies that torques of different physical origin have to cancel each other. At some critical value of the current such a solution cannot be found anymore and the net finite torque induces magnetization motion. This is the depinning current we are looking for.

4.3 GROUND STATE OF DOMAIN WALL WITH CURRENT BIAS

We consider the standard system of a magnetic nanowire with easy axis in the z-direction, containing a head-to-head transverse domain wall in the x-z plane. We approximate the total energy by a sum of several contributions that are computed separately by writing

$$F\left[\mathbf{M},j_{ext}\right]=F_{an}\left[\mathbf{M}\right]+F_{pin}\left[\mathbf{M}\right]+F_{el}\left[\mathbf{M}\right]\left(j_{ext}\right) \tag{4.4}$$

where the different contributions are F_{el}, the electronic energy, F_{pin}, the pinning energy and F_{an} the magnetic anisotropy. We compute the functional F_{el} quantum mechanically, but use micromagnetic models for the latter energy contributions.

4.3.1 MAGNETIC ENERGY

We model the magnetic dipolar energy of the domain wall by the anisotropy energy and a pinning energy for a notch in terms of a localized magnetic field $\mathbf{H}_0$ oriented perpendicular to the wire. The magnetic free energy can then be written as an integral over the domain wall texture:

$$F_M\left[\mathbf{M},j_{ext}\right]=\int^{DW} f_M\left[\mathbf{M},j_{ext}\right](z)\,dz-\int^{DW}\mu_0\mathbf{M}(z)\cdot\mathbf{H}_0\delta(z)dz \tag{4.5}$$

Here the micromagnetic energy density reads

$$f_M\left[\mathbf{M},j_{ext}\right]=\frac{\mu_0}{2}M_x^2(z)-\mu_0\frac{H_k M_z^2(z)}{2M_s}+\frac{D}{M_s^2}\left|\frac{\partial\mathbf{M}(z)}{\partial z}\right|^2, \tag{4.6}$$

μ_0 is the permeability of vacuum, H_k the anisotropy field, and D the exchange energy constant. The terms on the right hand side of Eq. (4.6) are the thin-film demagnetization energy, anisotropy energy, and exchange energy, respectively. The effective magnetic field is the functional derivative

$$\mathbf{H}_{\text{eff}}\left(\mathbf{r}\right)=-\frac{\delta\left(F_{an}+F_{pin}\right)}{\mu_0\delta\mathbf{M}\left(\mathbf{r}\right)}. \tag{4.7}$$

We disregard here the current-induced Oersted fields for simplicity, which implies that the magnetic energy does not explicitly depend on the current.

4.3.2 CONDUCTION ELECTRONS

The lateral dimension of a metallic wire (not considering atomic chains) is large compared to the Fermi wave length and we adopt for simplicity parabolic bands with spin-independent electron mass m. The Hamiltonian can be separated as $\hat{H} = \hat{H}_\perp + \hat{H}_z$.[1] $\hat{H}_\perp = (\hat{p}_x^2 + \hat{p}_y^2)/2m$ describes the lateral kinetic energy while

$$\hat{H}_z = \frac{\hat{p}_z^2}{2m} + \Delta \hat{\boldsymbol{\sigma}} \cdot \mathbf{n}(z), \tag{4.8}$$

where $\mathbf{n}(z)$ is the unit vector in the direction of the magnetization, $\Delta > 0$ the exchange energy, and $\hat{\boldsymbol{\sigma}}$ the vector of Pauli spin matrices. The eigenfunctions are $\Psi_{\mathbf{k},\sigma} = \psi_{k_z}(z) \exp[i(k_x x + k_y y)]/\sqrt{wt}$, and $E = E_{k_\perp} + E_{k_z}$, where w and t are the thickness in the x and y directions, respectively, and $E_{k_\perp} = \hbar^2 k_\perp^2/(2m)$, with $k_\perp^2 = k_x^2 + k_y^2$. We may safely disregard the pinning magnetic fields below $H_0 \lesssim 1$T on the electron motion.

We wish to determine the ground state of the system in the presence of an applied current density j_{ext}, i.e.

$$j_{ext} = \int d\mathbf{r}_\perp \sum_i f_i \langle \Psi_i | \hat{j}_z(\mathbf{r}_\perp, z) | \Psi_i \rangle \tag{4.9}$$

where f_i is the Fermi Dirac distribution function for an electron state $i = (\mathbf{k}, \sigma)$, at zero temperature $f_i = \Theta(\epsilon_F - E_i)$ where ϵ_F is the Fermi energy, and $\hat{j}_z$ is the current density operator in the wire direction

$$\langle \Psi_i | \hat{j}_z(\mathbf{r}_\perp, z) | \Psi_i \rangle = e \,\mathrm{Re}\, \Psi_i^*(\mathbf{r}_\perp, z) \hat{v}_z \Psi_i(\mathbf{r}_\perp, z) \tag{4.10}$$

where $\hat{v}_z$ is the velocity operator. The ground state is obtained by minimizing the energy functional including the current constraint and the normalization condition $\langle \Psi_i | \Psi_i \rangle = 1$ by introducing the Lagrange multipliers ε_i and λ:

$$\begin{aligned} F_{el}[\mathbf{M}, \{\Psi\}]\left(j_{ext}\right) = &\sum_i f_i \left(\langle \Psi_i | \hat{H} | \Psi_i \rangle - \varepsilon_i \left(\langle \Psi_i | \Psi_i \rangle - 1 \right) \right) \\ &- \lambda \left(j_{ext} - \int d\mathbf{r}_\perp \sum_i f_i \langle \Psi_i | \hat{j}_z | \Psi_i \rangle \right). \end{aligned} \tag{4.11}$$

[1] To avoid confusions, we distinguish operators with ˆ in this chapter.

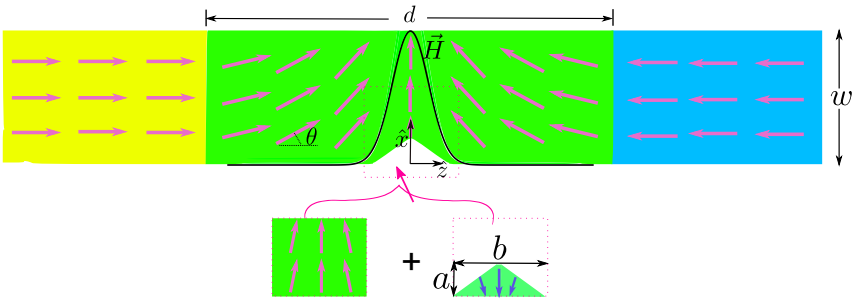

FIGURE 4.1: A schematic view of a ferromagnetic wire with domain wall head-to-head transverse. The wall is pinned by a local magnetic field generated by a notch at the center of the domain wall. Here the triangle notch has a base length of b, and height of a, and can be assumed as a summation of the domain wall without notch, coincide with a magnetic pattern in the shape of the notch with opposite direction of local magnetization of the wall.

The stationary condition of this functional with respect to the states $\langle\Psi_i|$ leads to an eigenvalue problem for a modified Hamiltonian

$$\hat{H}_z^j = \frac{\hat{p}_z^2}{2m} - \Delta\hat{\boldsymbol{\sigma}}\cdot\mathbf{n}(z) + \lambda\int d\mathbf{r}_\perp \hat{j}_z. \tag{4.12}$$

$\mathbf{A}(\mathbf{r}) \to \lambda$ is the effective vector potential that shifts occupation numbers, hence inducing a finite current in the ground state.

The magnetization texture $\mathbf{n}$ is usually modeled by the Walker profile, i.e. $\ln[\tan\theta(z)/2] = \pi z/d$, where $\theta(z)$ is the profile of the polar angle and the azimuthal angle is kept constant. Here d is the domain wall width (see Fig. 4.1). The domain wall is (initially) pinned at $z = 0$ by a magnetic field $\mathbf{H}_{pin}$, which represents a stray field discussed in the Appendix 4.6.3.

We assume that the pinning field is localized on a scale that is short compared to d, viz. $\mathbf{H}_{pin} = H_0\delta(z)\mathbf{e}_x$. We then do not have to take into account the full domain wall profile and describe the magnetization texture in vicinity to the notch by a half-period spin spiral state with a constant gradient equal to that of the Walker profile at the domain wall center, viz.

$$\theta(z) = \begin{cases} 0 & z \le -\frac{d}{2} \\ \Lambda(z+\frac{d}{2}) & \text{for} \quad -\frac{d}{2} \le z \le \frac{d}{2} \\ \pi & z \ge \frac{d}{2} \end{cases}, \tag{4.13}$$

where $\Lambda = \pi/d$ is the pitch of the spiral. By adapting the wave functions of electrons in an infinite spin spiral we sacrifice an accurate description of the states

in the tails of the domain wall, but avoid the artifacts of electron scattering at the edges of the profile Eq. (4.13).

We can diagonalize the Hamiltonian $\hat{H}_z$ by a local gauge transformation $\hat{\tilde{H}}_z = T^\dagger(z)\hat{H}_z T(z)$, which rotates the system to a local frame with magnetization along $\mathbf{e}_z$ direction [23–25]. Using $\hat{T}(z) = \hat{\sigma}_z \cos\theta/2 + \hat{\sigma}_x \sin\theta/2$ for $\theta(z) = \Lambda(z + \frac{d}{2})$:

$$\hat{\tilde{H}}_z = \frac{\hbar^2}{2m}\left(-i\frac{\partial}{\partial z}\right)^2 + i\frac{\Lambda\hbar^2}{2m}\frac{\partial}{\partial z}\hat{\sigma}_y - \Delta\hat{\sigma}_z. \tag{4.14}$$

Then the energies for each spin state $\sigma = \pm 1$ are

$$\tilde{E}_{k_z\sigma} = \frac{\hbar^2 k_z^2}{2m} + \sigma\frac{\Delta}{\cos\varrho(k_z)}, \tag{4.15}$$

and normalized eigenfunctions (for $k_z \neq 0$) are:

$$\widetilde{\psi}_{k_z,+}(z) = \frac{e^{ik_z z}}{\sqrt{L}}\begin{pmatrix} i\sqrt{\frac{\cos\varrho(k_z)}{-2+2\sec\varrho(k_z)}}(1-\sec\varrho(k_z)) \\ \sqrt{\frac{\cos\varrho(k_z)}{-2+2\sec\varrho(k_z)}}\tan\varrho(k_z) \end{pmatrix}, \tag{4.16}$$

$$\widetilde{\psi}_{k_z,-}(z) = \frac{e^{ik_z z}}{\sqrt{L}}\begin{pmatrix} \frac{1}{2}\left|\cos\varrho(k_z)\sec\varrho(k_z/2)\right|(1+\sec\varrho(k_z)) \\ -\frac{1}{2}i\left|\cos\varrho(k_z)\sec\varrho(k_z/2)\right|\tan\varrho(k_z) \end{pmatrix}. \tag{4.17}$$

Here

$$\varrho(k_z) = \arctan\frac{\hbar^2\Lambda k_z}{2m\Delta} \approx \frac{1}{\Delta}\frac{\hbar^2\Lambda^2}{2m}\frac{k_z}{\Lambda} \tag{4.18}$$

and the approximation we introduced in the above, holds in the limit of a wide domain wall and large exchange interaction, which is the case for elemental ferromagnetic metals and their simple alloys.

For a given Fermi energy, again invoking the wide domain wall limit, the two Fermi surfaces are the solutions of

$$\frac{\hbar^2\left(k_{z\sigma}^F\right)^2}{2m} + \sigma\frac{\Delta}{\cos\varrho k_{z\sigma}^F} \approx \frac{\hbar^2\left(k_{z\sigma}^F\right)^2}{2m}\left(1 + \sigma\frac{1}{2\Delta}\frac{\hbar^2\Lambda^2}{2m}\right) + \sigma\Delta = \epsilon_F - \frac{\hbar^2\left(k_{\perp\sigma}^F\right)^2}{2m}. \tag{4.19}$$

The domain wall deforms the originally spherical Fermi surfaces into prolate(oblate) ellipsoids along z.

$$\left(1 + \sigma\frac{1}{2\Delta}\frac{\hbar^2\Lambda^2}{2m}\right)\left(k_{z\sigma}^F\right)^2 = \frac{2m}{\hbar^2}\left(\epsilon_F - \sigma\Delta\right) - \left(k_{\perp\sigma}^F\right)^2 \tag{4.20}$$

$$\left(k_{z\sigma}^F\right)^2 = \left(\left(k_{0\sigma}^F\right)^2 - \left(k_{\perp\sigma}^F\right)^2\right)\left(1 - \sigma\beta\right) \tag{4.21}$$

where we defined $(k_{0\sigma}^F)^2 = 2m(\epsilon_F - \sigma\Delta)/\hbar^2$, and the above holds when

$$\beta = \frac{1}{2\Delta}\frac{\hbar^2\Lambda^2}{2m} \ll 1. \tag{4.22}$$

The total current operator in the z-direction is modified by the magnetization texture by an "anomalous velocity":

$$\hat{\tilde{v}}_z = \frac{\hbar}{im}\frac{\partial}{\partial z} - \frac{\Lambda\hbar}{2m}\hat{\sigma}_y \tag{4.23}$$

$\hat{\tilde{H}}_z^I = T^\dagger(z)\hat{H}_z^I T(z)$ is diagonal in k-space:

$$\hat{\tilde{H}}_z^I = \frac{\hbar^2}{2m}\left[(k_z+\lambda)^2 - \lambda^2\right] - \frac{\Lambda\hbar^2}{2m}(k_z+\lambda)\hat{\sigma}_y - \Delta\hat{\sigma}_z, \tag{4.24}$$

while $\hat{H}_\perp$ is modified by neither current constraint nor spin spiral. The eigenstates of the above Hamiltonian remain the same as in Eqs. (4.16) and (4.17), and the energies are modified to:

$$\tilde{E}_{k_z\sigma} = \frac{\hbar^2(k_z+\lambda)^2}{2m} + \sigma\frac{\Delta}{\cos\varrho(k_z+\lambda)}. \tag{4.25}$$

The current is reflected by replacing k_z by $k_z+\lambda$ and adding the constant $\sim\lambda^2$ that rigidly shifts the Fermi energy and can be disregarded. The lowest energy state for a given current therefore corresponds to a Fermi-Dirac distribution that is rigidly shifted in momentum space along the k_z direction.

The current in the domain wall as a function of λ reads

$$j_z = \sum_{k_z\sigma}\sum_{\mathbf{k}_\perp} f_{\mathbf{k}\sigma}\left\langle\tilde{\psi}_{k_z\sigma}\right|\hat{\tilde{j}}_z\left|\tilde{\psi}_{k_z\sigma}\right\rangle = \frac{A}{4\pi}\sum_{(k_z+\lambda)\sigma}^{k_{\perp\sigma}^2(k_z+\lambda)\geq 0}\left(k_{\perp\sigma}^F\right)^2(k_z)\left\langle\tilde{\psi}_{k_z\sigma}\right|\hat{\tilde{j}}_z\left|\tilde{\psi}_{k_z\sigma}\right\rangle \tag{4.26}$$

where

$$\left(k_{\perp\sigma}^F\right)^2(k_z) = \left(k_{0\sigma}^F\right)^2 - (k_{z\sigma})^2\left(1+\sigma\beta\right) \tag{4.27}$$

and the boundaries in the k_z summation are

$$k_{z\sigma}^{\pm} \approx -\lambda \pm k_{0\sigma}^F\left(1 - \sigma\frac{\beta}{2}\right) \tag{4.28}$$

To leading order in β

$$\left\langle\tilde{\psi}_{k_z\sigma}\right|\hat{\tilde{j}}_z\left|\tilde{\psi}_{k_z\sigma}\right\rangle \approx \frac{e}{V}\left(1-\sigma\beta\right)\frac{\hbar k_z}{m} \tag{4.29}$$

and

$$\sum_{k_z\sigma}\sum_{\mathbf{k}_\perp} f_{\mathbf{k}\sigma}\left\langle\widetilde{\psi}_{k_z\sigma}\right|\hat{\tilde{j}}_z\left|\widetilde{\psi}_{k_z\sigma}\right\rangle = \frac{e}{4\pi L}\sum_{k_z\sigma=k^-_{z\sigma}}^{k^+_{z\sigma}}\left(\left(k^F_{0\sigma}\right)^2-(k_z)^2\left(1+\sigma\beta\right)\right)\left(1-\sigma\beta\right)\frac{\hbar k_z}{m}$$
$$= \frac{e}{4\pi L}\frac{L}{2\pi}\sum_\sigma\int_{k^-_{z\sigma}}^{k^+_{z\sigma}} dk_z\left(\left(k^F_{0\sigma}\right)^2-(k_z)^2\left(1+\sigma\beta\right)\right)\left(1-\sigma\beta\right)\frac{\hbar k_z}{m}$$
$$\approx \frac{e}{4\pi^2 m}\lambda^3\left(2\sqrt{2m\left(\epsilon_F-\Delta\right)}+\beta\left(\sqrt{2m\left(\epsilon_F+\Delta\right)}-\sqrt{2m\left(\epsilon_F-\Delta\right)}\right)\right) \tag{4.30}$$

We can now determine λ by demanding that the current calculated is equal to the externally applied current bias j_{ext}:

$$\lambda^3 = \frac{\pi^2\sqrt{2m}j_{ext}}{e}\frac{1}{\sqrt{\epsilon_F-\Delta}}\frac{1}{1+\beta\left(\sqrt{\left(\epsilon_F+\Delta\right)}-\sqrt{\left(\epsilon_F-\Delta\right)}\right)/\left(2\sqrt{\left(\epsilon_F-\Delta\right)}\right)} \tag{4.31}$$
$$\approx \frac{\pi^2\sqrt{2m}j_{ext}}{e}\frac{1}{\sqrt{\left(\epsilon_F-\Delta\right)}}\left(1-\frac{\beta}{2}\left(1-\frac{\sqrt{\epsilon_F+\Delta}}{\sqrt{\epsilon_F-\Delta}}\right)\right). \tag{4.32}$$

To leading order in β (and $\epsilon_F > \Delta$) :

$$\lambda = \left(\sqrt{\frac{2m}{\epsilon_F-\Delta}}\frac{\pi^2 j_{ext}}{e}\right)^{1/3}. \tag{4.33}$$

Knowing λ, the Hamiltonian in Eq. 4.24, its eigenstates, and eigenvalues are fully determined.

4.3.3 ENERGY MINIMIZATION AND TORQUE CANCELLATION

We can now proceed to determine the magnetization profile. We assume that the magnetization texture including wall width and saturation magnetization does not depend on the current, i.e., the DW can move only rigidly with fixed width. The remaining free parameters are the domain wall center position Z and rotation angle out of the plane φ. This approximation can be relaxed by systematically including harder degrees of freedom by the collective coordinate method [26]. A stationary state exists when there is a minimum energy solution as a function of position, tilt angle, and applied current

$$\frac{\partial}{\partial\varphi}F\left(Z,\varphi,j_{ext}\right) = \frac{\partial}{\partial Z}F\left(Z,\varphi,j_{ext}\right) = 0, \tag{4.34}$$

i.e. when the total effective magnetic fields on the domain wall cancel each other. The electronic energy of a static texture in the presence of a current reads

$$F_{el}\left(Z,\varphi,j_{ext}\right)=\frac{\hbar^2}{2m}\sum_{\mathbf{k},\sigma}\left[(k_z+\lambda)^2-\lambda^2\right]-\Delta\int^{DW}\langle\hat{\boldsymbol{\sigma}}\cdot\mathbf{n}\rangle\,dz \tag{4.35}$$

$$\begin{aligned}&=\frac{\hbar^2}{2m}\sum_{\mathbf{k},\sigma}\left[(k_z+\lambda)^2-\lambda^2\right]\\&-\Delta\int_{-d/2-Z}^{d/2-Z}\langle\hat{\sigma}_x\rangle\sin(\Lambda(z+Z+d/2))dz-\Delta\int_{-d/2-Z}^{d/2-Z}\langle\hat{\sigma}_z\rangle\cos(\Lambda(z+Z+d/2))dz.\end{aligned} \tag{4.36}$$

which consists of kinetic and exchange energies.

We observe that this energy does not depend on the rotation angle φ because the magnetization is assumed static, while the lowest energy state in the absence of anisotropies is rotating with a constant velocity $\dot{\varphi}$. This issue could be solved by a generalized functional $F'_{el}\left(Z,\varphi,\dot{\varphi},I_{ext}\right)$. Here we sidestep the issue by not focusing on the free energy and its derivative with respect to φ, but by addressing the current-induced torques $d\mathbf{M}(z)/dt$. The field cancellation condition Eq. (4.34) is then equivalent to a torque cancellation condition. The time derivative of the spin angular momentum operator reads

$$\frac{d\hat{\mathbf{s}}}{dt}=\frac{\hbar}{2}\frac{d\hat{\boldsymbol{\sigma}}}{dt}=-\frac{i}{2}\left[\hat{\boldsymbol{\sigma}},\hat{H}\right]=\frac{\Delta}{2}\mathbf{n}(z)\times\hat{\boldsymbol{\sigma}}(z) \tag{4.37}$$

with expectation value

$$\frac{d\langle\hat{\mathbf{s}}\rangle}{dt}=\frac{\Delta}{2}\mathbf{n}(z)\times\langle\hat{\boldsymbol{\sigma}}(z)\rangle\,. \tag{4.38}$$

In Appendix 4.6.1 we compute the components of the spin polarization $\langle\hat{\boldsymbol{\sigma}}(z)\rangle$ from the electron wave functions determined above. The exchange interaction between conduction electrons and local magnetization conserves the total angular momentum of the system. So, the magnetization receives a reciprocal torque from the conduction electrons

$$\tau(z)=\frac{1}{\gamma}\frac{d\mathbf{M}}{dt}=-\mathbf{M}\times\frac{\partial F_{el}\left[\mathbf{M}\right]}{\partial\mathbf{M}} \tag{4.39}$$

where $\gamma=g\mu_B/\hbar$ in terms of the factor g and Bohr magneton μ_B. Its z-component reads:

$$\left.\frac{\partial F_{el}\left[\mathbf{M}\right]}{\partial\varphi}\right|_{\dot{\varphi}=0}=-\tau_z. \tag{4.40}$$

For the pinning potential we have:

$$F_{pin}\left(Z,\varphi,j_{ext}\right) = -\mu_0 H_0 M_s \sin\left(\Lambda\left(Z+\frac{d}{2}\right)\right)\cos\varphi. \tag{4.41}$$

The magnetic energy reads

$$\begin{aligned} &F_{an}\left(Z,\varphi,j_{ext}\right) \\ &= \int_{-d/2-Z}^{d/2-Z} dz\left\{\frac{\mu_0}{2}\left(M_x(z+Z)\right)^2 - \mu_0 H_k \frac{\left(M_z(z+Z)\right)^2}{2M_s} + \frac{D}{M_s^2}\left|\frac{\partial \mathbf{M}(z+Z)}{\partial z}\right|^2\right\} \quad (4.42) \\ &= \mu_0 \pi M_s^2 \cos^2\varphi \frac{d}{2} - \mu_0 \frac{H_k M_s}{2}\frac{d}{2} + D\Lambda^2 d. \quad (4.43) \end{aligned}$$

Now only the pinning energy depends on Z. Its minimum is found by

$$\frac{\partial F\left(M, j_{ext}\right)}{\partial Z} = -\mu_0 H_0 M_s \frac{\pi}{d}\cos\left(\frac{\pi}{d}\left(Z+\frac{d}{2}\right)\right)\cos\varphi = 0$$

to be at $Z=0$, independent of the current. Minimizing the energy with respect to ϕ at $Z=0$

$$\frac{\partial}{\partial\varphi}F\left(Z=0,\varphi,j_{ext}\right) = 0 \tag{4.44}$$

leads to

$$b\left(j_{ext}\right) = \left(\frac{\gamma}{\pi}H_0 - \gamma M_s d\cos\varphi\right)\mu_0\sin\varphi \tag{4.45}$$

where the current-induced torque $b\left(j_{ext}\right)$ has been defined in Appendix 4.6.1. Eq. (4.45) determines the tilt angle of the domain wall φ as a function of the applied current.

4.4 RESULTS

While $b\left(j_{ext}\right) \sim j_{ext}$, the right hand side of the equation of 4.45 has a maximum. This implies that above a critical current j_{th}, the static solution does not exist, the wall depins and starts to move. The maximum value occurs in an threshold angle, where for the threshold angle we obtain:

$$\varphi_{th} = -\arccos\left(\frac{-H_0 + \sqrt{H_0^2 + 8d^2M_s^2\pi^2}}{4dM_s\pi^2}\right)$$

Substituting this value into Eq. (4.45) give us the critical value of $b\left(j_{th}\right)$ and equivalently the critical value of the current to depin the wall. The critical value of $b\left(j_{th}\right)$

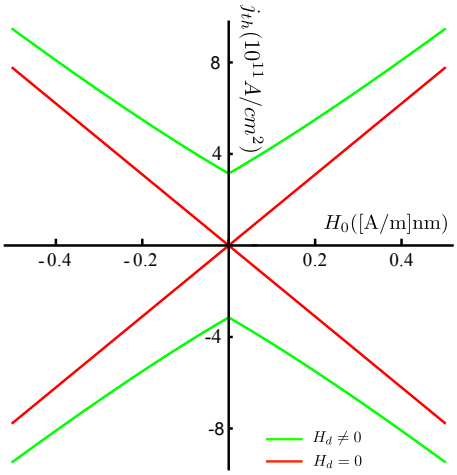

FIGURE 4.2: Critical current as a function of the pinning field. Here we plot the current density to depin the DW from the localized pinning magnetic field, in the presence and absence of the demagnetization field, red and green plots, respectively. For this plot, we have taken the spin spiral pitch of $\Lambda = 0.02\ \mathrm{nm}^{-1}$, and characteristic constants of permalloy, with $M_s = 86 \times 10^4$ A/m, Fermi energy $\epsilon_F = 1$eV, and exchange energy $\Delta = 0.5$ eV.

is:

$$b\left(j_{th}\right) = \frac{\pm\gamma\left(3\left|H_0\right| + \vartheta(H_0)\right)\sqrt{-H_0^2 + 4d^2M_s^2\pi^2 + \left|H_0\right|\vartheta(H_0)}}{8dM_s\sqrt{2}\pi^2} \tag{4.46}$$

where $\vartheta(H_0) = \sqrt{H_0^2 + 8d^2M_s^2\pi^2}$. In the limit of zero pinning this reduces to

$$b\left(j_{th}\right) \to \pm 2\pi d\gamma M_s \tag{4.47}$$

as derived by Tatara and Kohno [9].

Using Eq. (4.46), we obtain the value of critical current shown in Fig. 4.2, where we take the parameters for a permalloy wire. In the absence of the demagnetization field and pinning field, any current can drive the DW, i.e. the threshold current is zero. In the presence of the demagnetization field a threshold current is needed to move the wall, which is the intrinsic pinning derived by Tatara and Kohno [9]. As we see in Fig. 4.2, the pinning magnetic field in both cases, in the presence and absence of demagnetization field, causes an increase in threshold current.

4.5 CONCLUSION

We propose and implement a minimum energy principle to calculate the threshold current in the presence of localized pinning sites, such fabricated notches, thereby contradicting the common wisdom that this is not possible [21]. The trick is current density functional theory combined with the Lagrange multiplier method. In order to illustrate the method we consider a simple Hamiltonian for a magnetic wire. Through minimizing the energy in the presence of electric currents and in the adiabatic limit of wide domain walls we find analytical solutions for the eigenstates of the conducting electrons. We compute the torque quantum mechanically, which means that we can generalize the methods easily to include arbitrary spin-orbit torques. We calculate the minimum current beyond which the static solution does not exist, i.e. the DW depins and recover the intrinsic threshold current that exist [9] when there is no pinning potential and damping.

It is straightforward to treat more complicated magnetic textures, such as in non-adiabatic domain walls, vortices and skyrmions. In the case it is necessary to resort to numerical methods, but presumably much simpler than full-scale micromagnetic simulations. Going beyond the infinite spin spiral approximation will lead to non-adiabatic torques due to reflections at the domain wall that contribute to the field-like, so-called β term. As a side product we then obtain as well the deformations of the domain wall at currents below the depinning threshold.

The result can be extended to study the dynamics of the depinned DW by considering the full functional $F\left[\mathbf{M},\dot{\mathbf{M}},I\right]$, which leads to effective equations of motion on optimization. The weak point of the present calculation is disregard of the damping that has qualitative effects on the domain wall depinning. The dissipation induces a contribution to the field-like torque that induces sliding motion below the intrinsic threshold. It remains to be proven that the present formalism can be extended to take into account Gilbert damping, for example by including dissipation in terms of the Rayleigh functional [27].

4.6 APPENDIX

4.6.1 CURRENT INDUCED SPIN TORQUE

Here we compute the current-induced spin polarization, and spin-transfer torques by recovering the eigenstates in the lab frame using the inverse transformation $\psi_{k_z,\sigma} = \hat{T}^{\dagger}(z)\widetilde{\psi}_{k_z,\sigma}$, resulting in z-dependent spinors. Spin density is defined as

$$\boldsymbol{\rho}_s(z) = \sum_{\mathbf{k},\sigma} f_{\mathbf{k},\sigma}\Psi^{\dagger}_{\mathbf{k},\sigma}(z)\,\hat{\boldsymbol{\sigma}}\Psi_{\mathbf{k},\sigma}(z)\,. \tag{4.48}$$

Using the eigenstates and Fermi wave vectors in the lab frame, we obtain

$$\psi^{\dagger}_{k_z,\sigma}(z)\,\hat{\sigma}_x\psi_{k_z,\sigma}(z) = -\frac{1}{L}\sigma\cos\varrho(k_z)\sin(\Lambda(z+d/2)) \approx -\frac{1}{L}\sigma\sin(\Lambda(z+d/2)) \tag{4.49}$$

$$\psi^{\dagger}_{k_z,\sigma}(z)\,\hat{\sigma}_y\psi_{k_z,\sigma}(z) = \frac{1}{L}\sigma\tan\varrho(k_z) \approx \sigma\varrho(k_z) \tag{4.50}$$

$$\psi^{\dagger}_{k_z,\sigma}(z)\,\hat{\sigma}_z\psi_{k_z,\sigma}(z) = -\frac{1}{L}\sigma\cos\varrho(k_z)\cos(\Lambda(z+d/2)) \approx -\frac{1}{L}\sigma\cos(\Lambda(z+d/2)) \tag{4.51}$$

where the approximation is an expansion to first order in $\varrho(k_z)$. The spin density reads:

$$\begin{aligned}\rho^x_s(z) &= \frac{1}{8\pi^2}\sum_{\sigma}\int_{k^-_{z\sigma}}^{k^+_{z\sigma}} dk_z\left(\left(k^F_{0\sigma}\right)^2-(k_z)^2\left(1+\sigma\beta\right)\right)\psi^{\dagger}_{k_z,\sigma}(z)\,\hat{\sigma}_x\psi_{k_z,\sigma}(z)\\ &= \sin\theta(z)F(\lambda),\end{aligned} \tag{4.52}$$

where

$$\begin{aligned}f(\lambda) = \frac{1}{24\pi^2\hbar^2}\Bigg[&\frac{8}{\hbar}\left(\sqrt{(\epsilon_F+\Delta)^3\,m^3}\left(1+\frac{\beta}{2}\right)+\sqrt{(\epsilon_F-\Delta)^3\,m^3}\left(-1+\frac{\beta}{2}\right)\right)\\ &+6\hbar\lambda^2\left(\sqrt{(\epsilon_F+\Delta)\,m}\left(1+\frac{\beta}{2}\right)+\sqrt{(\epsilon_F-\Delta)\,m}\left(-1+\frac{\beta}{2}\right)\right)\Bigg],\end{aligned} \tag{4.53}$$

and

$$\begin{aligned}\rho^y_s &= \frac{1}{8\pi^2}\sum_{\sigma}\int_{k^-_{z\sigma}}^{k^+_{z\sigma}} dk_z\left(\left(k^F_{0\sigma}\right)^2-(k_z)^2\left(1+\sigma\beta\right)\right)\psi^{\dagger}_{k_z,\sigma}(z)\,\hat{\sigma}_y\psi_{k_z,\sigma}(z)\\ &= \frac{1}{8\pi^2}\frac{\hbar}{m\Delta}\lambda^3\Lambda\left(-\sqrt{2m(\epsilon_F-\Delta)}\left(1+\frac{\beta}{2}\right)+\sqrt{2m(\epsilon_F+\Delta)}\left(1-\frac{\beta}{2}\right)\right)\end{aligned} \tag{4.54}$$

$$\begin{aligned}\rho^z_s &= \frac{1}{8\pi^2}\sum_{\sigma}\int_{k^-_{z\sigma}}^{k^+_{z\sigma}} dk_z\left(\left(k^F_{0\sigma}\right)^2-(k_z)^2\left(1+\sigma\beta\right)\right)\psi^{\dagger}_{k_z,\sigma}(z)\,\hat{\sigma}_z\psi_{k_z,\sigma}(z)\\ &= \cos\theta(z)F(\lambda).\end{aligned} \tag{4.55}$$

We obtain the torque from the Heisenberg operator equation

$$\hat{\boldsymbol{\tau}} = (\hbar/2)\,d\hat{\boldsymbol{\sigma}}/dt = -i/2\left[\hat{\boldsymbol{\sigma}},\hat{H}\right] = (\Delta/2)\mathbf{n}\times\hat{\boldsymbol{\sigma}}, \tag{4.56}$$

Thus using Eqs. 4.52, 4.54, and 4.55 in Eq. 4.56, one can obtain the local torque as:

$$\sum_{\mathbf{k},\sigma} f_{\mathbf{k},\sigma}\Psi^{\dagger}_{\mathbf{k},\sigma}(z)\,\hat{\boldsymbol{\tau}}\Psi_{\mathbf{k},\sigma}(z) = C\left(j_{ext}\right)\frac{\partial}{\partial z}\mathbf{n}, \tag{4.57}$$

where

$$C\left(j_{ext}\right) \equiv \frac{\hbar\left(\sqrt{(\epsilon_F-\Delta)}(2+\beta)-\sqrt{(\epsilon_F+\Delta)}(2-\beta)\right)}{8e\left(\sqrt{(\epsilon_F+\Delta)}(2+\beta)+\sqrt{(\epsilon_F-\Delta)}(2-\beta)\right)} j_{ext}. \tag{4.58}$$

This could be consistently obtained from spin continuity equation in the stationary state. The above mentioned result can be rewritten in the common form the adiabatic torque in our geometry [28]

$$\boldsymbol{\tau}_a = -M_s b\left(j_{ext}\right)\mathbf{n}\times[\mathbf{n}\times(\mathbf{e}_z\cdot\frac{\partial}{\partial z})\mathbf{n}]. \tag{4.59}$$

Here $b\left(j_{ext}\right) \equiv \gamma C\left(j_{ext}\right)/M_s$ has the dimension of velocity. This result agrees with the phenomenological adiabatic torque obtained in Ref. [28]. Note that we did not ignore the nonadiabatic torque here. That torque for an infinite spin spiral domain wall in the absence of the impurities and diffusions vanishes.

4.6.2 CRITICAL CURRENT OBTAINED BY LANDAU-GILBERT-LIFSHITZ EQUATION

Here, we show that using the torque obtained in Appendix 4.6.1 in the LLG equation results in an equivalent equation for the critical current. The LLG equation reads [27]

$$\frac{\partial\mathbf{M}}{\partial t} = -\gamma\mu_0\mathbf{M}\times\mathbf{H}_{eff} + \alpha\mathbf{n}\times\frac{\partial\mathbf{M}}{\partial t} - b\left(j_{ext}\right)\mathbf{n}\times\left(\mathbf{n}\times\frac{\partial\mathbf{M}}{\partial z}\right). \tag{4.60}$$

The effective field reads

$$\mathbf{H}_{eff} = \frac{H_k M_z}{M_s}\hat{z} + \frac{2D}{\mu_0 M_s^2}\nabla^2\mathbf{M} - M_x\hat{x} + H_{ext}\hat{x} \tag{4.61}$$

where M_i is the i-th component of $\mathbf{M}$, H_k the anisotropy field, D the exchange constant, and M_x is demagnetization field. The x and y components of the LLG equation in polar coordinates read:

$$\begin{aligned}\alpha\frac{\partial\theta}{\partial t} - \frac{\partial\varphi}{\partial t}\sin\theta =& \gamma\mu_0 H_0\delta(z)\cos\theta\cos\varphi + \frac{2D\gamma}{M_s}\left(\frac{\partial^2\theta}{\partial z^2} - \cos\theta\sin\theta\left(\frac{\partial\varphi}{\partial z}\right)^2\right)\\ -H_k\gamma\mu_0\cos\theta\sin\theta - b\left(j_{ext}\right)\frac{\partial\varphi}{\partial z}\sin\theta &- M_s\gamma\mu_0\cos\theta\sin\theta\cos^2\varphi,\end{aligned} \tag{4.62}$$

and the z component give us:

$$\begin{aligned}\frac{\partial\theta}{\partial t} + \alpha\frac{\partial\varphi}{\partial t}\sin\theta =& \gamma\mu_0 H_0\delta(z)\sin\varphi + \frac{2D\gamma}{M_s}\left(\frac{\partial^2\varphi}{\partial z^2}\sin\theta + 2\cos\theta\frac{\partial\varphi}{\partial z}\frac{\partial\theta}{\partial z}\right)\\ &+ b\left(j_{ext}\right)\frac{\partial\theta}{\partial z} - M_s\gamma\mu_0\cos\varphi\sin\varphi\sin\theta.\end{aligned} \tag{4.63}$$

4

We solve these two partial differential equations using Walker's analysis of domain wall motion by introducing:

$$\varphi = \varphi(t);\ \ln\left[\tan\frac{\theta}{2}\right] = \frac{\pi}{d}(z - v_z t) \tag{4.64}$$

Since we are interested in the critical current, we assume that in the steady state φ is constant. The second equation postulates that the domain wall shape maintains its shape with constant width d and velocity v_z. By replacing these trial functions into Eqs. (4.62) and (4.63), and using the identities

$$\begin{aligned} &\frac{\partial\varphi}{\partial z} = \frac{\partial^2\varphi}{\partial z^2} = 0,\ \frac{\partial\varphi}{\partial t} = 0 \\ &\frac{\partial\theta}{\partial z} = \frac{\pi}{d}\sin\theta, \frac{\partial^2\theta}{\partial z^2} = \frac{\pi^2}{d^2}\sin\theta\cos\theta, \frac{\partial\theta}{\partial t} = -\frac{\pi}{d}v_z\sin\theta, \end{aligned} \tag{4.65}$$

and integrating over the z-axis, we obtain:

$$\alpha v_z + H_0\gamma\mu_0\cos\varphi\cos\left(2\arctan\left[\exp\left(-\frac{t v_z}{d}\right)\right]\right) = 0, \tag{4.66}$$

and

$$v_z + b\left(j_{ext}\right) + \frac{\gamma}{\pi}\mu_0 H_0\sin\varphi - \gamma\mu_0 M_s d\cos\varphi\sin\varphi = 0. \tag{4.67}$$

Eq. (4.66) is self-consistent for $v_z = 0$, while Eq. (4.67) at $v(t) = 0$ is identical to Eq. (4.45).

4.6.3 GEOMETRICALLY INDUCED PINNING MAGNETIC FIELD

In domain wall shift register devices, notch/anti-notches of different geometries allow the controlled trapping of DWs (Refs. [18]-[14]) in ferromagnetic nanowires. The strength of these trapping/pinning features depends on the form of the notch and the magnetic material [14–16, 29]. Tatara *et al.* model the pinning effects by a parabolic potential [9]. Here we suggest a simple model for fine (anti)notches interacting with wide domain walls in terms of a local pinning magnetic field. Such a notch causes a disturbance in the magnetic dipolar energy of the perfect wire, which outside the notch region can be treated in terms of an effective dipole. We consider here semicircular and triangular notches and antinotches. The missing magnetization is equivalent with an additional magnetization with direction opposite to the local magnetization of the wire, see Fig. 4.1. For an antinotch we simply attach additional magnetization to the wire edge. The dipole magnetic field caused by a distribution of magnetic moments can be written in terms of the scalar potential

$$\Phi_M(z) = \frac{\mathbf{M}\cdot\hat{\mathbf{r}}}{4\pi r^3} \tag{4.68}$$

related to the magnetic field as $\mathbf{H} = -\nabla\Phi_M(z)$, where $\mathbf{r} = r\hat{\mathbf{r}}$ and r the average distance from the area of missing or attached magnetic material. $\mathbf{M}$ is the total magnetization of the (anti)notch, which we calculate for two different shapes and a domain wall centered at the origin and far away from the notch.

Half disk (anti)notch

For a half disc (anti)notch with radius R centered at $z = 0$ in the x-z plane, we have:

$$\mathbf{m} = \int_0^t dy \int_0^R r' dr' \int_0^\pi d\varphi \mathbf{M} \tag{4.69}$$

Since the spin texture is initially in the x-z plane, $m_y = 0$, and because of the symmetry $m_z = 0$, therefore $\mathbf{M} = m_x \hat{\imath}$, and

$$\begin{aligned} m_x =& \iota M_s \int_0^t dy \int_0^R r' dr' \int_0^\pi d\varphi \cos\left(\frac{r'\cos\varphi}{d}\right) \\ \approx& \iota M_s t \frac{\pi R^2}{2}\left(1 - \frac{R^2}{4d^2}\right) \approx \iota M_s t \frac{\pi R^2}{2}, \end{aligned} \tag{4.70}$$

where $\iota = -(+)$ for the (anti)notch and we assumed $r'/d \ll 1$ and $R/d \ll 1$, *i.e.* the dimension of the notch is small compared to the width of the domain wall.

Isosceles triangle (anti)notch

For an isosceles triangle $m_y = m_z = 0$, and

$$m_x = \iota M_s t \int_{-b/2}^{b/2} dz \int_0^a dx \cos\left(\frac{z}{d}\right) = \iota 2 M_s t a d \sin\left(\frac{b}{2d}\right), \tag{4.71}$$

where b the base and a is the height of the triangle, see Fig 4.1. The pinning magnetic field is proportional to the value of $\mathbf{M}$, therefore, this result suggest that this field always increases linearly with a. However, b does not change this field much when its length becomes comparable with d, in agreement with the experimental observation in Ref [29]. In the small notch size limit $\mathbf{M} = \iota M_s abt\hat{\imath}$.

Dipolar field and pinning energy

$$\mathbf{H} = -\nabla\left(\frac{\mathbf{M}\cdot\hat{r}}{4\pi r^3}\right) = \frac{M_s\varpi}{4\pi r^3}\left(\hat{x} - 4\left(\frac{xz}{r^2}\hat{z} + \left(\frac{x}{r}\right)^2\hat{x}\right)\right), \tag{4.72}$$

Where $r = \sqrt{x^2 + z^2}$, and in the limit of small sized notch, for a half disk $\varpi = \pi R^2 t/2$, and for a isosceles triangle $\varpi = abt$. This field decreases as $1/r^3$ with the distance which makes the approximation of delta function field reasonable, and for $z \ll r$ the magnetic field is approximately in the x-direction.

REFERENCES

[1] S. D. Bader and S. S. P. Parkin, Ann. Rev. Cond. Matt. Phys. **1**, 71 (2010).

[2] D. A. Allwood, G. Xiong, C. C. Faulkner, D. Atkinson, D. Petit, and R. P. Cowburn, Science **309**, 1688 (2005).

[3] C. H. Marrows, Adv. Phys. **54**, 585 (2005).

[4] A. P. Malozemoff and J. C. Slonczewski, Magnetic Domain Walls and Bubble Materials (Academic, New York, 1976).

[5] N. L. Schryer and L. R. Walker, J. Appl. Phys. **45**, 5406 (1974).

[6] M. Hayashi, L. Thomas, C. Rettner, R. Moriya, X. Jiang, and S. S. P. Parkin, Phys. Rev. Lett., **97**, 207205 (2006).

[7] L. Thomas, M. Hayashi, X. Jiang, R. Moriya, C. Rettner, and S. S. P. Parkin, Nature (London) **443**, 197 (2006).

[8] L. Berger, Phys. Rev. B **54**, 9353 (1996).

[9] G. Tatara and H. Kohno, Phys. Rev. Lett. **92**, 086601 (2004).

[10] A. Thiaville, Y. Nakatani, J. Miltat, and Y. Suzuki, Europhys. Lett. **69**, 990 (2005).

[11] S. Zhang and Z. Li, Phys. Rev. Lett. **93**, 127204 (2004).

[12] S. E. Barnes and S. Maekawa, Phys. Rev. Lett. **95**, 107204 (2005).

[13] M. Kläui, C. A. F. Vaz, J. A. C. Bland, W. Wernsdorfer, G. Faini, E. Cambril, L. J. Heyderman, F. Nolting, and U. Rüdiger, Phys. Rev. Lett. **94**, 106601 (2005).

[14] M. Kläui, H. Ehrke, U. Rdiger, T. Kasama, R. E. Dunin-Borkowski, D. Backes, L. J. Heyderman, C. A. F. Vaz, J. A. C. Bland, G. Faini, E. Cambril, and W. Wernsdorfer, Appl. Phys. Lett. **87**, 102509 (2005).

[15] D. Petit, A. V. Jausovec, D. Read, and R. P. Cowburn, J. Appl. Phys. **103**, 114307 (2008).

[16] K. O'Shea, S. McVitie, J. N. Chapman, and J. M. R. Weaver, Appl. Phys. Lett. **93**, 202505 (2008).

[17] L. K. Bogart, D. Atkinson, K. O'Shea, D. McGrouther, and S. McVitie, Phys. Rev. B **79**, 054414 (2009).

[18] U. H. Pi, Y. J. Cho, J. Y. Bae, S. C. Lee, and S. Seo, Phys. Rev. B, **84**, 024426 (2011).

[19] M. Kläui, C. A. F. Vaz, J. Rothman, J. A. C. Bland, W. Wernsdorfer, G. Faini, and E. Cambril, Phys. Rev. Lett. **90**, 097202 (2003).

[20] S. Lepadatu, A. Vanhaverbeke, D. Atkinson, R. Allenspach, and C.H. Marrows, Phys. Rev. Lett. **102**, 127203 (2009).

[21] M.D. Stiles, W. M. Saslow, M.J. Donahue, and A. Zangwill, Phys. Rev. B **75**, 214423 (2007).

[22] G. Vignale, Phys. Rev. B **70**, 201102(R) (2004).

[23] V. K. Dugaev, J. Barnas, A. Łusakowski, and Ł. A. Turski, Phys. Rev. B **65**, 224419 (2002).

[24] Korenman, J. L. Murray, and R. E. Prange, Phys. Rev. B **16**, 4032 (1977).

[25] G. Tatara and H. Fukuyama Phys. Rev. Lett. **72**, 772 (1994).

[26] O. A. Tretiakov, D. Clarke, G. W. Chern, Ya. B. Bazaliy, O. Tchernyshyov, Phy. Rev. Lett. **100**, 127204 (2008).

[27] T. L. Gilbert, IEEE Trans. Magn. **40**, 3443 (2004).

[28] Z. Li and S. Zhang, Phys. Rev. B **70**, 024417 (2004).

[29] A. L. G. Oyarce, Y. Nakatani, and C. H. W. Barnes, Phys. Rev. B **87**, 214403 (2013).

5

AHARONOV-CASHER EFFECT IN QUANTUM RING ENSEMBLES

We study the transport of electrons through a single-mode quantum ring with electric field induced Rashba spin-orbit interaction that is subject to an in-plane magnetic field and weakly coupled to electron reservoirs. Modelling a ring array by ensemble averaging over a Gaussian distribution of energy level positions, we predict slow conductance oscillations as a function of the Rashba interaction and electron density due to spin-orbit interaction-induced beating of the spacings between the levels crossed by the Fermi energy. Our results agree with experiments by Nitta c.s., thereby providing an interpretation that differs from the ordinary Aharonov-Casher effect in a single ring.

The result presented in this chapter have been published in Phys. Rev. B **88**, 115410 (2013).

The Aharonov-Casher (AC) effect [1] is an analogue of the Aharonov-Bohm (AB) effect, but caused by the spin-orbit interaction (SOI) rather than an external magnetic field. Originally, Aharonov and Casher predicted in 1984 that a spin accumulates a phase when the electric charge is circling in an external electric field [1]. This situation is similar to a single-mode ballistic ring with Rashba spin-orbit interaction. Quantum rings in high-mobility semiconductor material have therefore attracted extensive attention, both experimentally and theoretically, as model devices to investigate fundamental quantum mechanical phenomena.

In the AC effect, the electrons injected into a quantum ring with SOI acquire spin phases when traversing the two arms due to precession in the effective spin-orbit magnetic field. Interference of the spinor wave functions at the exit point of the ring then leads to an oscillatory conductance as a function of the spin-orbit coupling constant that in Rashba systems can be tuned by an external gate voltage. The electrons injected into a quantum ring with SOI acquire spin phases when traversing the two arms due to precession in the effective spin-orbit magnetic field. Interference of the spinor wave functions at the exit point of the ring then leads to an oscillatory conductace as a function of the spin-orbit coupling constant that in Rashba systems can be tuned by an external gate voltage. König *et al.* [2] reported the first experimental evidence of the AC effect in a single HgTe ring by measuring the phase shift of the AB-type magneto-conductance oscillations caused by tuning the Rashba SO strength. Since several subbands in the ring were occupied, they supported their experiments by multi-mode transport calculations. This study focussed on the symmetry points, at which the Rashba SOI is small, and high values of the applied magnetic field [2]. Experiments on an array of InGaAs rings [4] agreed well with the theory provided for a single-mode quantum ring symmetrically and strongly coupled to the leads [3]. More recently, the zero magnetic field conductance as a function of gate field has been interpreted in terms of the modulation of (electron density-independent) Altshuler-Aronov-Spivak (AAS) oscillations by the SOI [5], emphasizing the importance of statistical averaging by the ring arrays.

In reality, however, the situation is not as simple as it appears. The assumed ideal link of the ring to the leads is equivalent to the strong coupling limit in terms of a connectivity parameter [6]. The implied absence of backscattering is at odds with the interpretation of the observed oscillations in terms of AAS oscillations due to coherent backscattering [5, 7]. Ref. [8] addresses the effects of scattering at the contacts of a single-mode Rashba ring to the reservoirs, interpolating between the fully open and isolated ring regimes. However, the experiments [4, 5] were not carried out on single rings in the one-dimensional quantum limit, but a large array of connected rings, each containing several transport channels. Some theoretical papers compute transport through an array of single-mode rings [9, 10], but

assuming a constant Fermi wave number, thereby disregarding the strong density changes associated with tuning the Rashba spin-orbit parameter [7]. In the present chapter, we offer an explanation of the robustness of the observed AC oscillations with respect to the complications summarized above.

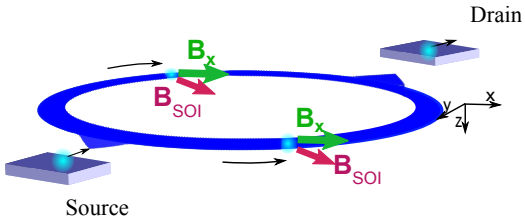

FIGURE 5.1: Schematic of a quantum ring weakly coupled to source and drain contacts in the presence of SOI effective field B_{SOI} and in-plane magnetic field B_x.

A quantitative analysis of the multi-mode ring array is challenging and requires large scale numerical simulations [11]. Here we proceed from a single single-mode quantum ring [3], taking backscattering into account by assuming weak coupling to the electron leads and correcting for the multimode character *a posteriori* (see below). The conductance of a quantum ring can be understood as resonant tunneling through discrete eigenstates at the Fermi energy [6] that are modulated by the SOI Rashba parameter. In-plane magnetic field [11] allows tuning of the conductance oscillations without interference of the AB oscillations (see Fig. 5.1). We consider a modulation of the Rashba interaction strength that is associated with an experimentally known large change in the electron density [7]. Small deviations between different rings in nanofabricated arrays can be taken into account by an ensemble averaging over slightly different single rings. We find that this procedure leads to an agreement with experiments that rivals that of previous theories.

We consider a ring with a radius of R, defined in the high-mobility two-dimensional electron gas in the xy-plane. The Rashba SOI with the strength α is is a known function of an external gate potential. The Hamiltonian of an electron in the ring has the form [12]

$$\hat{H}_{1D}^{(0)} = \frac{\hbar^2}{2mR^2}\left(-i\frac{\partial}{\partial\varphi}\right)^2 - \frac{\alpha}{R}\left(\cos\varphi\hat{\sigma}_x + \sin\varphi\hat{\sigma}_y\right)\left(i\frac{\partial}{\partial\varphi}\right) - i\frac{\alpha}{2R}\left(\cos\varphi\hat{\sigma}_y - \sin\varphi\hat{\sigma}_x\right), \tag{5.1}$$

where m is the effective mass, φ is the azimuthal angle, and $\hat{\sigma}_i$ are the Pauli matri-

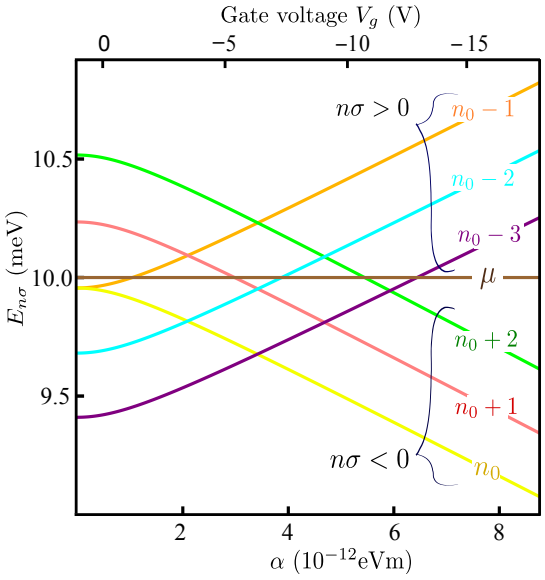

FIGURE 5.2: Energies of a quantum ring with the radius $R = 630$ nm close to the Fermi energy $\mu = 10$ meV as function of the SOI strength α. Energies are labeled as $n_0 + i$ and $n_0 = 72$, for $n > 0$, whereby, each level is Kramers degenerate with $-n_0 - i - 1$ and opposite spin direction. The effective mass for conduction electrons in InGaAs $m = 0.045\ m_0$, where m_0 is the electron mass. The conductance is nonzero when μ crosses an energy level.

5

ces in the spin space. The eigenstates are

$$E^{(0)}_{n\sigma} = E_R \left[\left(n + \frac{1}{2} \right)^2 + \frac{1}{4} + \sigma \frac{n + \frac{1}{2}}{\cos\theta} \right], \tag{5.2}$$

where $E_R = \hbar^2/(2mR^2)$, $\tan\theta = 2mR\alpha/\hbar^2$, the integer n is the angular momentum quantum number, and $\sigma = \pm$ denotes the spin degree of freedom.

An in-plane magnetic field B along the x-direction contributes the Zeeman energy $H' = E_B \hat{\sigma}_x$, where $E_B = g\mu_B B/2$, μ_B is the Bohr magneton and g the effective g-factor. We assume that the Zeeman energy is small compared to the (kinetic) Fermi energy and can be treated as a perturbation of the zero-field Hamiltonian, $H^{(0)}_{1D}$.

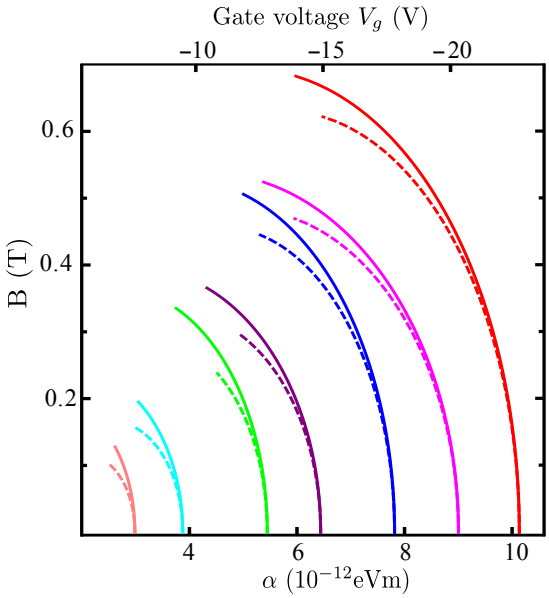

FIGURE 5.3: Shift of the conductance peaks, that for zero magnetic field coincide with the crossings of the Fermi energy in Fig. 2, by an in-plane magnetic field as obtained by perturbation theory. The magnetic field is seen to break Kramers spin degeneracy. The parameters are the same as in Fig. 5.2 and $g = -2.9$ for InGaAs.

To leading order in E_B the energies $E^{(0)}_{n\sigma}$ are shifted by the in-plane field as:

$$\Delta^{(2)}_{n\sigma} = \frac{E_B^2}{8E_R}\left[\frac{\sin^2(2\theta)}{(2n\cos\theta+\sigma)(2(n+1)\cos\theta+\sigma)} + \frac{4\sin^4\frac{\theta}{2}\cos\theta}{n(\cos\theta+\sigma)} - \frac{4\cos^4\frac{\theta}{2}\cos\theta}{(n+1)(\cos\theta-\sigma)}\right]. \tag{5.3}$$

The gate voltage V_g modifies the asymmetry of the electron confinement potential, thereby modulating the Rashba SOI strength α. We discuss here first the effects of varying SOI for constant Fermi energy and subsequently take the gate-induced density variation into account. In the absence of a magnetic field, the energy levels move with α according to Eq. (5.2). The four-fold degeneracy in the absence of SOI $E_{n,\sigma} = E_{n,-\sigma} = E_{-n-1,-\sigma} = E_{-n-1,\sigma}$ is broken when $\alpha \neq 0$ into two Kramers-degenerate doublets with $E_{n,\sigma} = E_{-n-1,-\sigma}$, see Eq. (5.2). For $\sigma n > (<) 0$ the energy increases (decreases) with α as indicated in Fig. 5.2. The experiments by Nitta c.s. were carried out in the low temperature regime with level spacings

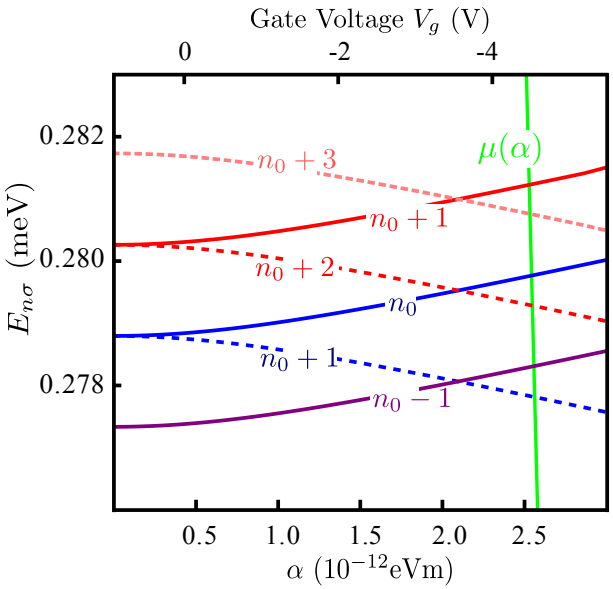

FIGURE 5.4: Energy levels around the Fermi energy for $\alpha \approx 2.4 \times 10^{-12}$ eVm relative to μ that strongly depends on the gate voltage tuning α. Here $n_0 = 380$, while dashed and solid lines represent $n\sigma < 0$ and $n\sigma > 0$, respectively. Similar to Fig. 5.2, we label the energies for $n > 0$, keeping in mind that the levels are twofold degenerate.

larger than the thermal energy [4, 5], therefore we assume zero temperature in the following.

Resonant tunneling occurs when the energy of the highest occupied level in the quantum ring, $E_{n_F,\sigma}$, equals the chemical potential μ in the leads, i.e. $E_{n_F,\sigma}(\alpha) = \mu$, as indicated in Fig. 5.2. Doublets of spin-split conductance peaks merge when $\alpha = 0$, $\mu = E_{n_F,\sigma}$, and the conductance becomes twice as large. The in-plane magnetic field shifts the energy levels as $\propto B^2$. As illustrated in Fig. 5.3, the resonant tunneling peaks at $E_{n_F,\sigma}(\alpha, B) = \mu$ are spin-split and non-parabolic. Fig. 5.3 agrees qualitatively with the experiments [11] when assuming the strong coupling limit and justifying the apparent independence on the large μ variation with gate voltage by coherent backscattering. In the following we suggest an alternative interpretation.

According to the experiments [4, 5], α depends on the gate voltage as $\alpha[10^{-12}\,\text{eVm}] = 0.424 - 0.47 \times V_G\left[10^{-12}\text{V}\right]$ and on the electron density as $\alpha\left[10^{-12}\text{eVm}\right] = 7.81 - 3.32 \times N_s\left[10^{12}\text{cm}^{-2}\right]$. In Fig. 5.4 we plot the ring energies as a function of

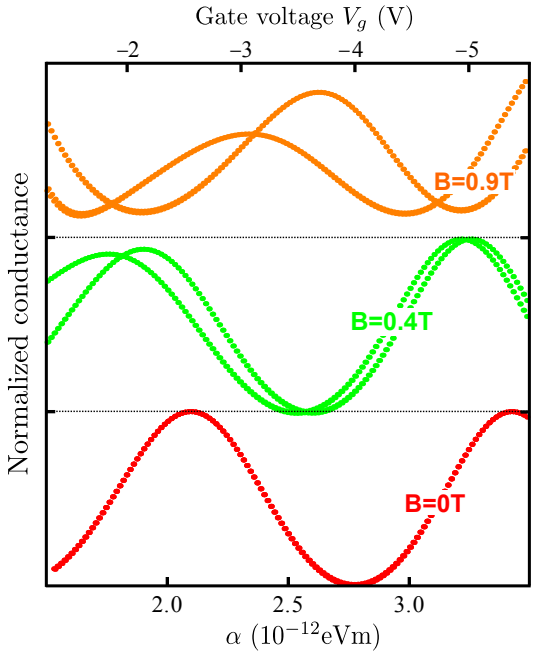

FIGURE 5.5: Conductance oscillations of an ensemble of rings with energy levels broadened by a Gaussian with Γ = 0.003 peV/m as a function of an in-plane magnetic field. The dashed lines are guides to the eye, to compare the oscillation amplitudes while varying the magnetic field. All amplitudes are scaled with those at B = 0 T that display a modulation of $(G_{max} - G_{min})/G_{max}$ = 50%. The in-plane magnetic field splits Kramers degenerate spin states that evolve differently with gate voltage.

α including the chemical potential μ that varies much faster with α than the single particle energies, leading to conductance peaks that as a function of gate voltage are very closely spaced. In ring arrays [4, 5] we do not expect to resolve such narrow resonances due to disorder, multi-mode contributions and ring size fluctuations. We can model the latter by averaging over an ensemble of rings with a Gaussian distribution of resonant energies or conductance peak positions with a phenomenological broadening parameter Γ. Fig. 5.5 illustrates the result of the averaging procedure in the form of the normalized conductance modulations [13]. While the resonant tunneling peaks are smeared out, slow (AC) oscillation as a function of α reappears, which represents the beating of the level spacings induced by the SOI, in qualitative agreement with experiments.

The experiments of AC oscillations in arrays with different ring radii [5] are compared in Fig. 5.6 with our results.

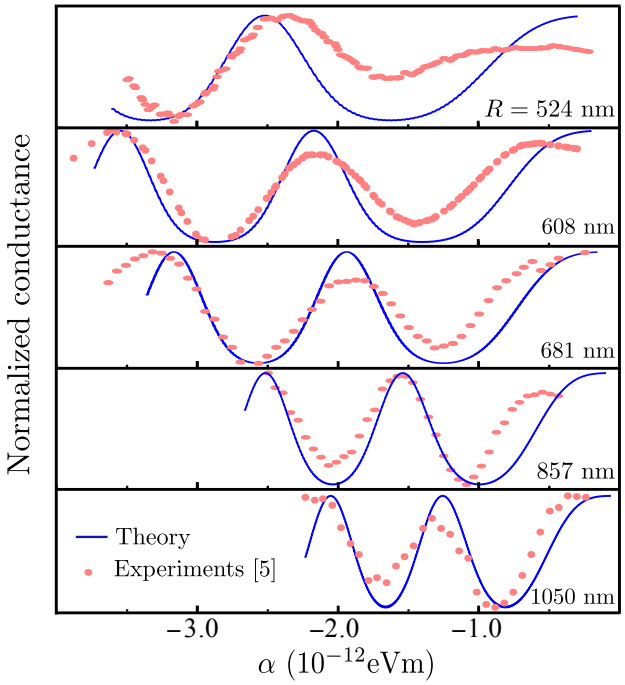

FIGURE 5.6: The conductance G of a array of rings modeled as an ensemble energy levels as a function of α broadened by a Gaussian for various nominal radii R. The broadening parameters are Γ = 0.005, 0.0035, 0.003, 0.002 and 0.001 peV/m, for R = 524; 608; 681; 857 and 1050 nm, respectively. All amplitudes are scaled to a panel height corresponding to $(G_{max} - G_{min})/G_{max}$ = 50%. We use the experimentally determined relations between Rashba constant and electron density as before. We compare our calculations (lines) with the experimental results (points) from Ref. [5] (see also Ref. [13]).

In Fig. 5.5, we also illustrate the effect of in-plane magnetic fields on the ensemble of Rashba rings. The magnetic field shifts the phase of the oscillation to lower values of the gate voltage or larger α and thus suppresses the amplitude of the conductance oscillations increasingly for lower values of the gate voltage. These features agree again well with those observed experimentally by Nitta *et al.* [11]. The magnetic field splits the Kramers degeneracy, thereby leading to two sets of superimposed oscillations that might be experimentally resolved in the form of different Fourier components.

The suppression of AAS oscillations in disordered ring arrays at constant density [9] can be interpeted in favor of our model. Most previous theories [3, 12] treat ideally open rings, while we consider the weak coupling limit. Both extremes

are likely not met in experiments. The intermediate regime can be modeled in terms of a connectivity parameter [6, 8]. An increased coupling causes a Lorentzian smearing of the conductance peaks, which is likely to effectively enhance the phenomenological broadening of the ensemble average and cannot be resolved in the experiments. The presence of several occupied modes in the rings also contributed to the average, since each radial node can be approximated as a ring with a slightly different radius. We therefore believe that our results are robust with respect to deviations from our Hamiltonian and these deviations can be captured by the phenomenological broadening parameter Γ.

In conclusion, we investigated the conductance of single rings and an ensemble of them as a function of the Rashba spin-orbit interaction in the limit of weak coupling to the leads. We considered both constant and gate voltage-dependent density of electrons. Both situations can in principle be realized experimentally by two independent (top and bottom) gate voltages. We compare results with experiments on ring arrays in which a single gate changes both the SOI α as well as the electron density. We found that, in agreement with experiments, the ensemble averaged conductance oscillates as a function of α. The oscillations undergo a phase shift under an in-plane magnetic field, and the period varies with the ring diameter, as observed. We conclude that experiments observe SOI-induced interference effects that are more complicated than the original Aharonov-Casher model but are robust with respect to the model assumptions. It should be possible to experimentally distinguish between the different models by separating effects of spatial inversion symmetry (and thereby α) and the Fermi wave number modulation. This should be possible by employing a double gate configuration in which the electric field is varied, but density is kept constant [14].

REFERENCES

[1] Y. Aharonov and A. Casher, Phys. Rev. Lett. **53**, 319 (1984).

[2] M. König, A. Tschetschetkin, E. M. Hankiewicz, J. Sinova, V. Hock, V. Daumer, M. Schafer, C. R. Becker, H. Buhmann, and L. W. Molenkamp, Phys. Rev. Lett. **96**, 076804 (2006).

[3] D. Frustaglia and K. Richter, Phys. Rev. B **69**, 235310 (2004).

[4] T. Bergsten, T. Kobayashi, Y. Sekine, and J. Nitta, Phys. Rev. Lett. **97**, 196803 (2006).

[5] F. Nagasawa, J. Takagi, Y. Kunihashi, M. Kohda, and J. Nitta, Phys. Rev. Lett. **108**, 086801 (2012).

[6] M. Büttiker, Y. Imry, and M. Ya. Azbel, Phys. Rev. A **30**, 1982 (1984).

[7] J. Nitta, J. Takagi, F. Nagasawa, and M. Kohda, Journal of Physics: Conference Series **302**, 012002 (2011).

[8] S. Bellucci, and P. Onorato, Phys. Rev. B **78**, 235312 (2008).

[9] Zh. Zhu, Y. Wang, K. Xia, X. C. Xie, and Zh. Ma, Phys. Rev. B **76**, 125311 (2007).

[10] O. Kálmàn, P. Földi, M. G. Benedict, and F. M. Peeters, Phys. Rev. B **78**, 125306 (2008).

[11] F. Nagasawa, D. Frustaglia, H. Saarikoski, M. Kohda, K. Richter, and J. Nitta, unpublished.

[12] F. E. Meijer, A. F. Morpurgo, and T. M. Klapwijk, Phys. Rev. B **66**, 033107 (2002).

[13] Experiments report resistances rather than conductances. The resistance oscillations $\delta R \ll R$ are measured on top of a large background resistance R. Thus, experiments are represented by $\delta R(\alpha \neq 0)/\delta R(\alpha = 0) = \delta G(\alpha \neq 0)/\delta G(\alpha = 0)$, which we may compare directly with our calculated normalized conductance oscillations.

[14] M. Yamaguchi, S. Nomura, K. Miyakoshi, H. Tamura, T. Akazaki, H. Takayanagi, J. Appl. Phys. **100**, 113523 (2006).

SUMMARY

THE INTERPLAY OF CURRENT AND SPIN IN NANOSTRUCTURES

Controlling magnetization on short time scales and/or small dimensions is a hot topic in the field of spintronics, owing to its fundamental physics and its applications for information technology. The most straightforward way to control magnetization is by using an external magnetic field. However, because of the technical limitation in using a magnetic field at smaller sizes and larger amplitudes, alternatives have been investigated such as using currents or light to control the magnetization. In this thesis, we study the interplay of current and spin in nanostructures. The charge current, in the work of this thesis, is generated by shining circularly polarized light on conducting rings, or by applying a voltage to magnetic wires. In Chapter 2, we study the electrons and holes in non-magnetic single mode quantum rings in the presence of Rashba or Dresselhaus type spin orbit interaction (SOI) and light induced circular currents. We consider the effect of circular currents induced by the circularly polarized light on orbiting holes and electron in the rings in the presence of only Dresselhaus or Rashba SOI. We show that the z-component of the polarization induced by the current vanishes for the case of electrons. However, the holes gain a non-zero polarization. This polarization has a higher value in the case of the Dresselhaus SOI compared to the case of Rashba SOI.

To investigate the effect of the polarization on magnetic rings, in Chapter 3, we consider electrons in the presence of Rashba SOI, and an exchange energy which breaks the Kramers degeneracy. We demonstrate in this chapter that current can change the polarization of the electrons, and the effect can be maximized by tuning the Fermi energy into the exchange gap such that only one band is occupied.

In Chapter 4, we study the current-induced motion of domain walls (DWs) in a metallic wire, that are initially pinned by the localized magnetic fields, e.g. generated intentionally by notches. In DWs, the current is locally magnetized by the noncollinear magnetization. Thus, the conducting electrons apply a torque on the magnetization when they arrive with a different polarization direction. We use the Lagrangian multiplier method to obtain the Hamiltonian of the system quantum mechanically. By only using energy considerations, we obtain the critical current needed to depin the wall. The calculated current-induced torque, for adiabatically varying magnetization textures agrees with known results. We also provide a sim-

ple mathematical expression for the localized magnetic field generated by notches with circular and triangular shapes.

The second part of this thesis focuses on an opposite effect, viz. the conductance controlled by SOI in an array of rings. In Chapter 5, we calculate the conductance oscillations of an ensemble of weakly coupled rings as a function of the SO coupling constant. We demonstrate that the oscillations for arrays of rings with different average radii are in good agreement with the experimental as well as the theoretical results obtained for a single mode ring strongly coupled to the leads. We suggest experiments to distinguish between these fundamentally different theoretical models.

SAMENVATTING

DE WISSELWERKING TUSSEN STROOM EN SPIN IN NANOSTRUCTUREN

De controle van magnetisatie op korte tijd- en/of lengteschalen is een *hot topic* in het onderzoeksveld van de spintronica, vanwege de fundamentele natuurkunde en de mogelijke toepassingen in informatietechnologie. De meest directe manier om magnetisatie te beïnvloeden is door gebruik te maken van een extern magnetisch veld. Door de technische beperkingen in het gebruik van magnetische velden op kleine lengteschalen en grote amplitudes zijn er echter ook alternatieven onderzocht, zoals het gebruik van elektrische stromen of van licht om de magnetisatie te beïnvloeden. In dit proefschrift onderzoeken we de wisselwerking tussen stroom en spin in nanostructuren. De ladingsstroom wordt, in het werk van dit proefschrift, gegenereerd door een geleidende ring te belichten met circulair gepolariseerd licht of door een spanning toe te passen op een magnetische draad. In hoofdstuk 2 worden elektronen en gaten bestudeerd in een niet-magnetische kwantumring, met een enkele mode, in de aanwezigheid van spinbaan interactie (SBI) van het type Rashba of Dresselhaus en in de aanwezigheid van circulair gepolariseerd licht. We beschouwen het effect van circulaire stromen, geïnduceerd door het circulair gepolariseerde licht, op rondcirkelende gaten en elektronen in de ring, in de aanwezigheid van alleen Rashba of Dresselhaus SBI. We tonen aan dat de z-component van de polarisatie, welke geïnduceerd is door de stroom, verdwijnt voor het geval van de elektronen. De gaten verkrijgen echter een polarisatie die ongelijk is aan nul. De waarde van deze polarisatie is groter in het geval van Dresselhaus SBI, vergeleken met het geval van Rashba SBI.

Om het effect van polarisatie op magnetische ringen te bestuderen, in hoofdstuk 3, beschouwen we elektronen in de aanwezigheid van Rashba SBI en omwisselingsenergie, welke de Kramers-ontaarding breekt. We demonstreren in dit hoofdstuk dat de stroom de polarisatie van elektronen kan veranderen. Dit effect kan gemaximaliseerd worden door de Fermi energie zodanig af te stemmen dat deze in het energiegat komt dat veroorzaakt wordt door de uitwisselingsenergie, zodat slechts één band gevuld is.

In hoofdstuk 4 bestuderen we de, door stroom geïnduceerde, beweging van domeinmuren (DM-en) in metalen draden welke aanvankelijk vastgepind zijn door gelokaliseerde magnetische velden, die bijvoorbeeld bewust gegenereerd zijn door inkepingen. In DM-en is de stroom lokaal gemagnetiseerd door niet-collineaire

magnetisatie. Als gevolg daarvan oefenen de geleidende elektronen een koppel uit op de magnetisatie als ze aankomen met een andere polarisatierichting. We maken gebruik van de methode van Lagrange-multiplicators om de Hamiltoniaan van het systeem kwantummechanisch te verkrijgen. Door alleen gebruik te maken van overwegingen met betrekking tot de energie, verkrijgen we de kritische stroom die nodig is om een DM te ontpinnen. De berekende, door stroom geïnduceerde, koppel waarmee magnetische texturen adiabatisch veranderen is in overeenkomst met bekende resultaten. We voorzien ook in een eenvoudige mathematische uitdrukking voor het gelokaliseerde magnetische veld dat gegenereerd wordt door inkepingen met circulaire en triangulaire vormen.

Het tweede deel van dit proefschrift is gericht op een tegengesteld effect, namelijk de geleiding die gecontroleerd wordt door SBI in een rij van ringen. In hoofdstuk 5 berekenen we de geleidingsoscillaties van een verzameling van zwak gekoppelde ringen als een functie van de koppelingsconstante van de SBI. We laten zien dat, in het geval van rijen van ringen met verschillende gemiddelde radii, deze oscillaties goed overeenstemmen met zowel de experimentele als de theoretische resultaten die verkregen zijn voor een ring met een enkele mode die sterk gekoppeld is aan de leidingen. We stellen experimenten voor om deze fundamenteel verschillende theoretische modellen van elkaar te onderscheiden.

CURRICULUM VITÆ

Fatemeh KAKO JOIBARI

June 16, 1983	Born in Sari, Iran.
2001–2005	B. SC. in PHYSICS, Atomic and Molecular Physics Amir Kabir University of Technology
2005–2008	M. SC. in PHYSICS, Solid State Physics and Electronics Tabriz University
2008–2009	GUEST RESEARCHER, Institute for research in Fundamental sciences (IPM)
2009–2014	PHD RESEARCHER, Delft University of Technology Promoter: Prof. dr. ir. G. E. W. Bauer Copromoter: Prof. dr. Y. M. Blanter

LIST OF PUBLICATIONS

- **F. K. Joibari**, Y. M. Blanter, and G. E. W. Bauer, *Aharonov-Casher effect in quantum ring ensembles*, Phys. Rev. B **88**, 115410 (2013).
- A. Qaiumzadeh, **F. K. Joibari**, and R. Asgari, *Dynamical Properties of Quasiparticles in a Gapped Graphene Sheet*, Eur. Phys. J. B **74**, 479 (2010).
- **F. K. Joibari**, Y. M. Blanter, and G. E. W. Bauer, *Light-induced spin accumulation in quantum rings*, Submitted to Phys. Rev. B.
- **F. K. Joibari**, P. Yan, and G. E. W. Bauer, *Current driven domain wall depinning in a ferromagnetic wire*, In preparation for submission.